

## INFORMATION TO USERS

This manuscript has been reproduced from the microfilm master. UMI films the text directly from the original or copy submitted. Thus, some thesis and dissertation copies are in typewriter face, while others may be from any type of computer printer.

**The quality of this reproduction is dependent upon the quality of the copy submitted.** Broken or indistinct print, colored or poor quality illustrations and photographs, print bleedthrough, substandard margins, and improper alignment can adversely affect reproduction.

In the unlikely event that the author did not send UMI a complete manuscript and there are missing pages, these will be noted. Also, if unauthorized copyright material had to be removed, a note will indicate the deletion.

Oversize materials (e.g., maps, drawings, charts) are reproduced by sectioning the original, beginning at the upper left-hand corner and continuing from left to right in equal sections with small overlaps. Each original is also photographed in one exposure and is included in reduced form at the back of the book.

Photographs included in the original manuscript have been reproduced xerographically in this copy. Higher quality 6" x 9" black and white photographic prints are available for any photographs or illustrations appearing in this copy for an additional charge. Contact UMI directly to order.

# UMI

A Bell & Howell Information Company  
300 North Zeeb Road, Ann Arbor MI 48106-1346 USA  
313/761-4700 800/521-0600



GEOPHYSICAL INVESTIGATIONS OF THE REYKJANES RIDGE  
AND KOLBEINSEY RIDGE SEAFLOOR SPREADING CENTERS

A DISSERTATION SUBMITTED TO THE GRADUATE DIVISION OF THE  
UNIVERSITY OF HAWAII IN PARTIAL FULFILLMENT OF THE  
REQUIREMENTS FOR THE DEGREE OF

DOCTOR OF PHILOSOPHY

IN

GEOLOGY AND GEOPHYSICS

December 1995

By

Bruce Appelgate

Dissertation Committee:

Alexander N. Shor, Chairman

Rodey Batiza

Margo Edwards

Richard Hey

Alexander Malahoff

Brian Taylor

**UMI Number: 9615507**

---

**UMI Microform 9615507  
Copyright 1996, by UMI Company. All rights reserved.**

**This microform edition is protected against unauthorized  
copying under Title 17, United States Code.**

---

**UMI**  
300 North Zeeb Road  
Ann Arbor, MI 48103

© Copyright 1995  
by  
Bruce Appelgate  
All Rights Reserved

## ACKNOWLEDGEMENTS

Following the unfortunate demise and burial at sea of the venerable SeaMARC II mapping system in 1991, my graduate career appeared tenuous. But I took heart in the sage words of a Famous Scientist who once explained to me, as I watched some expensive piece of equipment or other fail to return to the ship, "That's oceanography." From the precipice of ruin several people rose to the challenge of quickly developing and deploying a new, better mapping system - the HAWAII-MR1. Paving the way for the success of MR1, however, was an existing project by the the Hawaii Institute of Geophysics to build a more powerful swath mapping system, now known as SEAMAP, for the U.S. Naval Oceanographic Office. It was SEAMAP that I ultimately deployed to collect the data that's presented in Chapter 3. The success of these two systems is due to the (pick one: scientific foresight, technical skill, personal charm) of a host of key people: Sandy Shor, leader of the SeaMARC-cum-Hawaii Mapping Research Group; Carey Ingram and William Jobst at NAVOCEANO; Hank Fleming and Peter Vogt at NRL; and Mark Rognstad, Stan Zisk, Roger Davis, Mike Simpson, Margo Edwards, Joel Erickson, Steve Tottori, and Bev Adkins at the Hawaii Mapping Research Group. Without these guys I'd have ended up flipping teri-burgers at Zippy's.

I mercilessly annoyed the following people while I was a graduate student: Adam Klaus, Mary MacKay, Paul Johnson, Mark Dustman, Devi Joseph, Manny Leon, Les Kajiwara, Tina Mueller, and Karen Sender.

The best part of my tenure at UH was all the excellent Arctic Oceanographic Expeditions I got to go on, and the competent and/or interesting people I met thereon. Mike "BZ" Bendzlowicz (tireless if bombastic protector of the indigenous peoples of Norway), Dave Johanson (the Turtle Boy), Hunter, Dan Chayes, Penny Herring, Joan Gardner, Eric Halter, Les Kajiwara, Steve Tottori, Chris Jones. Thanks to Kathy Crane, Lynn Johnson and Roger Buck for inviting me to sail with them and their Russian colleagues on their cruise to the Reykjanes Ridge aboard the *Keldysh*.

I'm indebted to Terri Dunnebier for finding and extracting all kinds of data from all kinds of sources for me, and I suggest that she is the nicest person in the entire world.

Financial support for me and my work was provided by the United States Naval Oceanographic Office, which released the data from our joint UH/NAVOCEANO cruises in 1993 for scientific use (per written consent ); Office of Naval Research grant N00014-90-J-1834 to Alexander N. Shor; Joint Oceanographic Institutions, Inc. subcontract JSC5-90 to Alexander N. Shor; the United States National Science Foundation; the United States Naval Research Laboratory; The Society of Exploration Geophysicists Foundation Scholarship (sponsored by Exxon Production Research); The J. Watumull Merit Scholarship, administered by the University of Hawaii Department of Geology and Geophysics.

I thank my gorgeous wife Lisa for accompanying me. Aloha wa'u ia 'oe, ku'uipo.

## ABSTRACT

I used a suite of marine geophysical tools to study the structure and tectonics of the slow-spreading Kolbeinsey, Reykjanes and northern Mid-Atlantic Ridges. Including Iceland, these ridges constitute a continuous spreading center system more than 2055 km long, and vary in their structural expression and obliquity to the spreading direction. The northern Mid-Atlantic Ridge (MAR) and Reykjanes Ridge between 55°50'N and 63°00'N exhibit systematic along-strike variation in axial valley depth, axial boundary fault throw, relief along the neovolcanic axis, and degree of inter-segment structural discontinuity. The orthogonal northern MAR is separated from the Reykjanes Ridge by the Bight transform fault (56°47'N), a right-stepping linear fault 15 km wide. The volcanic axis of Reykjanes Ridge contains individual volcanic systems 4-45 km long (fourth-order segments), superimposed on intermediate-wavelength (13-65 km) axial topographic highs that constitute third- or second-order spreading segments. The modern Kolbeinsey Ridge axis contains three first-order segments oriented orthogonally to the spreading direction. These segments are separated by large right-stepping nontransform offsets, the Spar (69.0°N) and Eggvin (70.4°N) discontinuities. The northern KR segment is a robust volcanic edifice 125 km long and more than 1000 m high. Shallow crust extends east from the northern KR axis to Jan Mayen Island, and I suggest the Jan Mayen hotspot is located beneath the northern KR rather than near Jan Mayen Island. A tectonic reconstruction based on aeromagnetic data indicates that the axial structure of the KR changed from continuous to segmented after anomaly 4. The subsequent structural evolution of the ridge involved ridge propagation, along-strike migration of axial discontinuities, asymmetric spreading, and lateral migration of segment axes that occurred via ultrafast propagation or synchronous ridge jumps. Two of the three original discontinuities still exist and contain active north-directed propagators. An ephemeral, catalytic change in plate motion is inferred to have triggered the axial reorientation at anomaly 4 time, which initiated the subsequent phase of ridge propagation and migration of nontransform offsets.

## TABLE OF CONTENTS

ACKNOWLEDGEMENTS.....	iv
ABSTRACT .....	v
LIST OF TABLES .....	viii
LIST OF FIGURES.....	ix
CHAPTER 1: THE NORTHERN MID-ATLANTIC AND REYKJANES RIDGES:	
SPREADING CENTER MORPHOLOGY BETWEEN 55°50'N AND 63°00'N .....	1
ABSTRACT .....	1
INTRODUCTION .....	1
DATA AND METHODS .....	2
REGIONAL STRUCTURE .....	4
TERMINOLOGY .....	5
AXIAL PROFILE .....	5
NORTHERNMOST MID-ATLANTIC RIDGE.....	7
THE BIGHT TRANSFORM FAULT .....	9
SOUTHERN REYKJANES RIDGE.....	11
<i>The 56°47'-56°55'N segment .....</i>	<i>11</i>
<i>The 56°55'-57°18'N segment .....</i>	<i>12</i>
<i>The 57°18'-57°36'N segment .....</i>	<i>12</i>
<i>The 57°36'-57°51'N segment .....</i>	<i>12</i>
<i>The 57°51'N discontinuity.....</i>	<i>12</i>
<i>The 57°51'-58°12'N segment .....</i>	<i>13</i>
<i>The 58°12'-58°26'N segment .....</i>	<i>15</i>
<i>The 58°26'-58°47'N segment .....</i>	<i>15</i>
NORTHERN REYKJANES RIDGE.....	15
<i>The 58°47'-59°21'N segment .....</i>	<i>16</i>
<i>The 59°21'-60°00'N segment .....</i>	<i>16</i>
<i>The NRR between 60°-63°N .....</i>	<i>19</i>
DISCUSSION .....	22
<i>Spreading Center Segmentation.....</i>	<i>22</i>
<i>Faulting .....</i>	<i>25</i>
<i>Volcanism .....</i>	<i>29</i>
<i>Tectonic Homogenization .....</i>	<i>30</i>

<i>Fracture Zones</i> .....	32
CONCLUSIONS .....	32
CHAPTER 2: RAPID REORIENTATION OF A SLOW SEAFLOOR SPREADING	
CENTER: THE STRUCTURAL EVOLUTION OF KOLBEINSEY RIDGE SINCE 10 MA .....	34
ABSTRACT .....	34
INTRODUCTION .....	34
DATA .....	36
OBSERVED MAGNETIC FIELD AND INTERPRETATION OF ANOMALIES .....	38
TECTONIC EVOLUTION OF KOLBEINSEY RIDGE SINCE ANOMALY 5.....	41
INITIAL SEGMENTATION AND SUBSEQUENT MIGRATION OF	
DISCONTINUITIES ON KR.....	45
CONCLUSIONS .....	48
CHAPTER 3: AXIAL STRUCTURE AND RECENT TECTONICS OF THE KOLBEINSEY	
RIDGE SEAFLOOR SPREADING CENTER.....	50
ABSTRACT .....	50
INTRODUCTION .....	50
METHODS .....	52
GEOLOGIC SETTING .....	55
KOLBEINSEY RIDGE AXIAL PROFILE .....	55
TJÖRNES FRACTURE ZONE .....	56
SOUTHERN KOLBEINSEY RIDGE (SKR) .....	58
SPAR OFFSET .....	62
MIDDLE KOLBEINSEY RIDGE (MKR) .....	65
EGGVIN OFFSET .....	68
NORTHERN KOLBEINSEY RIDGE (NKR).....	70
DISCUSSION .....	72
<i>Structural and Geochemical Axial Segmentation</i> .....	72
<i>Axial volcanism on the MKR</i> .....	73
<i>The NKR, and Eggvin Bank: Implications for the Jan Mayen hotspot</i> .....	74
CONCLUSIONS .....	75
REFERENCES .....	77

## LIST OF TABLES

## TABLE

1.1	Spreading segments of the Reykjanes Ridge .....	17
1.2	Reykjanes Ridge segment boundaries .....	23
2.1	Chronology of tectonic events on the Kolbeinsey Ridge since 5 Ma .....	43
2.2	Propagation rates of the Kolbeinsey Ridge segments .....	47

## LIST OF FIGURES

## FIGURE

1.1	Regional Bathymetry of Reykjanes Ridge .....	3
1.2	Axial bathymetric profile of the Reykjanes Ridge .....	6
1.3	Bathymetry, acoustic imagery and structure of the northernmost MAR.....	8
1.4	Bathymetry, acoustic imagery and structure of the Bight transform fault .....	10
1.5	Bathymetry, acoustic imagery and structure of the 57°51'N nontransform offset .....	14
1.6	Bathymetry, acoustic imagery and structure of the 59°40'N spreading segment.....	18
1.7	Distribution of equant volcanoes along the axis of Reykjanes Ridge .....	20
1.8	Bathymetry, acoustic imagery and structure of Reykjanes Ridge near 61°20'N .....	21
1.9	Frequency histogram of azimuths of axial faults and volcanic systems .....	26
1.10	Azimuths of axial volcanic systems versus latitude .....	27
1.11	Comparison of axial structural azimuths with experimental results .....	28
2.1	Bathymetry and magnetic anomalies of the southern and middle Kolbeinsey Ridge.....	35
2.2	Shaded-relief image of residual magnetic field of Kolbeinsey Ridge.....	37
2.3	Anomaly picks for Kolbeinsey Ridge.....	39
2.4	Tectonic reconstruction of KR.....	42
3.1	Location of Kolbeinsey Ridge and surrounding plate tectonic features .....	51
3.2	Regional bathymetry of the Greenland Sea .....	53
3.3	Bathymetric profile of Kolbeinsey Ridge .....	57
3.4	Bathymetry and structure of Tjörnes Fracture Zone and the southern Kolbeinsey Ridge.....	59
3.5	Acoustic imagery and structure of the northern SKR.....	61
3.6	Acoustic imagery and structure of the Spar Nontransform Offset .....	63
3.7	Acoustic imagery and structure of the Middle Kolbeinsey Ridge .....	66
3.8	Acoustic imagery and structure of the Eggvin Nontransform Offset.....	69
3.9	Bathymetry of the Northern Kolbeinsey Ridge .....	71

THE NORTHERN MID-ATLANTIC AND REYKJANES RIDGES: SPREADING CENTER  
MORPHOLOGY BETWEEN 55°50'N AND 63°00'N

ABSTRACT

SeaMARC II and Hydrosweep acoustic imagery and bathymetry reveal that the northern Mid-Atlantic Ridge (MAR) and Reykjanes Ridge between 55°50'N and 63°00'N are segmented seafloor spreading centers that exhibit structural morphologies that vary with distance from Iceland. The northern 100 km of the MAR (55°50'N-56°47'N) is oriented 005° (perpendicular to the spreading azimuth) and contains four third-order spreading segments separated along strike by right- and left-stepping axial discontinuities. The boundary between MAR and Reykjanes Ridge occurs at 56°47'N, where the Bight transform fault offsets the neovolcanic axis 15 km right laterally across a single linear fault oriented 092°. This is the only transform fault between 55°50'N and 63°00'N and is inferred to have generated the Bight Fracture Zone. The Reykjanes Ridge lies between the Bight transform and Iceland's Reykjanes Peninsula and is oriented ~30° oblique to the spreading-orthogonal direction. Axial faults and volcanic systems on the Reykjanes Ridge are arranged in a right-stepping *en echelon* pattern and display strikes intermediate between the spreading-orthogonal direction and the strike of the ridge, which is compatible with experimental models of oblique extension. Spreading segments on the northern MAR and Reykjanes Ridge are defined structurally and bathymetrically. At the smallest scale, the volcanic axis is segmented into individual volcanic systems 4-45 km long, which are separated along strike by intervolcano gaps or offsets. These features are analogous to fourth-order spreading segments documented elsewhere on the MAR. Axial volcanic systems are superimposed on intermediate-wavelength (13-65 km) axial topographic highs that constitute third- or second-order spreading segments. Segment boundaries occur at axial depth maxima, which correspond to offsets in the volcanic axis. Four primary characteristics of the spreading axis (axial valley depth, axial boundary fault throw, relief along the neovolcanic axis, and degree of inter-segment structural discontinuity) decrease toward the north. This variation is consistent with higher crustal temperatures near Iceland, due to either thicker crust or elevated mantle temperatures.

INTRODUCTION

The Reykjanes Ridge was among the first seafloor spreading centers recognized from symmetry of magnetic anomaly patterns [Heirtzler *et al.*, 1966; Vine, 1966] and was an early target for geophysical studies of midocean ridges. The Reykjanes is not a typical spreading ridge: it is located next to the robust Iceland hotspot, it is anomalously shallow, and it is oriented ~30° oblique to the spreading-orthogonal direction [Vogt, 1971; Vogt and Avery, 1974]. However, the significance of the Reykjanes Ridge lies in its very abnormality: its intermediate position between

the northern Mid-Atlantic Ridge (MAR) and the hotspot-dominated, subaerial spreading center on Iceland provides an opportunity to study the along-strike variation in spreading center processes between these two extremes. The obliquity of the Reykjanes Ridge facilitates the study of structures that, although common to all ridge crests, are best expressed in this environment. Previous studies have documented the general structure of the ridge [Laughton *et al.*, 1979; Schilling, 1973; 1986; Searle and Laughton, 1981; Shih *et al.*, 1978; Talwani *et al.*, 1971; Vogt, 1971; 1974; 1976] although the fine-scale morphology of the spreading axis and the degree of along-strike morphological variability have remained unknown due to limitations in the resolution and areal extent of the geophysical surveys.

We acquired a nearly continuous swath of SeaMARC II imagery and Hydrosweep bathymetry of the Reykjanes Ridge and northernmost MAR spreading axis between 55°50'N and 63°00'N (Figure 1.1). These data are important because they resolve the axial structure of the spreading center at a scale fine enough to evaluate the structure of individual volcanic systems, facilitating the comparison of the Reykjanes Ridge with other well-studied mid-ocean ridges. Swath bathymetry surveys elsewhere on the slow spreading MAR have shown that the spreading axis is typically segmented at several length scales [Purdy *et al.*, 1990; Sempéré *et al.*, 1990; 1992] and segmentation of fast and intermediate rate spreading centers is also well documented [Macdonald *et al.*, 1991]. Recent models [Bell and Buck, 1992; Phipps Morgan and Chen, 1993; Rabinowicz *et al.*, 1993; Sempéré *et al.*, 1992] suggest that mid-ocean ridge segmentation and morphology may be controlled by the thermal structure beneath the spreading centers. As a slow spreading ridge that displays physical characteristics typically associated with both fast and slow spreading ridges, the Reykjanes Ridge is an ideal area to test these models.

The primary objectives of this survey were to determine the volcanic and tectonic expression of the Reykjanes Ridge spreading axis along strike, to evaluate the nature and scale of ridge segmentation, and to establish whether axial morphology systematically varies with proximity to the Iceland hotspot. This paper presents the structure of the spreading axis between 55°50'N and 63°00'N, discusses the style of axial volcanism and faulting, and compares the pattern of axial segmentation here with other parts of the slow spreading MAR.

## DATA AND METHODS

We surveyed the spreading axis of the mid-Atlantic ridge between 55°50'N and 63°00'N using the SeaMARC II and Hydrosweep seafloor imaging systems aboard the R/V *Maurice Ewing* in 1990 (Figure 1.1). This was a transit leg, and our data are limited to a single track line along most of the spreading axis. However, a short survey at 59°50'N extended coverage to 15 km on either side of the neovolcanic zone, and a few other brief excursions allowed off-axis seafloor to be surveyed elsewhere as well (Figure 1.1). Navigation was by Global Positioning System (70%) and transit satellite.

SeaMARC II [Blackinton *et al.*, 1983; Shor, 1990] was a shallow-towed 11-12 kHz swath seafloor imaging system that simultaneously recorded digital side scan sonar imagery and bathymetry

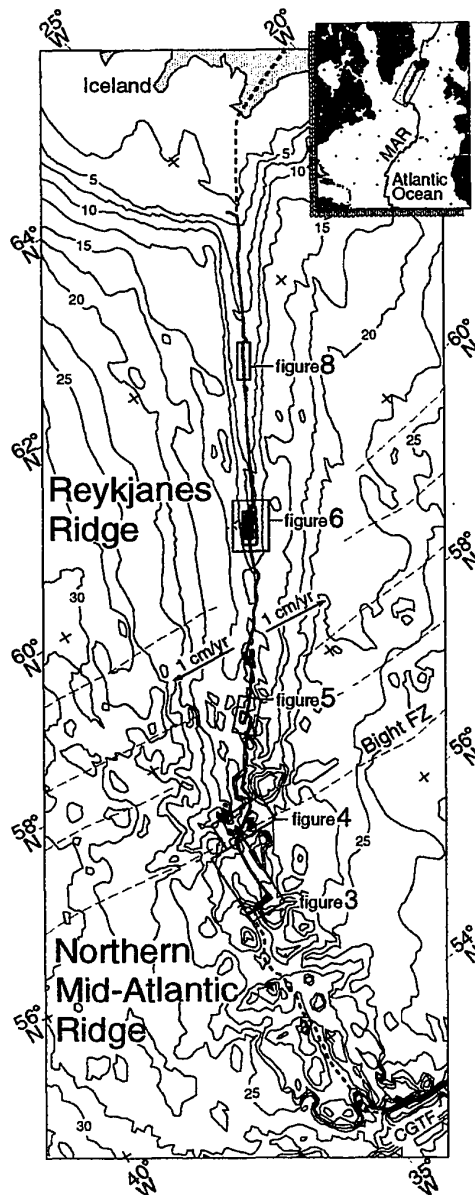


**Figure 1.1.** Bathymetry near the Reykjanes Ridge, showing the SeaMARC II/Hydrosweep trackline (bold line). The ship's track roughly marks the spreading axis, which elsewhere is shown by a bold dashed line. Arrows show the  $097^\circ$  spreading direction at  $59^\circ\text{N}$ , which is oblique to the trend of the Reykjanes Ridge axis. The Bight transform fault at  $56^\circ47'\text{N}$  separates the oblique Reykjanes Ridge from the spreading-orthogonal Mid-Atlantic Ridge to the south. Light dashed lines show fracture zone picks from Müller and Roest [1992]. Locations of detailed side scan figures are shown. Depth contour interval is 250 m, annotated in hundreds of meters. Inset shows the location (shaded) of the survey area within the North Atlantic Ocean. CGTF is Charlie-Gibbs Transform Fault. This and the following figures were generated using the Generic Mapping Tools (GMT) software package [Wessel and Smith, 1991].

data. (The SeaMARC II system was lost at sea in February 1991.) We collected SeaMARC II side scan data using swath widths of 10 and 5 km and obtained bathymetry swath widths of up to 3.4 times the water depth. Hydrosweep is a 15.5 kHz hull-mounted multinarrow beam bathymetry system that samples a swath width twice water depth [Grant and Schreiber, 1990]. The two systems were operated simultaneously throughout the survey, allowing the data sets to be directly compared. These data are complementary because Hydrosweep provides a high-resolution swath of bathymetry centered beneath the ship, and SeaMARC II extends bathymetric coverage over an even wider swath and provides textural information (side scan imagery) that allows tectonic, volcanic, and sedimentary features to be resolved. For the purposes of this study, SeaMARC II side scan images were especially useful as a means of discriminating volcanic ridges from fault scarps and for defining the locus of recent volcanism along the spreading axis.

Side scan data were postprocessed to normalize system gains [Sender *et al.*, 1989] allowing direct comparison of backscatter amplitudes on different images. Side scan images were plotted by merging the digital side scan data with ship navigation, and mapping side scan pixels onto a geographic coordinate system using a flat-bottom assumption. On the side scan images presented herein, high-amplitude echoes are displayed as dark shades of gray, and acoustic shadows appear white.

Geological interpretations of SeaMARC II backscatter data were drawn following the rationale of previous workers [Edwards, 1991; Edwards *et al.*, 1991; Vogt, 1986a]. We interpret fault scarps as long, narrow features that display little or no internal structure. The backscatter measured from a fault scarp is variable depending on the imaging geometry and the relief and slope of the scarp: fault scarps that face nadir display high backscatter, and scarps that face away from the towfish cast acoustic shadows. Volcanoes typically form cones (some with flat tops and summit craters) or ridges, and volcanic surfaces often exhibit a botryoidal appearance indicative of smaller-scale eruptive and flow structures. Younger lavas typically display high backscatter relative to older, sedimented areas, and the average backscatter intensity of broad regions can be used as a measure of relative crustal age [Hagen *et al.*, 1990]. However, this is at best a qualitative means of establishing age relationships due to the dependence of backscatter amplitude on the material properties and surface roughness of the seafloor, acoustic grazing angle, and sonar frequency [Gardner *et al.*, 1991; Jackson *et al.*, 1986].

## REGIONAL STRUCTURE

The midocean ridge between the Charlie-Gibbs transform fault system (53°N) and Iceland (64°N) is a slow (~1 cm/yr half rate) seafloor spreading center that separates the Eurasian and North American lithospheric plates [DeMets *et al.*, 1990; Minster and Jordan, 1978]. Regional bathymetry (Figure 1.1) and magnetic anomaly patterns [Vogt, 1986b; Vogt and Avery, 1974] show that the spreading center consists of three linear sections characterized by different strikes. The northernmost part of the Mid-Atlantic Ridge (MAR) is a 460-km-long section of the spreading axis that lies between the Charlie-Gibbs transform and 56°47'N. The 005° strike of the northern

MAR is orthogonal to the 095° local spreading azimuth calculated from the NUVEL-1 plate velocity model [DeMets *et al.*, 1990]. Magnetic data [Fleischer, 1974; Vogt, 1986c; Vogt and Avery, 1974] indicate that the northern MAR probably contains several smaller-scale segments separated by axial discontinuities.

The spreading axis at 56°47'N is marked by a sharp 31° clockwise change in strike, which separates the spreading-orthogonal MAR from the oblique Reykjanes Ridge to the north. This bend corresponds to the point where the Bight Fracture Zone (BFZ) intersects the ridge axis [Müller and Roest, 1992]. The Reykjanes Ridge is oriented roughly 30° oblique to the spreading-orthogonal direction (Figure 1.1) and is composed of two linear sections that are divided by a 5° bend in the ridge axis at ~59°N [Fleischer, 1974]. The southern Reykjanes Ridge extends 350 km between 56°47'N and 59°00'N, and the northern Reykjanes Ridge spans 650 km between 59°00'N and Iceland's subaerial Reykjanes Peninsula at 63°20'N. Previous surveys have documented several unique structural characteristics of the ridge, including overlapping volcanic ridges along the spreading axis, axial faults oriented nearly perpendicular to the spreading direction, off-axis faults that trend roughly parallel to the Reykjanes Ridge axis, and an along-strike transition in axial morphology from a median valley in the south to a central high in the north [Johnson *et al.*, 1971; Talwani *et al.*, 1971; Shih *et al.*, 1978; Laughton *et al.*, 1979; Searle and Laughton, 1981; Bogdanov *et al.*, 1985; Rudenko, 1986; Parson *et al.*, 1993]. The following sections describe the structural characteristics of the northern MAR and Reykjanes Ridge spreading axis.

#### TERMINOLOGY

The northern MAR and Reykjanes Ridge display structural segmentation similar to that described for other slow spreading ridges, and I discuss the axial morphology here using descriptive terminology developed for slow spreading ridges by previous workers [Grindlay *et al.*, 1991; Macdonald *et al.*, 1991; Sempéré *et al.*, 1993]. This hierarchical scheme classifies axial segments and discontinuities as first-order (large-scale, long-lived) through fourth-order (small-scale, ephemeral) features. Following Sempéré *et al.* [1993], I define a segment as a part of the spreading axis that is bounded at each end by offsets that disrupt the continuity of the axial valley (i.e., first-through third-order discontinuities). A segment may contain one or more fourth-order volcanic systems that are separated from each other by intervolcano gaps or small (<4 km) offsets that do not disrupt the continuity of the axial valley. On the Reykjanes Ridge, individual volcanic systems commonly form elongate axial volcanic ridges (described by Parson *et al.*, [1993] and Murton and Parson [1993]) or sets of aligned cones and low-relief lava flows.

#### AXIAL PROFILE

Figure 1.2 shows an axial profile along the spreading center, which illustrates depth variations along the neovolcanic axis. This profile was constructed by identifying individual axial volcanic systems from SeaMARC II imagery, digitizing the bathymetry along the long axis of each volcanic system, and combining them into a single composite profile (Figure 1.2, inset). In cases

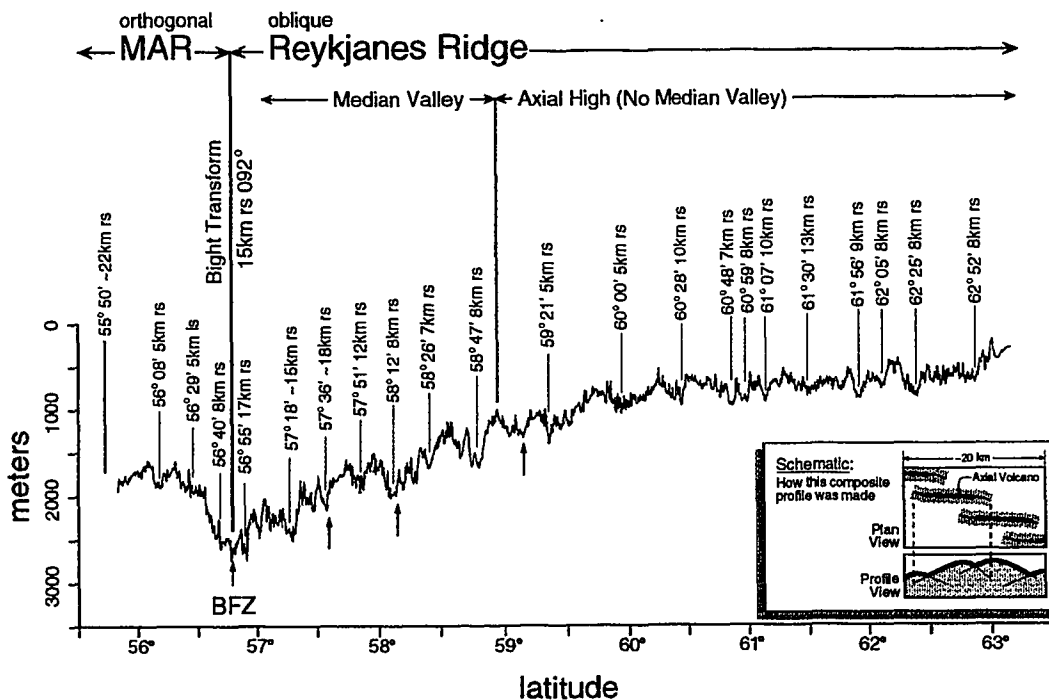


**Figure 1.2.** Axial bathymetric profile of the Reykjanes Ridge. The locations of axial discontinuities are shown above the profile, along with the magnitude and sense of offset (rs is right-stepping, ls is left-stepping). The deepest part of the profile marks the intersection of the ridge with the Bight Fracture Zone. The unlabeled bold arrows beneath the profile mark the points where off-axis fracture zones [Müller and Roest, 1992] are predicted to intersect the ridge axis, if in fact they extend on-axis. This is a composite of longitudinal profiles from 86 individual volcanic systems identified from side scan imagery. Inset schematically depicts how the composite profile was produced by combining profiles of the overlapping, en echelon axial volcanic systems. Vertical exaggeration is ~55x.

where volcanic systems overlap, the shallower of the two profiles is shown. Major structural features identified in the text are indicated on the profile.

The axial profile illustrates the segmented nature of the northern MAR and Reykjanes ridge spreading centers. The deepest point on the axis occurs at 56°47'N, and the MAR axis south of this point shoals rapidly, reaching 2000 m at 56°32'N. Axial depths farther south (to 55°50'N) range from 1900-1600 m. The axial gradient north of 56°47'N is less steep, and the rate of depth change progressively decreases to the north. Superimposed on this long-wavelength shoaling are several intermediate-wavelength (13-65 km long) topographic highs, which in turn contain even shorter-wavelength features. Axial topography is roughest on the southern Reykjanes Ridge, where intermediate-wavelength highs display 300-500 m of relief, in contrast to 200-300 m on the northern Reykjanes and MAR. *Vogt and Johnson* [1973] observed a similar distribution of roughness on a ridge-parallel seismic section east of the axis that imaged crust as old as 1-6 m.y.

#### NORTHERNMOST MID-ATLANTIC RIDGE

The northern 100 km of the MAR contains four ridge segments that lie within a fault-bounded median valley at least 500 m deep (Figure 1.1). The ridge segments are separated along strike by axial discontinuities at 56°08'N, 56°29'N, and 56°40'N. The axial neovolcanic zone displays high backscatter relative to the surrounding, presumably sedimented, seafloor within the axial valley. The neovolcanic zone is marked by a series of elongate volcanic ridges, which display between 75 and 200 m of relief and range in length from 18 to 42 km. A few small (~1 km diameter) circular volcanoes occur along the volcanic ridges and elsewhere within the axial valley. Volcanoes outside the neovolcanic zone are faulted and display lower backscatter than the axial volcanoes. Recent volcanic activity appears to have been restricted to the axial volcanic ridges.

Three of the segments on the northern MAR are shown in more detail in Figure 1.3. These segments are offset from one another, and the tips of neighboring segments bend toward one another at each axial discontinuity. At 56°08'N, the southern and middle segments are separated by a 5-km, right-stepping offset, and their ridge tips overlap by about 4 km. The middle and northern segments overlap by 5 km and are offset 5 km at 56°29'N. The southern segment, which was not completely surveyed, appears to be bounded to the south by a major right-stepping axial discontinuity at ~55°50'N based on bathymetry, the westward curvature of the tip of the southern ridge, and magnetic anomaly patterns [*Vogt*, 1986c]. The exact nature of this discontinuity (transform versus nontransform) cannot be determined from our data.

The volcanic systems are composite features, constructed from many smaller ridges and cones superimposed upon one another. For instance, the southern segment at 56°05'N displays small (<1 km diameter) circular volcanoes along its base, which are partially buried on their uphill sides by presumably younger lavas. The middle segment exhibits a continuous band of high backscatter 3-4 km wide along its axis and contains several small cones and elongate constructional ridges. The northern segment (20 km long) contains a single 16-km-long volcanic system constructed from subsidiary ridges and cones. The fine-scale morphology of these

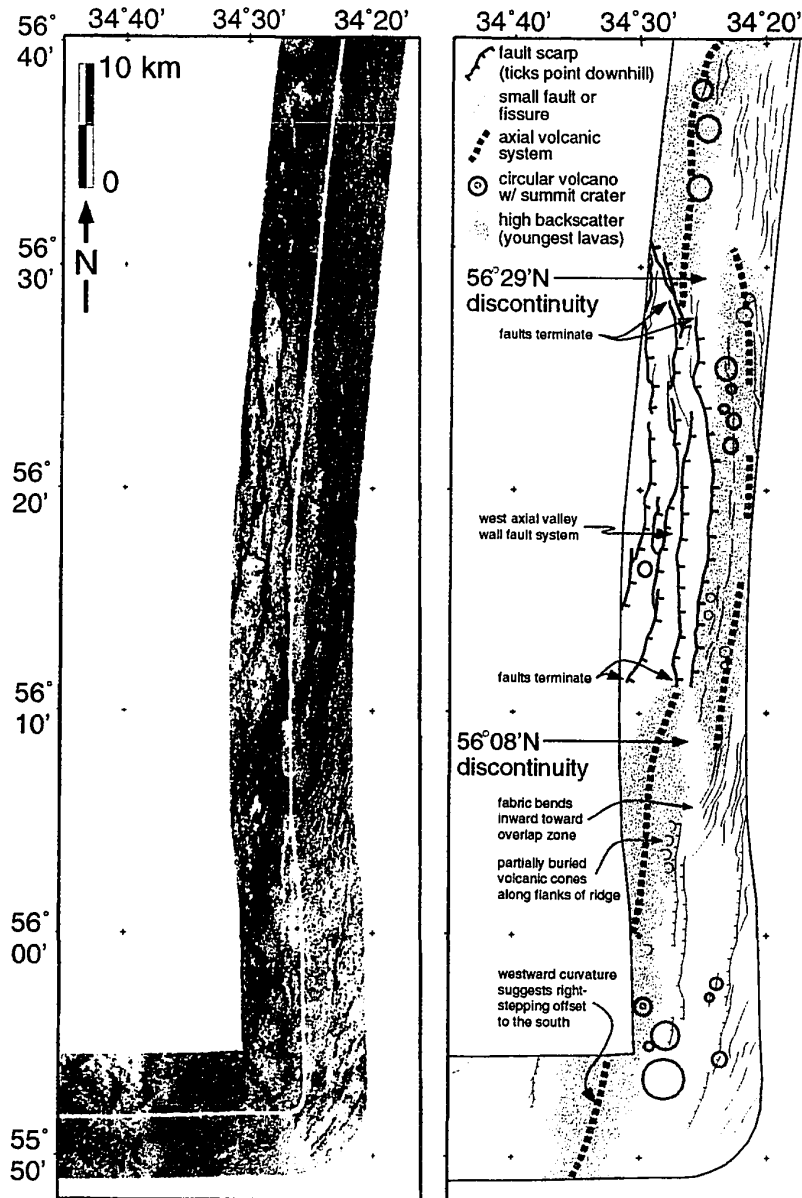


**Figure 1.3.** SeaMARC II side scan imagery and geological interpretation of the northernmost MAR. In this and all subsequent side scan images, high backscatter appears dark. Three distinct spreading segments are evident, marked by high-backscatter lavas. The segments are separated along strike by third-order axial discontinuities, with the middle segment offset to the east of the other two.

volcanic systems is similar to other parts of the MAR and Reykjanes Ridge, where detailed bathymetry and deep-towed side scan data show axial volcanic systems to be constructed from myriad small volcanoes and fissure ridges [Smith and Cann, 1990; 1992; 1993; Parson *et al.*, 1993].

The volcanic axes of each segment are bounded laterally by inward facing, small-offset faults within 1 km of the neovolcanic zone. Faults strike roughly  $005^\circ$ , parallel to the ridge axis, and curve toward axial discontinuities. The walls of the axial valley are constructed from multiple inward facing fault scarps with individual throws of up to 120 m (Figure 1.3). No outward facing fault scarps are evident.

The three segments shown in Figure 1.3 are separated by third-order axial discontinuities. By definition, third-order discontinuities on slow spreading centers disrupt the axial boundary faults but do not leave an off-axis trace, indicating that they are short-lived features [Grindlay *et al.*, 1991; Sempéré *et al.*, 1993]. Although our coverage is not wide enough to evaluate the presence of off-axis discordant zones here, the continuity of boundary faults on the west side of the axial valley is disrupted at each of the offsets. The scale of these offsets (4-6 km) is also compatible with that of other documented third-order discontinuities on the MAR. The smaller-scale volcanic systems contained within each third-order segment represent fourth-order features.

#### THE BIGHT TRANSFORM FAULT

The northernmost transform fault on the Mid-Atlantic Ridge occurs at  $56^\circ47'N$  (Figure 1.4), just north of the previously described spreading segments, and is the only transform fault on the northern MAR or Reykjanes Ridge between  $55^\circ50'N$  and  $63^\circ00'N$ . This transform separates the spreading-orthogonal MAR axis to the south from the oblique Reykjanes Ridge to the north (Figure 1.1), and offsets the spreading axis 15 km right-laterally along a single linear fault oriented  $092^\circ$ . This orientation is nearly parallel to the local plate motion azimuth of  $095^\circ$  predicted by the NUVEL-1 model [DeMets *et al.*, 1990]. The Bight Fracture Zone intersects the ridge crest at  $56^\circ47'N/34^\circ06'W$  [Müller and Roest, 1992] and was probably generated by the  $56^\circ47'N$  transform (hereinafter referred to as the Bight transform). The BFZ extends off-axis into crust at least 36 Ma old [Müller and Roest, 1992]. Magnetic anomalies on either side of the BFZ display a  $\sim 30^\circ$  change in strike similar to the modern spreading axis [Vogt, 1986b], indicating that the Reykjanes Ridge and MAR have been separated by this structural boundary since 36 Ma.

The Bight is the smallest-offset transform yet surveyed in the North Atlantic. The presence of a well-defined, persistent transform at such a small discontinuity (17 km, 1.7 m.y. age offset) is anomalous given that none of the axial discontinuities between  $24^\circ00'$  and  $30^\circ40'N$  on the MAR display transform faults, despite offsets ranging up to 30 km [Sempéré *et al.*, 1990]. Other well-known small discontinuities on the MAR, such as the Kurchatov (22 km), the  $23^\circ15'N$  offset in the MARK area (8 km), and Fracture Zones A and B at FAMOUS ((20 and 25 km), are probably second- or third-order nontransform offsets [Sempéré *et al.*, 1993].

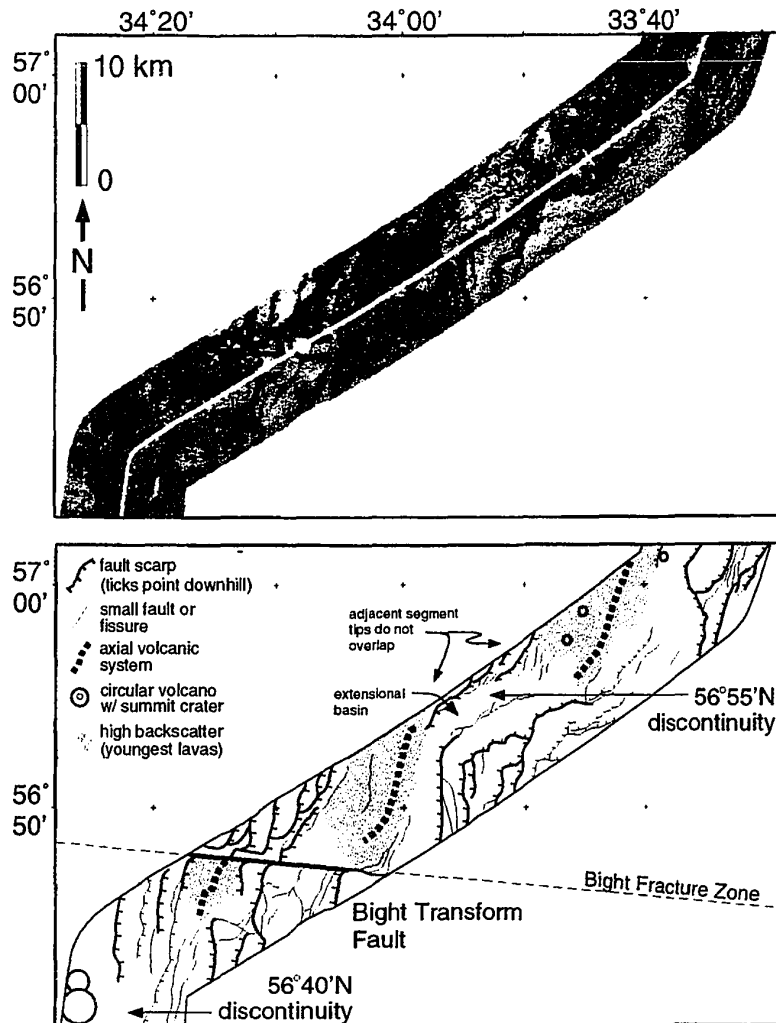


**Figure 1.4.** SeaMARC II imagery and interpretation of the Bight transform fault, which offsets the volcanic axis 15 km right-laterally along a single, 092° trending fault. The Bight transform separates the spreading-orthogonal MAR from the oblique Reykjanes Ridge and is the only transform fault between 55°50'N and 63°00'N. Also evident is the 56°55'N nontransform offset, a second-order axial discontinuity that contains an amagmatic extensional basin. A 15-km-long spreading segment lies between the transform and the nontransform offset, and spreading segments north and south of the two discontinuities are also evident.

## SOUTHERN REYKJANES RIDGE

The southern 350 km of the Reykjanes Ridge axis (between 56°47'N and 59°00'N) exhibit axial morphology and tectonic segmentation similar to other parts of the slow spreading MAR. The spreading axis lies within a median valley [Laughton *et al.*, 1979; Searle and Laughton, 1981] that is 40 km wide at 58°00'N (measured parallel to 095° between the highest points on the rift flanks) and displays 1300 m of vertical relief between the flanking rift mountains and the deepest basins along the spreading axis (B. Murton *et al.*, unpublished data, 1990). The volcanically active part of the median valley is nested within a 6-8 km wide inner valley defined by inward facing normal faults. The inner valley is 100-500 m deeper than the outer valley, with this relief accommodated in some places by a single major fault and in others by several smaller-offset fault scarps. The seafloor outside the inner valley displays low backscatter, indicating that recent volcanic activity has been confined within the inner valley [Laughton *et al.*, 1979; Searle and Laughton, 1981].

The southern Reykjanes Ridge axis is composed of seven offset, right-stepping segments that share several common characteristics. Each segment contains one to six volcanic systems along strike, which typically construct ridges that are 100-350 m high, 2-6 km wide, and 5-37 km long; these are the axial volcanic ridges originally described by [Searle and Laughton, 1981] and are similar to axial volcanic ridges on the northern Reykjanes described by Jacoby [1981]. The axial volcanic ridges that characterize these systems are the primary source of recent lavas. Each ridge segment is offset from its neighbors in a right-stepping sense; there are no left-stepping offsets. The axes of many volcanic ridges curve in a clockwise sense as their tips are approached, and as a result, these volcanic ridges appear S-shaped in plan view.

Although these characteristics are generally applicable to the southern Reykjanes, the axial valley morphology changes along strike. Progressing northward, the relief of the axial valley decreases, until it is replaced by a broad axial high north of 58°47'N. The following sections describe the segments and axial discontinuities of the southern Reykjanes, which are also summarized in Tables 1.1 and 1.2.

### *The 56°47'-56°55'N segment*

North of the Bight transform is a 15-km-long segment that contains a single volcanic system (Figure 1.4). This segment is bounded to the north by a 17-km-wide, right-stepping nontransform offset (NTO) at 56°55'N. The low-backscatter floor of this nontransform offset (NTO) contains an elongate extensional basin with a long axis oriented 060°. The neovolcanic zones of the spreading segments on either side of this NTO underlap by several kilometers. This NTO differs from the axial discontinuities on the northern MAR (Figure 1.3) in its greater offset and disruption of the axial valley's major boundary faults and is inferred to be a second-order discontinuity. The structural disruption evident at this NTO is probably sufficient to have generated an off-axis trace indicative of the migration history and age of the discontinuity, although our data do not extend far enough off axis to tell.

*The 56°55'-57°18'N segment*

North of the 56°55'N NTO is a 43-km-long segment that contains three volcanic systems separated by right-stepping offsets 3-4 km wide. The volcanic systems lie within a ~100-m-deep, 7-km-wide inner valley, which is defined by a series of discontinuous faults. The floor of the inner valley is flooded by lavas from the volcanic systems. The northern end of this segment occurs at about 57°18'N, where the neovolcanic zone is offset ~15 km to the east. Although the neovolcanic zone is not imaged between 57°15' and 57°20'N, this offset is inferred to be a segment boundary based on the disruption of the axial valley's western boundary faults, which make a series of right steps across several ~090° trending faults near 57°20'N. The 090° faults do not offset the NE trending faults, and are inferred to accommodate relative motion between the right-stepping normal faults here.

*The 57°18'-57°36'N segment*

The next segment to the north is inferred to contain at least two volcanic systems between 57°22' and 57°36'N. The volcanic systems are offset 4 km in a right-stepping sense and lie within an inner valley that is at least 7 km wide and bounded to the west by a 150-m fault scarp. The northern volcanic system is dominated by a flat-topped, cratered cone at its midpoint, with a pair of volcanic ridges that extend to the north and south. The cone is 2 km in diameter, displays 150 m of relief, and marks the shallowest point of the segment. The valley floor west of the neovolcanic zone is primarily a smooth-surfaced area that has been block faulted, although small patches of older, faulted constructional volcanic terrain are evident. The northern tip of this segment occurs at an ~18-km-wide right-stepping nontransform offset at 57°36'N, which is inferred to be a third-order axial discontinuity.

*The 57°36'-57°51'N segment*

The neovolcanic axis of the next segment to the north is marked by a single robust volcanic system which has constructed a ridge at least 26 km long (Figure 1.5). The ridge is S-shaped in plan view and displays 400-m vertical relief near its midpoint. Inward facing normal fault scarps laterally bound the ridge and mimic its S shape and define a 7-km-wide inner valley. The inner valley is completely filled by high backscatter lavas associated with the volcanic ridge. Faults located in the outer axial valley east and west of the volcanic axis strike ~005°, parallel to the trend of the axial volcanic ridge.

*The 57°51'N discontinuity*

The next axial discontinuity, at 57°51'N, is a 12-km-wide, right-stepping nontransform offset that separates ridge segments that overlap by ~2 km (Figure 1.5). Volcano-tectonic fabric at the tips of each segment bend inward toward the overlap zone, and many short fractures within the offset strike nearly parallel to the spreading direction. Within the overlap zone is a 2300-m-deep basin, which is part of a crustal block on the downthrown side of a major fault that marks the west side of the inner valley north of the offset.

This is a second-order discontinuity, evidenced by a wake of basins and fault scarps preserved to the west of the neovolcanic zone. Prominent faults northwest of the discontinuity exhibit the same sense of curvature as the segment's western inner boundary fault (Figure 1.5). The southern ends of these faults end abruptly northwest of the discontinuity. These faults define the western edges of several semienclosed basins, which are aligned roughly parallel to the flow line ( $\sim 275^\circ$ ) west of the offset. The basins represent the deep southern ends of fault blocks that are backtilted along the faults in the outer valley. These basins are structurally similar to the present overlap basin and are inferred to define the location of the discontinuity through time. Positive Bouguer gravity anomalies associated with these basins indicate that thin crust and/or high-density mantle underlies the overlap basin and its off-axis trace [Owens *et al.*, 1991], similar to the off-axis expression of long-lived nontransform offsets elsewhere on the MAR [Lin *et al.*, 1990; 1992]. The Brunhes-Matuyama reversal boundary and Anomaly 2 are offset 3 km right-laterally across the trace [Searle *et al.*, 1994].

The faults and basins of the western outer valley constitute discordant topography that extends  $\sim 20$  km west of the volcanic axis (measured parallel to the spreading azimuth). Given the  $\sim 1$  cm/yr half spreading rate, this discontinuity has persisted here for at least 2 m.y. without detectably migrating along axis. Owens *et al.* [1991] noted the absence of similar discordant topography east of the discontinuity, perhaps indicative of a long-lasting asymmetry in the structural expression of the offset.

#### *The 57°51'–58°12'N segment*

The segment north of the 57°51' NTO contains six volcanic systems, which are arranged in a right-stepping, *en echelon* pattern, separated by offsets of 2–3 km. The neovolcanic zone is bounded to the west by a single major (350–500 m high) fault scarp and to the east by a series of small-offset (50–100 m) inward facing faults. The volcanic systems at the south end of the segment form prominent ridges that display up to 300 m of vertical relief. In the northern part of this segment, volcanic systems display less relief, and the inner valley floor is marked by a series of fractures oriented parallel to the spreading direction. Although these fractures are pervasive between 58°08' and 58°12'N, they do not offset axial volcanic ridges or boundary faults. The northern end of this segment occurs at an 8-km-wide, right-stepping axial discontinuity at 58°12'N, coincident with a 005° trending fracture.

This discontinuity may represent a rare case where a transform fault has developed across a small axial discontinuity. However, the pattern of the 005° trending fractures within the northern part of this segment could represent an accommodation zone rather than a series of small transform faults. Accommodation zones elsewhere on slow spreading ridges have been inferred to occur where parts of the median valley that display distinctly different structural expressions are juxtaposed along strike [Karson and Rona, 1990]. Accommodation zones allow adjacent parts of the median valley to respond to extension independently, resulting in different structural styles and perhaps slightly different rates of extension. The 58°12'N area marks a discontinuity in

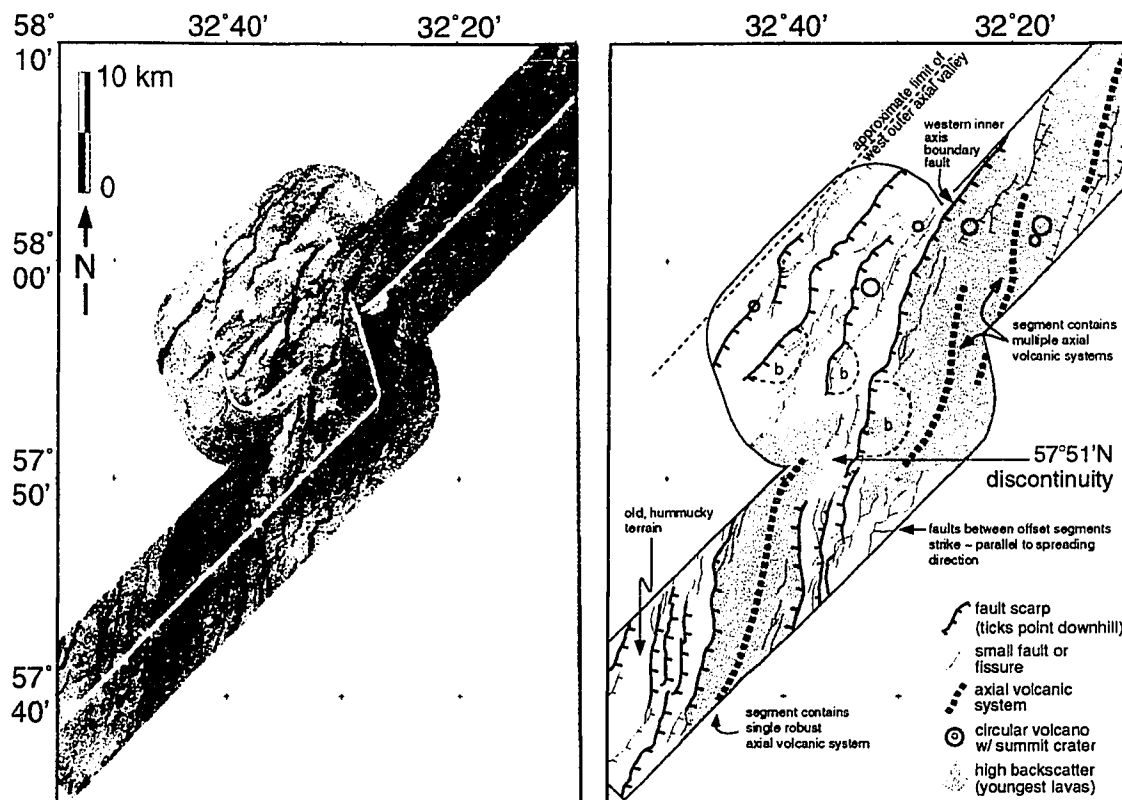


**Figure 1.5.** SeaMARC II side scan imagery and geological interpretation of the 57°51' nontransform offset. The neovolcanic zone is contained within an inner axial valley defined by inward-facing fault scarps. Three basins (marked "b") located west of the discontinuity occur at the southern ends of backtilted fault blocks and are inferred to mark the off-axis trace of the discontinuity. The western boundary of the axial valley is inferred to occur along the northwest edge of this image; the total width of the axial valley here is ~40 km, measured parallel to the spreading direction [Murton and Parson, 1991].

the structure of the inner axial valley boundary faults. The axial valley between 57°51'N and 58°12'N is asymmetric, with a single major fault bounding the west side of the inner axial valley and several smaller-relief faults scarps along the eastern side. This sense of asymmetry reverses at 58°12'N, where a single major fault scarp bounds the inner valley's east side.

*The 58°12'-58°26'N segment*

The segment north of the 58°12'N discontinuity is 26 km long and contains three volcanic systems that are offset from one another in a right-stepping sense. The middle volcanic system completely overlaps the northern one. Each volcanic system displays high backscatter indicative of recent lavas, although it is not possible to discern whether the ridges were volcanically active simultaneously, or whether one system has shut down and the other taken over. The northern system is composed of a circular, flat-topped, cratered volcano near its midpoint, with volcanic ridges that extend to the north and south in a manner similar to the volcanic system at 57°32'N. This segment overlaps the next segment to the north by 4 km at the 58°26'N discontinuity, a 7-km-wide right-stepping offset. At this discontinuity the overlapping ridge segments surround a corridor of low-backscatter seafloor that contains a pair of old circular volcanoes that each host summit craters.

*The 58°26'-58°47'N segment*

The next segment to the north is 39 km long and contains four volcanic systems. At the segment's southern end, the neovolcanic zone lies within a 6-km-wide inner valley defined by boundary faults 50-75 m high. The western boundary fault progressively decreases in relief to the north, and at the segment's northern end the inner axial valley is defined by a series of discontinuous, low relief (~25m) inward facing faults. The northern end of this segment occurs at 58°47'N and is marked by a pronounced axial depth maximum (Figure 1.2). At this discontinuity, both the volcanic axis and the inner valley's eastern boundary fault system are offset to the east by 7 km.

#### NORTHERN REYKJANES RIDGE

The regional bathymetry indicates that the general strike of the Reykjanes Ridge changes by ~5° at 59°00'N (Figure 1.1), which is also the approximate location of the transition from axial valley to central high observed in GLORIA imagery [Laughton *et al.*, 1979; Searle and Laughton, 1981]. Our data show that the fine-scale structure of the ridge axis changes at the 58°47'N discontinuity: north of this point axial volcanic systems occupy a topographic high; a deep axial valley does not exist, although inward facing faults continue to define the axial zone; and faults that define the axial zone are shorter and display lower relief than their counterparts to the south. Although our side scan data do not image the axis between 59°05'N - 59°20'N, the bathymetry indicates that a distinct structural boundary (such as a transform fault or major ridge-axis discontinuity) does not separate the northern and southern sections of the Reykjanes Ridge. The transition between rift valley and axial high is accommodated gradually by diminishing throw along axial boundary faults.

North of 58°47'N the neovolcanic zone contains a series of volcanic systems arranged in a right-stepping, en echelon pattern, separated by discontinuities 3-7 km wide. Despite this well-defined interval volcanic segmentation, larger-scale structural axial discontinuities (third- and second-order) are not clearly expressed on the northern Reykjanes. This may be due in part to the lack of major axial boundary faults that can be used as a measure of the degree of structural segmentation. However, the axial bathymetric profile (Figure 1.2) shows that axial volcanic systems group together to form intermediate-wavelength (15-65 km long) topographic highs having length scales similar to the second- and third-order segments on the southern Reykjanes Ridge. Adjacent intermediate-wavelength highs are separated by bathymetric maxima that occur at offsets between axial volcanic systems. Based on the axial bathymetry profile I have identified 12 intermediate-wavelength axial topographic highs, which contain between 1 and 10 individual axial volcanic systems (Table 1.1).

*The 58°47'-59°21'N segment*

A segment is inferred to occur between 58°47' and 59°21'N based on Hydrosweep bathymetry and available SeaMARC II data. The southernmost volcanic system within this segment consists of a prominent ridge 27 km long and 450 m high. High-backscatter lavas from the ridge are contained within a 5-km-wide graben constructed from small-offset (< 25 m), inward facing faults. Additional axial and off-axis bathymetry at 59°00'N (B. Murton et al., unpublished data, 1990) indicate that the 40-km-wide axial valley that was evident near 57°52'N is not present here; instead, axial volcanic systems lie on a broad topographic high.

*The 59°21'-60°00'N segment*

The next segment to the north illustrates the unique structure of the northern Reykjanes relative to the southern part of the ridge. Our widest coverage on the northern Reykjanes occurs between 59°40' and 60°10'N, where I surveyed a 30-km-wide area centered over the axial volcanic zone (Figure 1.6). Axial volcanic systems here are arranged en echelon on a topographic high. All adjacent volcanic systems overlap to some degree, in cases by more 50%. Axial volcanic ridges strike  $010^{\circ} \pm 5^{\circ}$  near their midpoints and curve in a clockwise sense as their tips are approached. The volcanic ridges range in length from 11 to 20 km, are 1 to 2.5 km wide, and display 150 to 350 m of relief, shoaling to 700 m depth.

Axial fault orientations mimic the trends of the volcanic systems and extend obliquely outward from the neovolcanic zone into older crust. At a distance of about 8 km from the volcanic axis (measured parallel to the spreading direction), most faults bend to approach the orientation of the Reykjanes Ridge and merge with fault systems on either side of the axis. The fault systems trend  $\sim 035^{\circ}$  (parallel to the trend of the Reykjanes Ridge axis), although individual fault azimuths vary. Another set of faults occurs about 15 km on either side of the axis. The outer fault systems also trend parallel to the Reykjanes Ridge trend and are composed of discontinuous faults that display strikes intermediate between the spreading-orthogonal and Reykjanes Ridge trends. Relief across the outer fault systems (up to 250 m) is greater than for the

**Table 1.1.** Spreading Segments of the Reykjanes Ridge

Segment Latitude	Segment ID	Length km	Volcanic Systems	Fourth- Order Offsets
55°50' - 56°08'	NMAR 1	33	≥ 1	?
56°08' - 59°29'	NMAR 2	39	3	2 no
56°29' - 56°40'	NMAR 3	20	1	0
56°40' - 56°47'	NMAR 4	13	1	0
56°47' - 56°55'	SRR 1	15	1	0
56°55' - 57°18'	SRR 2	43	3	2 rs
57°18' - 57°36'	SRR 3	33	2	1 rs
57°36' - 57°51'	SRR 4	28	1	0
57°51' - 58°12'	SRR 5	39	6	5 rs
58°12' - 58°26'	SRR 6	26	3	2 rs
58°26' - 58°47'	SRR 7	39	6	5 rs
58°47' - 59°21'	NRR 1	63	8	7 rs
59°21' - 60°00'	NRR 2	65	11	10 rs
60°00' - 60°28'	NRR 3	59	4	3 rs
60°28' - 60°48'	NRR 4	37	4	3 rs
60°48' - 60°59'	NRR 5	20	2	1 rs
60°59' - 61°07'	NRR 6	15	2	1 rs
61°07' - 61°30'	NRR 7	43	3	2 rs
61°30' - 61°56'	NRR 8	48	9	7 rs, 1 ls
61°56' - 62°05'	NRR 9	16	1	0
62°05' - 62°25'	NRR 10	37	7	6 rs
62°25' - 62°52'	NRR 11	50	8	7 rs

Segments are defined as parts of the spreading axis that are bounded at each end by first-through third-order axial discontinuities. The 22 segments are inferred from the axial structure revealed by side scan sonar imagery and bathymetry. Individual segments contain one or more volcanic systems separated by fourth-order discontinuities. Segment lengths are measured parallel to 005° (the spreading-normal direction). NMAR, northern Mid-Atlantic Ridge; SRR, south Reykjanes Ridge; NRR, north Reykjanes Ridge; no, no offset; rs, right-stepping offset; ls, left-stepping offset.

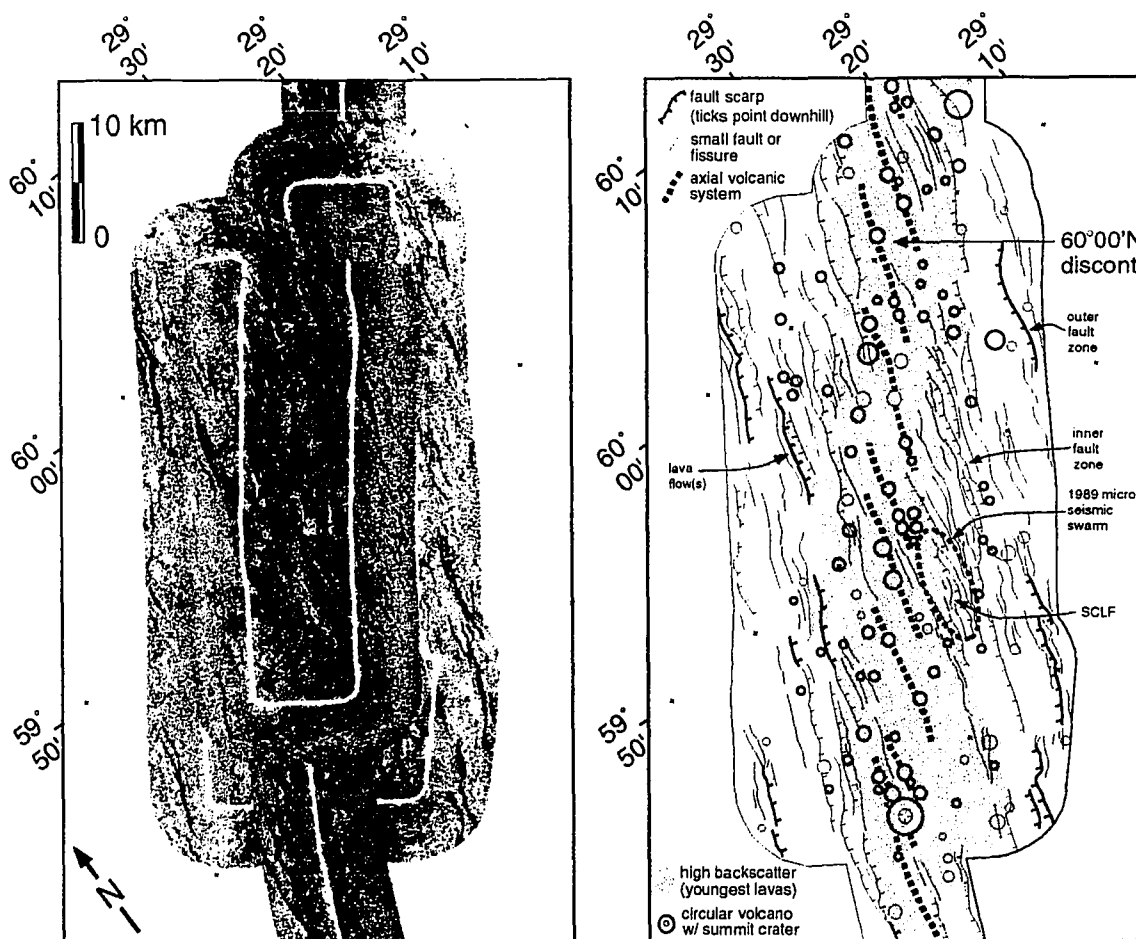


**Figure 1.6.** SeaMARC II side scan imagery and geological interpretation of the northern part of the 59°21'N-60°00'N segment. The neovolcanic axis contains several right-stepping volcanic systems that overlap by as much as 50%. Small-throw, inward facing normal faults form an inner fault zone that defines the boundaries of the axial zone. A second fault zone occurs farther outboard, which contains larger-throw faults. Despite the presence of the fault zones, an axial valley is not developed. Heavy dashed ellipse indicates region of sonobuoy-detected microseismic events of the 1989 swarm [Nishimura *et al.*, 1989]. The suspected coseismic lava flow within this region is marked (SCLF). The structural expression of the 60°N axial discontinuity (a depth maximum in Figure 1.2) is not significantly different from nearby intervolcano offsets. Bold circles represent volcanoes having aspect ratios < 2 and more than 50-m relief; fine circles indicate volcanoes with less than 50-m relief.

near-axis faults (up to 50 m). Out of 243 faults mapped in this area, all are inward facing except one.

This segment contains an anomalously high number of small circular volcanoes (Figure 1.7). Sixty-six individual volcanoes within and near the neovolcanic zone conform to the criteria of *Smith and Cann* [1990; 1992], which considers only individual volcanoes with plan view aspect ratios less than 2 that display at least 50 m of relief on all sides. Many smaller volcanoes are also present that do not meet these formal criteria. Most of the volcanoes occur along the crests or flanks of axial volcanic ridges. The few volcanoes that are evident outside the axial zone are inferred to be inactive, relatively old features because they are crosscut by faults and display low backscatter.

This segment was the site of a teleseismic earthquake swarm in May/June 1989 that was detected on both the World-Wide Standard Seismograph Network and Icelandic seismic network [Bergman and Solomon, 1990]. A subsequent sonobuoy deployment on June 13, 1989, recorded high microseismic activity (> 100 events) along the inner fault zone east of the axis near 59°48'N [Nishimura *et al.*, 1989]. A patch of high backscatter near the epicentral region of the microseismic swarm (Figure 1.6) led *Shor et al.* [1990] to suggest that the seismicity accompanied a volcanic eruption. Subsequent submersible observations indicated that no recent volcanic activity has occurred here [Crane *et al.*, 1992], and I infer the seismicity to have resulted from extensional tectonics rather than volcanic activity.

The northern terminus of this segment is defined largely on the basis of the axial bathymetry, which indicates a depth maximum near 60°00'N (Figure 1.2). This point corresponds with a ~5 km right step in the eastern inner fault zone (Figure 1.6). However, the degree of structural disruption at this discontinuity is much less than observed on the southern Reykjanes Ridge, and the amount of offset between the volcanic systems on either side of the boundary is similar in scale to intervalcano offsets within each of the segments.

#### *The NRR between 60°-63°N*

North of 60°05'N our side scan coverage is limited to a single 10-km swath along the spreading axis. The east edge of the axial neovolcanic zone is continuously imaged between 60°00' and 63°00'N, and in areas where the neovolcanic zone is narrower than 10 km (e.g., 60°55'N, 61°15'N, 61°35'N) the entire axis is evident. Figure 1.8 shows the axial region between 61°10' and 61°30'N, which exhibits characteristics that are representative of this part of the Reykjanes Ridge as a whole. Adjacent volcanic systems are separated by 5-6 km wide, right-stepping discontinuities, and their tips commonly overlap. Individual volcanic systems appear S-shaped in plan view and occur within shallow graben defined by low-relief inward facing faults that mimic the S-shape geometry of the ridges. Faults near the center of the neovolcanic zone strike ~010° and bend to new strikes of 020°-038° at a distance of about 3 km from the axis. Boundary faults oriented 036° are evident on the western side of the axis at ~61°15'N, indicating that this image covers nearly the full width of the axial zone.

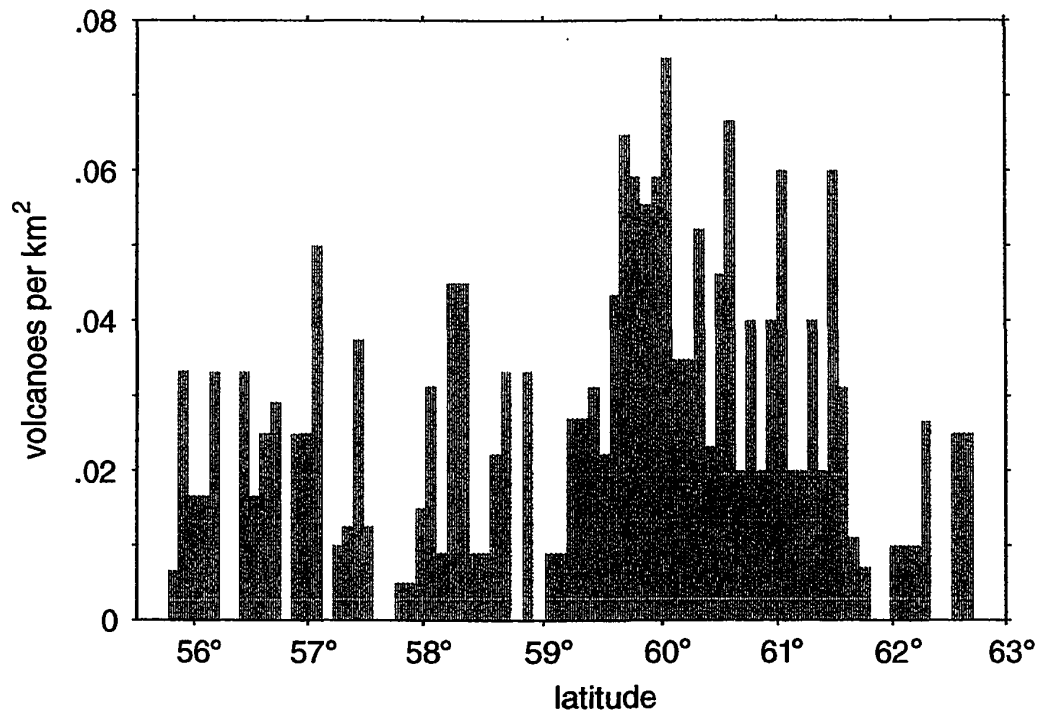


**Figure 1.7.** Distribution of circular volcanoes along axis, binned in intervals of 5 arc min of latitude. Volcanoes are defined as equant (aspect ratio  $<2$ ) features that display more than 50 m vertical relief, following *Smith and Cann* [1991]. These values have been normalized with respect to area. An anomalously high population of volcanoes occurs near 59°50'N.

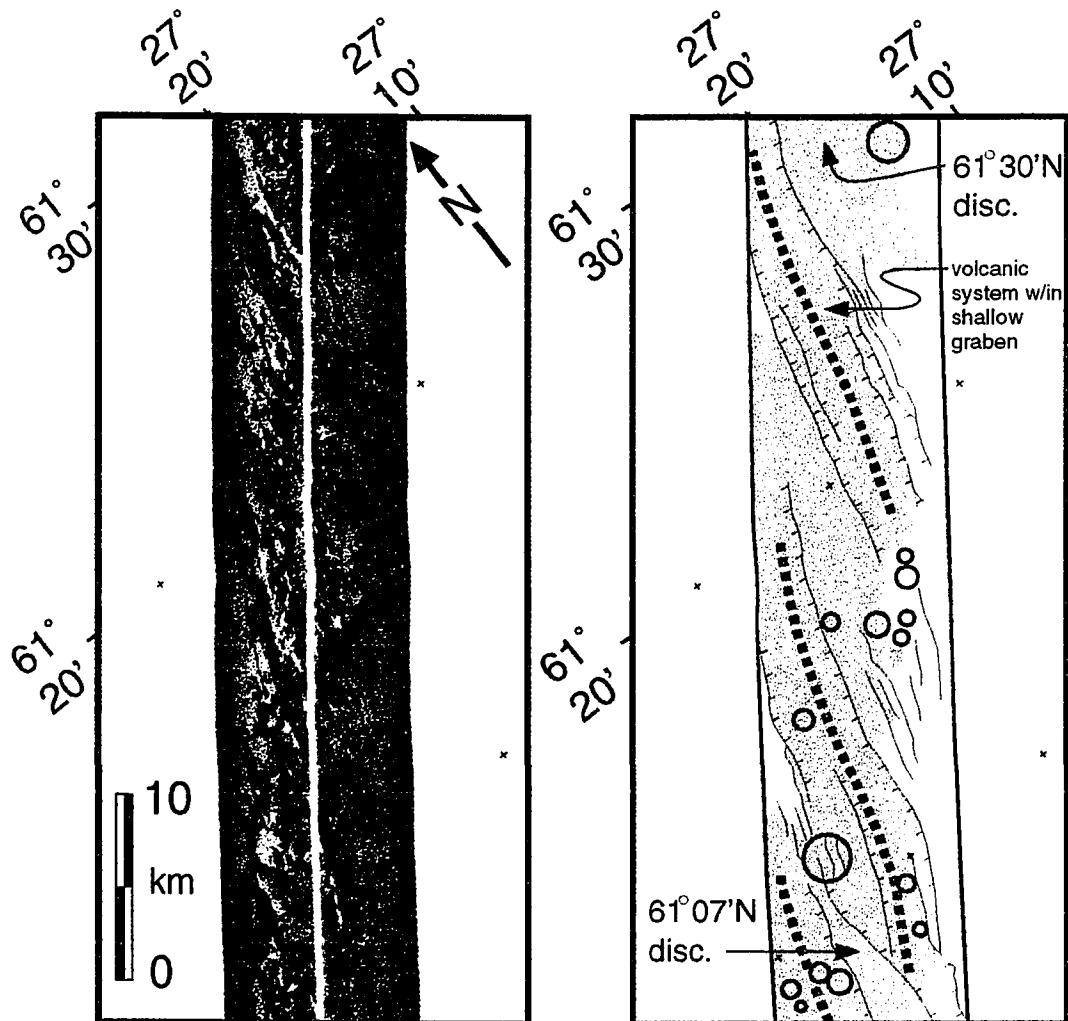


**Figure 1.8.** SeaMARC II side scan imagery and geological interpretation of the northern Reykjanes Ridge near 61°20'N. Axial volcanic systems exhibit S-shaped plan morphologies and lie within shallow graben. Axial faults strike parallel to the volcanic systems. The axial morphology expressed here is representative of the ridge axis structure north of 60°00'N.

## DISCUSSION

### *Spreading Center Segmentation*

At the smallest scale, the volcanic axis of the Reykjanes Ridge is segmented into discrete volcanic systems (fourth-order segments). The volcanic systems are dextrally offset from one another, with a mean offset of 5.4 km. Individual volcanic systems display 50-200 m vertical relief and range in length between 4 and 45 km. We identified 86 volcanic systems between 55°50'N and 63°00'N, although this may slightly underestimate the total number due to our incomplete coverage of the neovolcanic zone. These volcanic systems constitute the short-wavelength undulations evident on the axial topographic profile (Figure 1.2).

Axial volcanic systems are superimposed on intermediate-wavelength (13-65 km) axial highs that constitute third- and second-order spreading segments. Each segment contains between 1 and 11 volcanic systems, and adjacent segments are offset in a right-stepping sense by an average distance of 10 km (Table 1.2). On the northern MAR and southern Reykjanes Ridge, segments are separated by structural discontinuities that disrupt the axial valley boundary faults and correspond to axial depth maxima (Figure 1.2). These segments display 300-500 m vertical relief, comparable to segments on other parts of the MAR [Sempéré *et al.*, 1990; 1993]. On the northern Reykjanes Ridge, second- and third-order segments exhibit axial relief of only 200-300 m, which is more similar to the relief observed along the fast spreading East Pacific Rise than other slow spreading ridges [Bell and Buck, 1992]. Adjacent segments on the northern Reykjanes Ridge are separated by depth maxima (Figure 1.2), although the degree of structural discontinuity between adjacent segments is not as strongly developed as it is on the southern Reykjanes. For example, consider the segment boundary at 60°00'N. The axial profile indicates a depth maximum here between two intermediate-wavelength axial highs (Figure 1.2). However, the side scan imagery (Figure 1.6) shows that although several offset volcanic systems occur within the neovolcanic zone here, a distinctive structural discontinuity is not evident. Structural segmentation on the northern Reykjanes Ridge may be difficult to recognize largely due to the lack of significant axial valley boundary faults, which provide the standard measure for evaluating the scale of axial discontinuities on slow spreading ridges [Grindlay *et al.*, 1991; Macdonald *et al.*, 1991; Sempéré *et al.*, 1993]. These data suggest that segmentation on the northern Reykjanes Ridge is similar to that of the southern Reykjanes in some respects (length scales of second- and third-order segments, segments composed of multiple axial volcanic systems) while different in others (amplitude of axial relief, degree of inter-segment structural discontinuity).

At the largest scale, the ~1000-km-long Reykjanes Ridge is a first-order segment, with no transform faults between the Bight transform (56°47'N) and the point where the ridge emerges subaerially on Iceland's Reykjanes peninsula. The overall geometry and obliquity of the Reykjanes Ridge are enigmatic. Vogt and Avery [1974] proposed that prior to 40 Ma the plate boundary south of Iceland consisted of a series of short, orthogonal spreading segments separated by transform faults. Between 40 and 10 Ma a new rift propagated southwestward from

**Table 1.2. Segment Boundaries**

Discontinuity	Order	Offset km	Overlap
55°50'	2 (?)	~22 rs	~4
56°08'	3	5 rs	4
56°29'	3	5 ls	5
56°40'	3	8 rs	-10
56°47'	1	15 rs	-4
56°55'	2	17 rs	-7
57°18'	3	~15 rs	-15 <sup>a</sup>
57°36'	3 (?)	~18 rs	-9 <sup>a</sup>
57°51'	2	12 rs	1
58°12'	3	8 rs	0
58°26'	3	7 rs	3
58°47'	3	8 rs	-2
59°21'	3	5 rs	-3
60°00'	3	5 rs	8
60°28'	3	10 rs	7
60°48'	3	6 rs	1
60°59'	3	8 rs	3
61°07'	3	10 rs	2
61°30'	3	13 rs	-4
61°56'	3	9 rs	3
62°05'	3	11 rs	1
62°25'	3	8 rs	-1
62°52'	3	~4 rs	~2

Segment boundaries occur at first- through third-order axial discontinuities, which exhibit disrupted axial boundary faults and bathymetric maxima at spreading center offsets (following *Sempéré et al.* [1993]). The offset across a discontinuity is measured parallel to the spreading direction (~095°). rs, right-stepping offset; ls, left-stepping. Segment overlap at a discontinuity is measured perpendicular to the spreading direction (~005°), with negative overlap values indicating an along-strike gap between segments.

<sup>a</sup>Offset and overlap magnitudes are approximate due to incomplete sonar coverage.

the Iceland hotspot, which replaced the ridge-transform axial configuration with the linear, oblique spreading axis that has persisted ever since. *Vogt and Avery* [1974] suggested that the ridge's linear plan geometry and oblique orientation are maintained by subaxial asthenospheric flow moving southwest from the Iceland hotspot. This implies that the present configuration of the ridge results from structural control by the hotspot and that without the controlling influence of the hotspot the spreading axis might be differently oriented and might occur in a different location. This idea is compatible with geoid/topography data, which have been interpreted to indicate that the Reykjanes Ridge crest occurs east of a linear axis of shallow mantle upwelling [*Goslin and Aslanian*, 1992]. On other mid-ocean ridges this sort of shallow upwelling occurs directly beneath the spreading axis. These data suggest that the distance between the axis of shallow upwelling and the Reykjanes spreading axis increases from south to north, compatible with the model that the Iceland hotspot focuses spreading farther east than would occur otherwise. Other hotspots and off-axis volcanoes influence the position and morphology of spreading centers, for instance, near Axial Volcano on the Juan de Fuca Ridge [*Delaney et al.*, 1981; *Hammond and Delaney*, 1985], and on the East Pacific Rise (EPR) near 1°20'S [*Lonsdale*, 1989]. Therefore the location, strike, and gross axial structure of the northern Reykjanes spreading axis may all be heavily influenced by the presence of the Iceland hotspot.

The axial structure of the Reykjanes Ridge varies with proximity to Iceland, manifested by decreasing fault throw, intersegment structural discontinuity, and the change from axial valley to axial high near 59°00'N. The magnitude of axial relief and the degree of structural segmentation along ridge axes have been related to crustal thermal structure, with higher temperatures associated with lower relief and less structural discontinuity [*Bell and Buck*, 1992; *Sempéré et al.*, 1992; *Rabinowicz et al.*, 1993]. Elevated crustal temperatures may result from higher subjacent mantle temperatures [*Sempéré et al.*, 1992; *Rabinowicz et al.*, 1993] or thicker crust [*Bell and Buck*, 1992], either of which may be applicable near the Iceland hotspot [*RRISP Working Group*, 1980; *White et al.*, 1992; *Zhang and Tanimoto*, 1992]. The observed structural variation of the Reykjanes Ridge is compatible with these models, suggesting decreasing crustal temperatures with distance from the Iceland hotspot. The southern Reykjanes, which exhibits a different orientation and axial morphology than the northern Reykjanes, may represent a structural transition zone between the hotspot-dominated northern Reykjanes Ridge and the orthogonal MAR axis south of the Bight transform.

Structural segmentation of the slow spreading MAR is thought to reflect the degree of mantle upwelling and the along-axis distribution of magma [*Lin et al.*, 1990; *Sempéré et al.*, 1990; *Macdonald et al.*, 1991]. Axial depth variations that display wavelengths of 200-1000 km may be indicative of asthenospheric upwelling between first-order discontinuities, and along-strike variations in the pattern of upwelling may result in the segregation of discrete spreading segments along axis [*Crane*, 1985; *Schouten et al.*, 1985] separated by second- or third-order nontransform offsets. The axial structure of the Reykjanes Ridge may therefore provide clues to

the pattern of mantle upwelling beneath the ridge. *Parmentier and Phipps Morgan* [1990] suggest that the mode of mantle flow is dependent on spreading rate, with fast spreading ridges characterized by sheetlike upwelling, and slow spreading ridges by diapiric upwelling. *Bell and Buck* [1992] propose an alternate model in which diapiric upwelling occurs universally, with axial structure controlled by crustal temperature. Where axial crust is relatively cold (such as along slow spreading ridges), along-axis variations in crustal thickness that result from diapiric upwelling are quickly frozen into the crust and preserved, whereas along hot ridge axes (for instance, fast spreading ridges), ductile crustal flow occurs rapidly enough to even out differences in crustal thickness. The Reykjanes Ridge is unique because it is a slow spreading ridge that exhibits smooth intermediate-wavelength axial topography (similar to fast spreading ridges) along its northern part and high relief (more typical for of slow spreading ridges) along its southern section. The axial structure of the Reykjanes Ridge suggests two possibilities: (1) mantle upwelling changes from sheet like to diapiric at  $\sim 59^{\circ}00'N$ ; or (2) diapiric upwelling is ubiquitous but crustal temperature decreases away from the hotspot: north of  $\sim 59^{\circ}00'N$  the crust is hot and undergoes crustal flow, whereas south of  $\sim 59^{\circ}00'N$ , cold crustal temperatures prevent crustal flow and variations in crustal thickness that result from diapiric upwelling are preserved.

#### *Faulting*

We digitized fault traces observed in the side scan imagery to construct a histogram showing orientations of axial and near-axial faults along the northern MAR and Reykjanes Ridge (Figure 1.9a). On the northern MAR, fault azimuths are distributed nearly symmetrically about  $009^{\circ}$ . In contrast, Reykjanes Ridge faults exhibit a modal strike of  $\sim 020^{\circ}$ , which is intermediate between the spreading and spreading-orthogonal directions. Similar azimuthal distributions are displayed by axial volcanic systems (Figure 1.9b). Most axial volcanic systems strike closest to the spreading-orthogonal direction near their midpoints, yet even here most volcanic systems on the Reykjanes Ridge exhibit strikes that are oblique to the spreading-orthogonal direction.

The relationship between fault strike and stretching direction has been addressed in laboratory modeling of oblique extension [*Withjack and Jamison*, 1986; *Tron and Brun*, 1991]. Figure 1.11a shows experimentally derived fault orientations that result from stretching directions that vary from pure extension to pure strike slip. The value  $\alpha$  represents the angle between the stretching direction and the strike of the ridge crest, and  $q$  indicates the angle between faults and the stretching direction (Figure 1.11b). For the Reykjanes Ridge the stretching direction is  $095^{\circ}$  and the ridge strike is  $036^{\circ}$ , yielding  $\alpha \approx 60^{\circ}$ . The observed modal azimuths of axial faults and volcanic systems are each  $\sim 020^{\circ}$  (Figure 1.9), resulting in  $Q \approx 75^{\circ}$  (Figure 1.10, solid circle), and midpoint azimuths of axial volcanic systems range from  $61^{\circ} < Q < 97^{\circ}$  (Figure 1.10, bar). These values fall within the range of experimentally derived fault orientations. *Tron and Brun* [1991] found that the highest fault density occurs for stretching directions of  $45^{\circ} < \alpha < 60^{\circ}$ , and therefore the Reykjanes may experience more pervasive faulting than other parts of the MAR that spread at similar rates but are oriented more orthogonally to the spreading direction. Modeled faults that formed

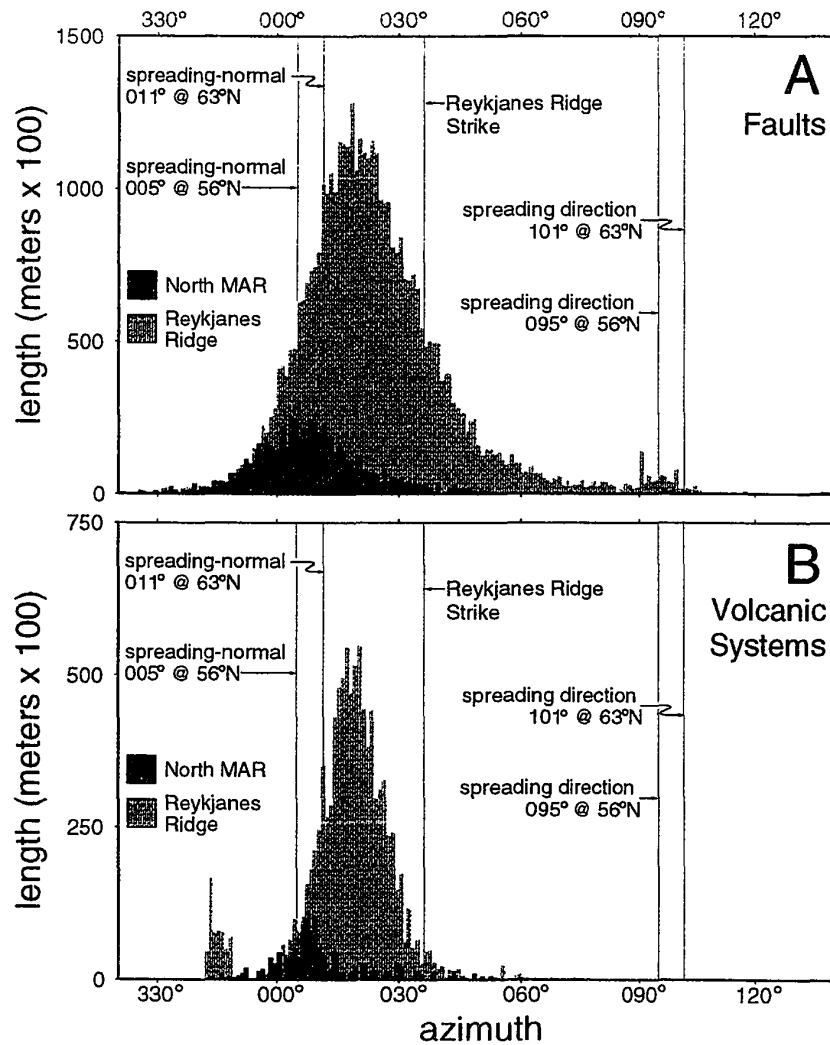


**Figure 1.9.** Frequency histograms showing strikes of (a) faults and (b) axial volcanic systems for the northern MAR and Reykjanes Ridges, digitized from SeaMARC II side scan images and binned at 1° intervals. For reference, the strike of the Reykjanes Ridge ( $\sim 036^\circ$ ) is shown, as are the spreading and spreading-orthogonal directions predicted by the NUVEL-1 plate model [DeMets *et al.*, 1990] for 56°N and 63°N. On the Reykjanes Ridge, the dominant strike of axial faults and volcanic systems ( $\sim 020^\circ$ ) is intermediate between the spreading-orthogonal and Reykjanes Ridge azimuths.

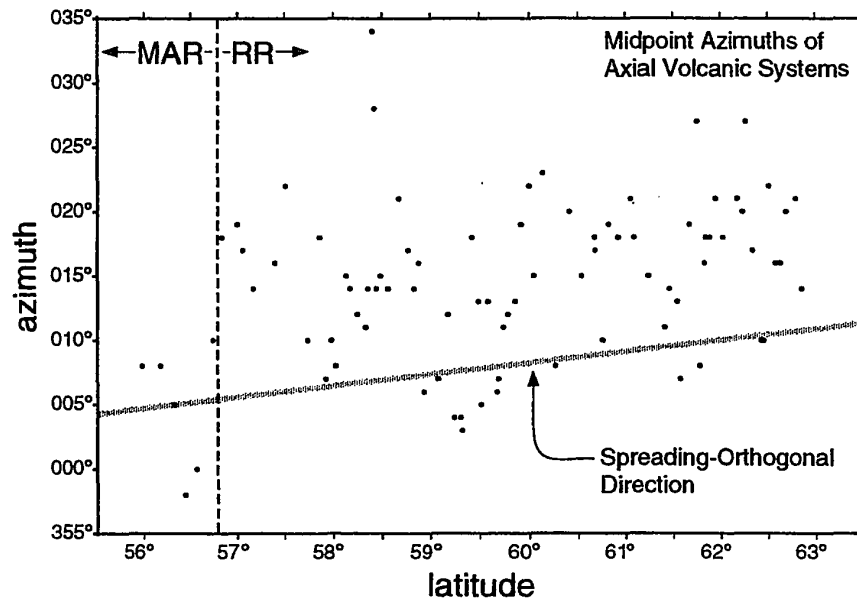


**Figure 1.10.** Orientation of axial volcanic systems plotted versus latitude. The strike of each volcanic system was measured at its midpoint. Heavy gray line shows the predicted spreading-orthogonal direction, calculated from *DeMets et al.* [1990]. Most volcanic systems on the Reykjanes Ridge exhibit midpoint strikes that are intermediate between the spreading and spreading-orthogonal directions.

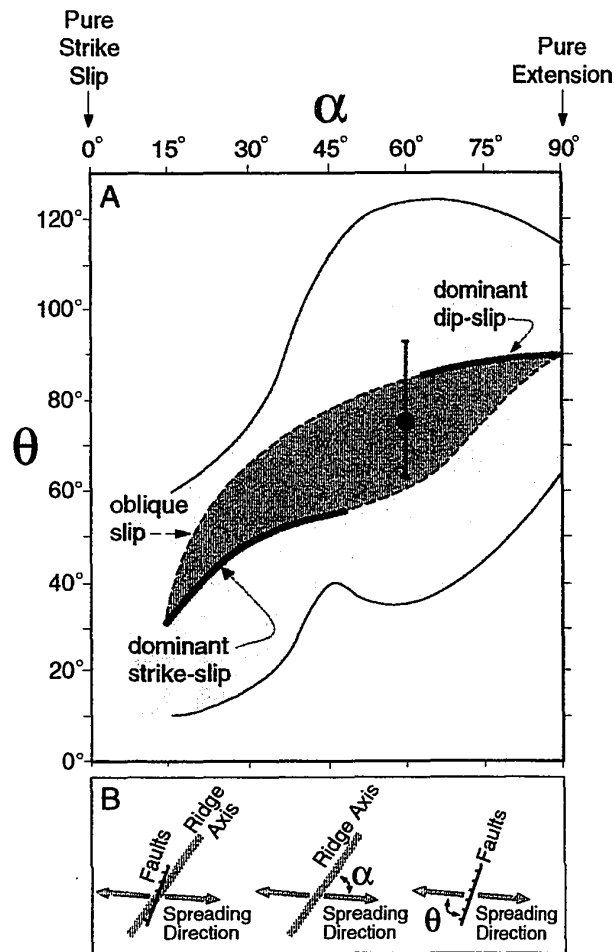


**Figure 1.11.** (a) Results from laboratory models of oblique extension [Tron and Brun, 1991] illustrating the range of fault orientations that result from different degrees of obliquity. (b) The angle between ridge axis and extension direction is given by  $\alpha$ , and the angle between the extension direction and the resulting faults is shown by  $\theta$ . For  $15^\circ < \alpha < 90^\circ$  the experimental fault distributions were bimodal, and the values between the observed bimodal peaks define the dark-shaded central region. The light shading represents the full range of fault orientations observed. For obliquely-extending regions, the dominant fault strike is not perpendicular to the extension direction. The Reykjanes Ridge is oriented  $036^\circ$ , and the local spreading direction is  $095^\circ$ , yielding  $\alpha \approx 60^\circ$ . The observed modal azimuths of axial faults and volcanic systems are each  $\sim 020^\circ$  (Figure 1.9), resulting in  $Q \approx 75^\circ$  (black circle), and midpoint azimuths of axial volcanic systems range from  $61^\circ < Q < 97^\circ$  (bar). The strikes of axial faults and volcanic systems on the Reykjanes Ridge are compatible with the azimuth predicted for obliquely-extending environments.

between  $45^\circ < \alpha < 60^\circ$  were also observed to display S-shaped plan geometries arranged en echelon, and exhibited dominantly dip-slip behavior near their midpoints and strike-slip behavior near their tips. This geometry is observed on the Reykjanes, and therefore the style of offset along the S-shaped axial faults may be similar as well. *Tron and Brun* [1991] suggest that faults within obliquely stretching environments never form perpendicular to the stretching direction, and in fact, the observed axial fault orientations on the Reykjanes Ridge agree well with experimentally derived values using the plate boundary configuration and spreading direction of the Reykjanes Ridge. Similar agreement is observed on the obliquely spreading Mohns Ridge near  $72^\circ 20' N$  [*Dauteuil and Brun*, 1993].

#### *Volcanism*

Volcanism along the spreading axes of both the Reykjanes Ridge and the northern MAR is largely confined to the axial volcanic systems that constitute fourth-order segments. Most volcanic systems construct elongate volcanic ridges that are oriented parallel to axial faults and fissures. At a smaller scale, these ridges appear to be constructed from mosaics of narrow fissure ridges, small cones, or both. Fissure ridges occur both along the flanks and on the crests of axial volcanic systems and may appear as either massive walls or as a series of aligned, coalesced volcanic mounds that give the ridge the appearance of narrowing and widening along strike. Assuming that the morphology of small volcanoes reflects the geometry of their eruptive vent system [*Batiza and Vanko*, 1983], the axial volcanic ridges probably erupted along fissures or closely spaced, aligned point sources. Axial volcanic systems are usually oriented parallel to axial fault and fissure systems, suggesting that the orientations of eruptive fissures are controlled by the same stress field as the axial fault systems. The ends of some volcanic systems terminate within fissure swarms, and some merge along strike with inward facing normal faults that define the axial valley, suggesting a common genesis. For the volcanic systems of the Reykjanes Ridge, *Parson et al.* [1993] suggest a cyclic pattern of volcanic construction and tectonic dismemberment to account for the observed morphology of volcanic systems, involving initial fissure eruptions, localized point source eruptions, and subsequent dismemberment by faulting. The structure of axial volcanic systems on the Reykjanes Ridge is similar in many ways to those observed elsewhere on the MAR [*Smith and Cann*, 1990; 1992; 1993; *Lawson et al.*, 1991], suggesting that the fundamental eruptive styles on these ridges are the same.

*Sempéré et al.* [1993] suggest that volcano-tectonic segmentation on the MAR may be associated with geochemical segmentation, if distinct upper mantle sources feed individual spreading segments. This sort of geochemical segmentation has been documented on the East Pacific Rise [*Langmuir et al.*, 1986]. The Reykjanes Ridge exhibits volcanic and structural segmentation, manifested by the echelon arrangement of individual volcanic systems, which reflects the ridge's obliquity to the spreading direction. An implication of this structural segmentation is that it provides a mechanism for the isolation of magmatic systems that are closely spaced along strike. If volcanic systems here are fed by magmatic point sources aligned along strike, then ascending

packages of magma located relatively close together along strike may be physically separated from one another as they rise through the crust. Volcanic systems and presumably their crustal plumbing systems are oriented nearly orthogonally to the spreading direction rather than parallel to the Reykjanes Ridge strike, and thus do not merge along strike. For example, the volcanic systems along the orthogonal northern MAR near 56°20'N (Figure 1.3) and the volcanic systems on the northern Reykjanes Ridge at 61°20'N (Figure 1.8) display similar lengths and spacing along strike, yet much different degrees of spatial isolation. In a study of 60 precisely located, closely spaced samples, *Johnson* [1992] observed no significant geochemical difference between lavas from two adjacent volcanic systems near 59°54'N and found that all of the lavas could be related by fractional crystallization of a similar parent source. Further studies at this level of detail are needed to determine whether this sort of intrasegment homogeneity is common and to document the degree of intersegment geochemical variation.

Isolated volcanic cones occur within the neovolcanic zone, although less frequently than axial volcanic ridges. Cones occur both independently from axial volcanic ridges as well as superimposed on them. The summits of individual cones display either sharp, pointed tops or flat tops with or without summit craters. Over most of the ridge crest these volcanoes occur at a rate of ~0.015-0.025/km<sup>2</sup>, although an anomalously large population of conical volcanoes occurs near 59°50'N, where these volcanoes occur at a rate of 0.05-0.06/km<sup>2</sup> (Figure 1.7). The large number of volcanic cones here may simply reflect the wider sonar coverage, although I have attempted to account for swath width by expressing the number of cones as a function of the area surveyed. The reason for so many individual volcanoes is not clear. The cones are distributed unevenly rather than being aligned in chains, indicating ephemeral magma sources. The presence of these cones near the transition between northern and southern Reykjanes is also intriguing, and I speculate that these cones may represent the distal end of hotspot/ridge crest interaction. These cones may be a manifestation of a subaxial pulse of mantle material away from the Iceland hotspot, such as those described by *Vogt* [1971] that are thought to have spawned wakes of diachronous topography on either side of the Reykjanes Ridge. One such time-transgressive topographic feature converges on the ridge axis at about 59°30'N [*Vogt*, 1986c]. If high seamount production results from the along-axis propagation of asthenospheric pulses from the Iceland hotspot, then the V-shaped wakes of basement topography may be zones of higher-than-normal seamount populations rather than continuous volcanic ridges.

#### *Tectonic Homogenization*

An important characteristic of the ridge is the absence of unbroken volcanic edifices preserved off-axis. Although our off-axis coverage is limited, I observe a consistent pattern at each location where data exist. Figure 1.5 shows that very little volcanic topography is evident to the west of the spreading axis near 58°00'N, despite the presence of volcanoes that display up to 400 m vertical relief within the neovolcanic zone. With the exception of a few isolated cones, the terrain off-axis consists of smooth surfaces offset by faults. The paucity of off-axis volcanic topography

is also evident on the northern Reykjanes Ridge around 59°50'N (Figure 1.6). Here the neovolcanic axis is marked by a continuous series of volcanic cones and ridges that display up to 500 m of vertical relief. Beyond ~6 km of the axis, however, large volcanic edifices are absent. The only volcanic features outside the axial zone are small circular volcanoes, most of which are faulted, or patches of hummocky volcanics that occur on the outboard side of inward facing fault scarps. Off-axis topographic relief varies by 100-200 m, usually in association with fault scarps. Similar characteristics are observed elsewhere on the southern and northern Reykjanes where our data extend off axis (e.g., 55°55'; 57°20'; 57°40'; 58°35'; 61°42'N).

The absence of volcanic topography outside the axial neovolcanic zone may be explained in two ways. Either modern volcanic processes are unlike those that occurred before about 0.5 Ma, or the observed morphology results from a steady state process that constructs volcanoes along the axis and summarily wipes them out before they can be transported off-axis. Burial of volcanic structures by sediments or flat-lying lava flows contributes to the smoothing of the surface with age, although burial alone is almost certainly not sufficient to swamp 200-500 m tall volcanic features within 0.5 Ma of the volcanic axis. The pelagic sedimentation rate here, although variable, averages 37 m/m.y. [Vogt, 1986d]. Several lava flows within our survey area are inferred to have erupted along the axial volcanic systems and flowed outward from the neovolcanic zone (Figure 1.6); however, voluminous flat-lying flows are relatively rare on the Reykjanes Ridge, and most volcanism elsewhere on the MAR forms volcanic cones or ridges rather than large sheet flows [Smith and Cann, 1992; 1993]. The explanation I prefer for the disappearance of volcanic features with age involves the tectonic dismemberment of volcanic edifices as they are transported off-axis by seafloor spreading, similar to the model proposed by Parson *et al.* [1993].

The side scan imagery presented above shows that extensive faulting occurs within the axial zone, with additional faulting concentrated along fault zones located ~8 and ~15 km on either side of the axis. Observations from deep-towed side scan sonar and submersible surveys indicate pervasive faulting of axial volcanic systems and show that axial volcanic features experience extensive tectonic deformation at an early age [Crane *et al.*, 1992; Parson *et al.*, 1993]. Our data indicate that this sort of rapid tectonic dismemberment of axial volcanic systems is ubiquitous along the entire Reykjanes Ridge. Significant destruction of major extrusive volcanic features must occur within a few kilometers of where the ridges formed, as demonstrated by the scarcity of volcanic ridges at a distance of 6-8 km from the axis. Additional faulting occurs along the bands of faults located 8 and 15 km off-axis, and volcanic features located within these zones are highly faulted, suggesting that they are being destroyed as they pass over the fault zones. These observations suggest that crust generated by the Reykjanes Ridge experiences an early history of intense, pervasive deformation by faulting. In contrast, intermediate-rate spreading centers such as the EPR near 23°00'N [Lewis, 1979] and Juan de Fuca ridge [Kappel and Ryan, 1986] are bordered by split volcanic ridges, indicating that at faster spreading rates either (1) axial faulting is not as

extensive, (2) magmatically robust periods swamp the effects of axial faulting, or (3) faster spreading rates allow axial volcanic ridges to escape the axial tectonic zone relatively unscathed.

#### *Fracture Zones*

Four fracture zones identified from satellite altimetry occur on either side of the southern Reykjanes Ridge [Müller and Roest, 1992]. If projected onto the ridge crest, the southern three fracture zones would intersect the ridge near axial discontinuities (Figure 1.2). The northern fracture zone intercepts the ridge near the axial rift valley/no rift valley transition, although it does not correspond with any modern axial discontinuity. Only one of the southern three offsets is a first-order discontinuity (the Bight transform) inferred to be long-lived and thus capable of generating a fracture zone. With the exception of the Bight, these fracture zones probably formed between 42 and 10 Ma, when the Reykjanes Ridge axis was a series of short spreading segments offset by transform faults [Vogt and Avery, 1974]. If so, these fracture zones probably do not extend onto the modern spreading axis, and their correspondence with small discontinuities is fortuitous. An alternative possibility is that small axial discontinuities have persisted at these locations, although magnetic anomalies around the Reykjanes younger than chron 5 are not offset. Additional off-axis bathymetry is needed to resolve the geometry and significance of these fracture zones.

#### CONCLUSIONS

SeaMARC II and Hydrosweep acoustic imagery and bathymetry of the spreading axis between 55°50'N and 63°00'N show that the northern Mid-Atlantic and Reykjanes Ridges are segmented seafloor spreading centers that exhibit structural morphologies that vary with proximity to the Iceland hotspot and with the degree of obliquity to the spreading direction. Our observations support several conclusions:

1. The northernmost MAR strikes 005° (perpendicular to the local spreading azimuth) and contains four third-order ridge segments within a fault-bounded axial valley at least 500 m deep. Segments are separated along strike by both right- and left-stepping axial discontinuities and contain one or more constituent axial volcanic systems.
2. The Bight transform fault at 56°47'N separates the spreading-orthogonal northern MAR from the spreading-oblique Reykjanes Ridge. This is the only transform fault located between 55°50'N and 63°00'N and probably generated the Bight Fracture Zone.
3. The axial morphology of the Reykjanes Ridge varies with proximity to Iceland. Axial valley depth, axial boundary fault throw, relief along the neovolcanic axis, and degree of intersegment structural discontinuity all decrease toward the north. A bend in the ridge axis at ~59°00'N corresponds to the point where the median valley is replaced by an axial high and loosely defines a boundary that separates the different structural provinces of the north and south Reykjanes Ridge.
4. The spreading axis between 55°50'N and 63°00'N is strongly segmented. At the smallest scale, the volcanic axis is segmented into individual volcanic systems 4-45 km long, which are

separated along strike by intervolcano gaps or offsets. These features are analogous to fourth-order spreading segments documented elsewhere on the MAR. Axial volcanic systems are superimposed on intermediate-wavelength (13-65 km) axial topographic highs that constitute third- or second-order spreading segments. Segment boundaries occur at axial depth maxima, which correspond to offsets in the volcanic axis. Axial relief and the degree of intersegment structural discontinuity decrease toward Iceland, which may reflect increasing crustal temperatures as the Iceland hotspot is approached.

5. The distribution of strikes of axial structures (faults and volcanic systems) on the Reykjanes Ridge is consistent with results from laboratory models of oblique extension that employed boundary conditions similar to those of the Reykjanes Ridge. Modeling also predicts that the S-shaped faults on the Reykjanes Ridge experience dip-slip motion near their midpoints and oblique-slip motion near their tips. Oblique extension across the Reykjanes Ridge may also account for the extreme segmentation of the ridge's volcanic axis.
6. Volcanism is generally confined to the volcanic systems that constitute fourth-order segments. Volcanic systems construct elongate axial ridges that are composed of superimposed and coalesced cones and fissure ridges. Isolated volcanic cones are less common, although an anomalously high population occurs around 59°50'N.
7. Despite the high relief of axial volcanoes, old volcanic topography is rarely observed beyond 6-8 km of the neovolcanic axis. This, in conjunction with the observed fault distribution, suggests that volcanic edifices are tectonically dismembered before they can be translated out of the axial zone by seafloor spreading.

## CHAPTER 2

## RAPID REORIENTATION OF A SLOW SEAFLOOR SPREADING CENTER: THE STRUCTURAL EVOLUTION OF KOLBEINSEY RIDGE SINCE 10 MA

## ABSTRACT

We use reprocessed aeromagnetic data to infer the tectonic evolution of the slow-spreading Kolbeinsey Ridge (KR) between 66.8°N and 70°N. The axial structure of the KR changed from being continuous to segmented following a counterclockwise reorientation of the spreading axis after anomaly 4, which resulted in the separation of the ridge into 4 segments. The subsequent structural evolution of the ridge involved the propagation and death of adjacent segments, the along-strike migration of axial discontinuities, asymmetric spreading, and lateral migration of segment axes that occurred via ultrafast propagation or synchronous ridge jumps. Two of the three original discontinuities still exist (the Spar Offset and an unnamed discontinuity at 68°43'N) and contain active north-directed propagators. We suggest that an ephemeral, catalytic change in plate motion triggered the axial reorientation at anomaly 4 time, which initiated the subsequent phase of ridge propagation and migration of nontransform offsets. As a result, the initial S-shaped geometry of the axis was replaced by orthogonal ridge segments separated by propagating nontransform offsets.

## INTRODUCTION

The Kolbeinsey Ridge (KR) is a 625 km long spreading center located north of Iceland, bounded by the Tjörnes Fracture Zone to the south and Jan Mayen Fracture Zone, a 220 km offset transform fault to the north (Figure 2.1). The KR is a slow-spreading ridge, characterized by a full spreading rate of ~2 cm/year that has remained steady since ~13 Ma [Vogt *et al.*, 1980]. The modern ridge axis is divided into three second-order discontinuities separated by large (> 30 km) right-stepping nontransform offsets. The segments generally strike perpendicular to the local extension direction, and are further divided by smaller axial discontinuities.

The KR has not always exhibited segmentation. Anomalies older than 4A are continuous, sinuous features that indicate the absence of axial discontinuities for the 15 million year period following the initiation of KR spreading [Vogt *et al.*, 1980]. Anomalies younger than anomaly 4A, however, are complexly disrupted. Vogt *et al.* [1980] suggested the disruption resulted from ephemeral fracture zones that form and anneal quickly, and noted that disruptions south of 69°N could have been produced by the passage of a propagating rift. However, the mechanism by which the initial segmentation of the KR occurred, and the events that produced the observed anomaly pattern, have remained unknown.

This paper describes a kinematic model for the evolution of the KR that accounts for the observed magnetic anomaly pattern. Our model, based on reprocessed aeromagnetic data,

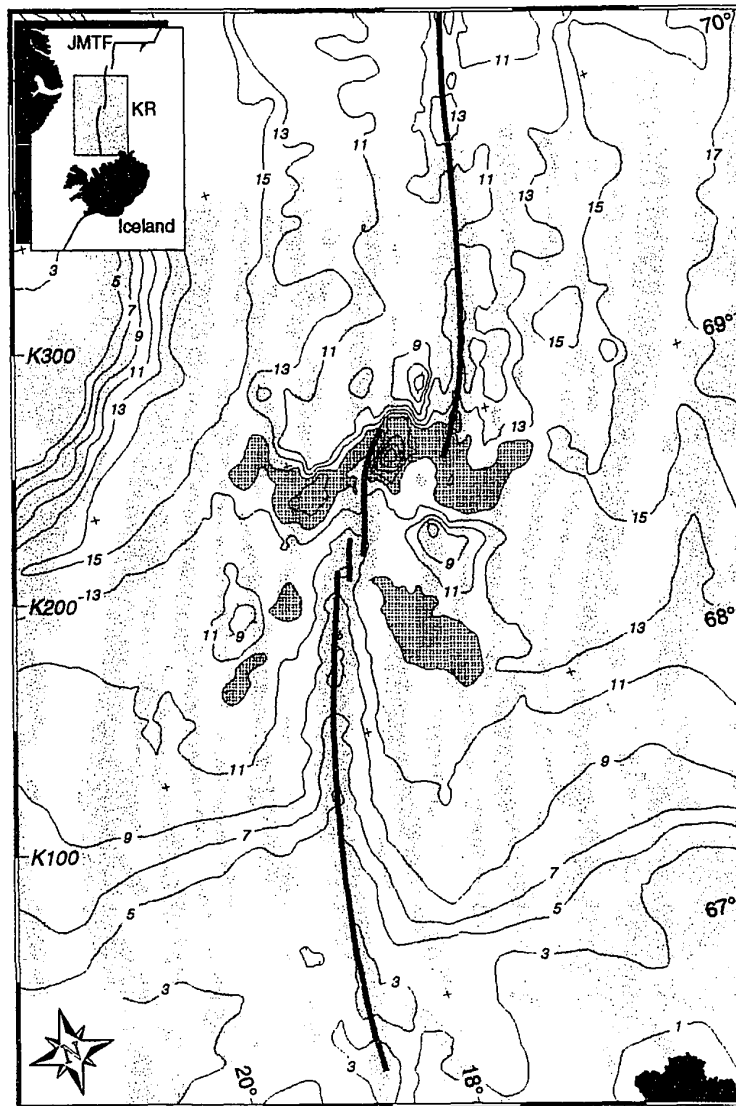


**Figure 2.1.** Bathymetry and magnetic anomalies of the southern and middle Kolbeinsey Ridge. This and following figures are oblique Mercator projections from the NUVEL-1 Eurasian/North American rotation pole [DeMets *et al.*, 1990], so the predicted extension direction is horizontal and the spreading-orthogonal direction is vertical. The spreading axis (bold line) is interrupted by two discontinuities, the 34 km wide Spar Offset at 69°N and the 10 km wide 68°43'N discontinuity. Positive magnetic anomalies are shaded. Bathymetry is NGDC trackline data and Sea Beam and SEAMAP swath data, contoured at 200 m intervals and annotated in hundreds of meters. Basins associated with the axial and off-axis trace of the Spar and 68°43'N offsets are shaded. Ticks on closed contours point downhill. Annotation on left side of map (e.g. K200) indicates distance in kilometers north of a reference point on the North American plate (67°N/22.2°W) used in the reconstruction in Figure 2.4. The outer basemap frame shows increments of 50 km north and east of this point; the interior frame shows latitude and longitude. Inset shows location; KR is Kolbeinsey Ridge, JMTF is Jan Mayen Transform Fault.

incorporates ridge propagation and concomitant along-strike migration of axial discontinuities as a fundamental component, and successfully reproduces many of the observed magnetic anomaly patterns. In addition to steady propagation, however, our reconstruction requires episodes of rapid lateral migration of the ridge axis that resulted from asymmetric spreading, fast propagation and synchronous lateral jumps.

## DATA

Our analysis is based on aeromagnetic data collected by the United States Naval Oceanographic Office in 1973 as part of Operation MAGNET [Vogt *et al.*, 1981; Vogt, 1986b; Vogt *et al.*, 1980]. In order to apply these data towards a detailed kinematic model, I corrected navigation errors in the original data set. Flight lines were flown using inertial navigation, and errors are manifested as mismatched anomaly patterns between sets of flight lines that individually are internally consistent. To correct for the observed mismatch between sets, I assumed that anomaly 5 on the west side of the ridge is a continuous, unbroken feature. This assumption is reasonable because each offset in anomaly 5 occurs between adjacent flight lines that show consistent mismatches across the survey area. Independent evidence for the continuity of Anomaly 5 is observed on the east side of the ridge, where the north half of the anomaly was imaged within a single set of flight lines.

We identified five coherent flight line sets, and eliminated the mismatch between them by shifting entire blocks of data along the path of the flight lines until offsets in anomaly 5 were eliminated. Three sets were held constant, and two were shifted 3.5 km to the northeast. In each instance where anomalies extend beyond the boundaries of shifted blocks, the along-strike continuity of the anomaly is restored. This method allows us to constrain relative positions in the across-axis direction, although it does not account for mismatch in the direction parallel to the anomaly pattern.

The corrected data are shown in Figure 2.2. This is a shaded-relief image of the residual magnetic field after removing the IGRF from total-field measurements, and accounting for diurnal variation. A surface was fit to the data, and the surface was artificially illuminated using a light source from the east. This presentation illustrates the continuity of peaks and troughs in the data, regardless of amplitude, more effectively than contour images. Anomaly peaks occur at the light/dark break between illuminated east-facing limbs and darkened west-facing limbs. This is an oblique Mercator map, projected from the present Eurasia - North America pole of rotation at 62.4°N/135.9°E [DeMets *et al.*, 1990]. This projection emphasizes the orientation of the ridge with respect to the spreading direction: flowlines or transform faults that follow small-circles about the Euler pole are oriented horizontally across the page. The vertical axis is the spreading-orthogonal direction. Corresponding bathymetry and a contour plot of the zero magnetic anomaly contour are shown in Figure 2.1.

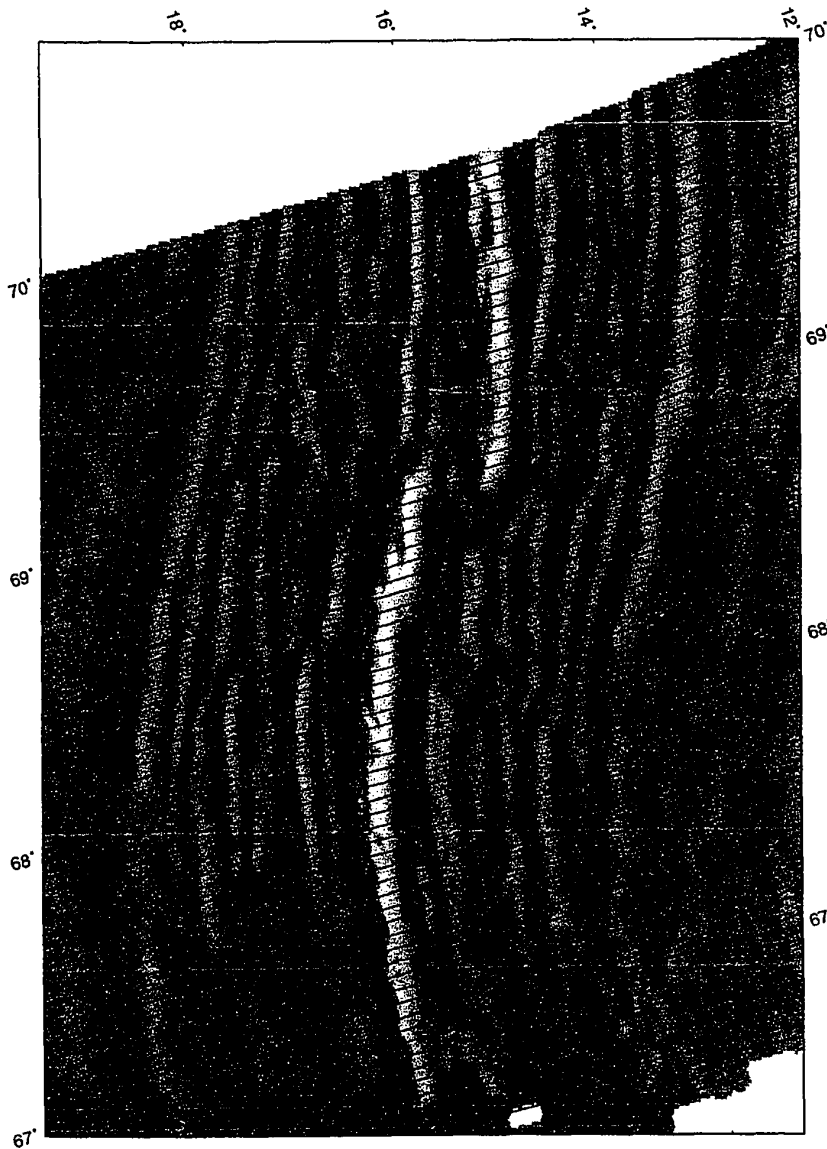


**Figure 2.2.** Shaded-relief image of residual magnetic field (total field - IGRF) from reprocessed aeromagnetic data. Data were gridded and fit with a surface that is illuminate from right to left such that the east flanks of positive anomalies appear bright. The linear anomaly fabric is disrupted by the off-axis wakes of the Spar and 68°43'N discontinuities. The wake of the 68°43'N offset exhibits the shape of an inverted "V", the Spar scar has a shape that more closely resembles the letter "W". Anomalies north off Spar Offset are irregular, discontinuous and difficult to correlate across the axis, and thus cannot be reconciled with simple spreading models. A reconstruction that accounts for the observed anomaly pattern is shown in Figure 2.4. Inset shows aeromagnetic coverage; line spacing is 5.5 km except southeast of 68.5°N/15°W, where spacing is 11 km.

## OBSERVED MAGNETIC FIELD AND INTERPRETATION OF ANOMALIES

The modern ridge axis is marked by a high-amplitude central anomaly that is offset 34 km at 69°N by the right-stepping Spar Offset, a nontransform axial discontinuity [Vogt *et al.*, 1980]. A second nontransform discontinuity occurs at 68°43'N, where the spreading axis is offset in a right lateral sense by 10 km. Zones of disrupted magnetic fabric extend off axis from each of these discontinuities. Magnetic anomalies are offset across these zones, which are characterized by 10-15 km wide swaths of attenuated magnetic amplitude (Figure 2.2), and occur within areas of deep seafloor (Figure 2.1). The disruption zones mark pseudofaults and corridors of transferred lithosphere that result from ridge propagation and the along-strike migration of axial discontinuities, and are used in a later section to reconstruct the histories of each of these offsets.

Our anomaly picks are shown in Figure 2.3. In the following discussion I abbreviate anomaly identifications according to anomaly number, supplemented where necessary with the side of the ridge where the anomaly originally formed (e.g. A4A-E indicates anomaly 4A, east of the axis). Positions of features discussed below are based on an orthogonal reference grid oriented with respect to theoretical flowlines, with distances expressed in kilometers (e.g. K-38) measured from a reference point southwest of Anomaly 5 on the North American plate (present coordinates 67.0°N/22.2°W).

Anomaly identification is straightforward in the southern part of the survey, and is not discussed further. The complexity of the anomaly pattern north of the Spar offset requires the following detailed explanations. North of 69°N the modern ridge axis is situated asymmetrically within A5, and anomaly stripes are discontinuous and oriented obliquely to the trend of A5. Anomalies west of the axis are typically more discontinuous than those to the east. To aid in the identification of these anomalies, I constructed a forward model based on extension rates measured between unambiguous anomaly picks south of 69°N.

Several significant relationships are revealed in the anomaly pattern. Three positive anomalies occur north of K-325 between A2A-W and A4-W (labeled X, Y, and Z in Figure 2.3), where only two anomalies are predicted (A3A-W and A3-W). To resolve the nature of these anomalies I look to the east side of the axis. Anomaly 3A-E can be traced southward to K-325, where it terminates. In general A3A-E is oriented ~5° counterclockwise to the trend of A5-E, although it curves in a clockwise direction near its southern tip. Anomaly 4-E is also discontinuous, but in this case the discontinuity occurs as a 50 km-long gap that coincides with the encroachment of A3A-E, and the tips of A4-E exhibit no curvature on either side of the gap. The absence of curvature indicates that the gap in A4-E did not result from an offset spreading axis; this inference is further supported by the continuity of A4-W. Forward modeling based on symmetric spreading indicates that anomaly X occurs at the predicted location for the A3A spreading axis. When A3A-E is rotated back to a position on the axis, it coincides with anomaly Y. Based on these observations, I suggest that anomaly X represents the position of the spreading center during early 3A time, and that later in 3A time the axis assumed a new position to the east.

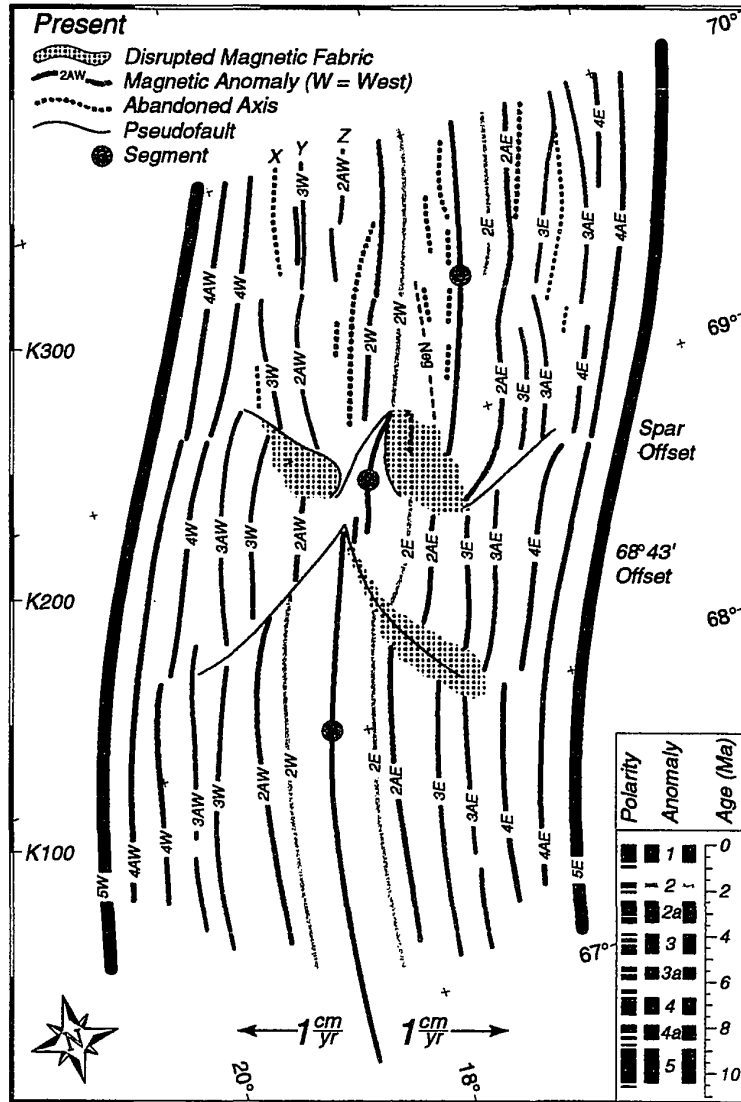


Figure 2.3. Anomaly picks and based on the magnetic field in Figure 2.2. Detailed explanation of structures are discussed in text. The lower left corner of the image occurs on a point on the North American plate that is used as a reference point on the panels in Figure 2.4. Basemap annotations show distance in kilometers from this point. Magnetic reversal scale is from Berggren *et al.* [1985].

The new axis was oriented oblique to the trend of the earlier spreading axis, and the easternmost part the new axis established itself within A4-E crust. The late-A3A spreading center generated anomalies Y and A3A-E.

Several observations indicate ridge reorganization occurred rapidly, and that the new spreading locus was established laterally away from the old spreading center without disrupting the magnetization of the crust between the old and new spreading centers. First, the distance between the old and new spreading centers is greater than can be accounted for by asymmetric spreading over the available time period, and the geometry of the anomalies requires that the A3A spreading axis was superimposed on A4-E crust. Second, crust between the old and new axes exhibits irregular magnetization rather than the uniformly magnetized crust expected from a steadily spreading asymmetric system. Third, a low-amplitude positive anomaly between anomalies X and Y exhibits the proper geometry to be a sliver of A4-E that was trapped between the old and new spreading centers and thus transferred to the North American plate. Within the resolution limits imposed by the magnetic reversal chronology, the new spreading center may have been established by either a synchronous lateral ridge jump or a fast southward propagation event. If the mechanism of emplacement was by southward propagation from 70°N, the minimum propagation rate required is 18 cm/year, which is nearly an order of magnitude faster than the full spreading rate.

Based on the foregoing interpretation, I identify anomaly Z as A3-W. Anomaly 3-W is divided into two sections, with the southern of the two offset west of the northern section. On the east side of the axis, A3-E is a broad positive anomaly that exhibits two peaks between K-325 that merge into a single peak north of K-380. The outermost of the two peaks exhibits the same sense of curvature as A3A-E, although the distance between the two anomalies increases towards the south. The observed geometry is indicative of asymmetric spreading that began after A3A and continued through A3 time, adding more crust to the Eurasian plate and resulting in the westward migration of the spreading axis. Reconstruction of the axis at A3 time indicates that A3-W and A3-E generally match, although the shapes of the anomalies differ. We speculate that this morphological disparity resulted from along-strike variations in the degree of spreading asymmetry.

Anomaly 2A is characterized by single- and double-peaked anomalies. North of K-280, A2A-W occurs as a doublet that merges into a single peak at K-360. Anomaly 2A-E exhibits the opposite structure, occurring as a doublet north of K-360 and a singlet to the south. We suggest that in the case of each doublet, the outboard peaks represent the initial position of the spreading axis, which migrated during A2A time to a position recorded by the inboard peaks. This indicates that during A2A time the southern part of this segment migrated towards the east while the northern part migrated west. The geometry of A2A could have been produced either by steady asymmetric spreading or a discrete lateral jump. However, I suggest that the presence of well-defined amplitude peaks observed on the doublets is indicative of a rapid lateral jump,

whereas asymmetric spreading would simply produce a broad anomaly stripe on the side of the axis where more crust is added.

Anomaly A2-W is continuous from the north edge of the survey area to K-275, and is parallel to A2A-W over this distance. Anomaly A2-E is similarly parallel to A2A-E, but can only be traced south to K-330, where it abuts the east flank of anomaly 1. Anomaly 1 occurs east of the symmetric axis between A2-E and A2-W, and is oriented  $\sim 7^\circ$  counterclockwise to the strike of A2-W. As a result, A1 exhibits progressively more asymmetry towards the south.

#### TECTONIC EVOLUTION OF KOLBEINSEY RIDGE SINCE ANOMALY 5

A kinematic reconstruction of KR is shown in Figure 2.4. This reconstruction was generated by rotating each anomaly pair back to the axis using a single Euler pole at  $62.4^\circ\text{N}/135.9^\circ\text{E}$  [DeMets *et al.*, 1990] and a constant full spreading rate of 2 cm/year [Vogt *et al.*, 1980]. Significant events in the evolution of KR are summed in Table 2.1.

At anomaly 5 time the KR axis is continuous albeit sinuous, curving eastward at K-200 and back northward at K-300. Although the continuous nature of Anomaly 5 was assumed as a boundary condition, older anomalies east of Anomaly 5 are continuous as well [Vogt *et al.*, 1980], indicating that there were no preexisting axial discontinuities that could have been inherited by the ridge. At A4A time the ridge exhibits the same sinuosity, although a right-stepping offset (offset A) develops at K-265 km. This offset is the incipient Spar Offset. By the end of A4 time a second offset (offset B) appears at K-169 km, which will develop into the  $68^\circ 43'\text{N}$  discontinuity. We infer that these two offsets were nontransform discontinuities due to their small scale ( $< 5$  km offset), by analogy with similar scale discontinuities on modern slow spreading centers [Grindlay *et al.*, 1991; Sempéré *et al.*, 1990].

The broad, S-shaped morphology of the ridge changed dramatically after A4. By the end of A3A the axis separated into four segments (Figure 2.4), each oriented counterclockwise relative to the preexisting axis. The degree of rotation decreases to the south such that segment 4 exhibits the greatest change in strike and segment 1 the least. On segment 4, reorientation was manifested by the eastward displacement of the axis, and the early A3A axis was abandoned. Relict early-A3A axes also occur on segment 3, evident as the outboard peak of the doublet on the south part of A3A-W and a short isolated positive anomaly on the northeast side of A3A-E. Based on the timing inferred for the eastward jump of segment 4, the clockwise orientation appears to have occurred completely within A3A time, a period of  $< 540$  ka. The clockwise reorientation resulted in the widening of offsets A and B, and spawned a new right-stepping discontinuity (offset C) at 335 km.

Immediately following the ridge reorientation, the tips of neighboring segments overlapped. This is especially evident on either side of offsets A and B, where the restored A3A anomalies overlap by 12 and 24 km, respectively. The observed anomaly pattern could have been produced either by synchronous asymmetric spreading at the tips of the overlapping segments or by short-

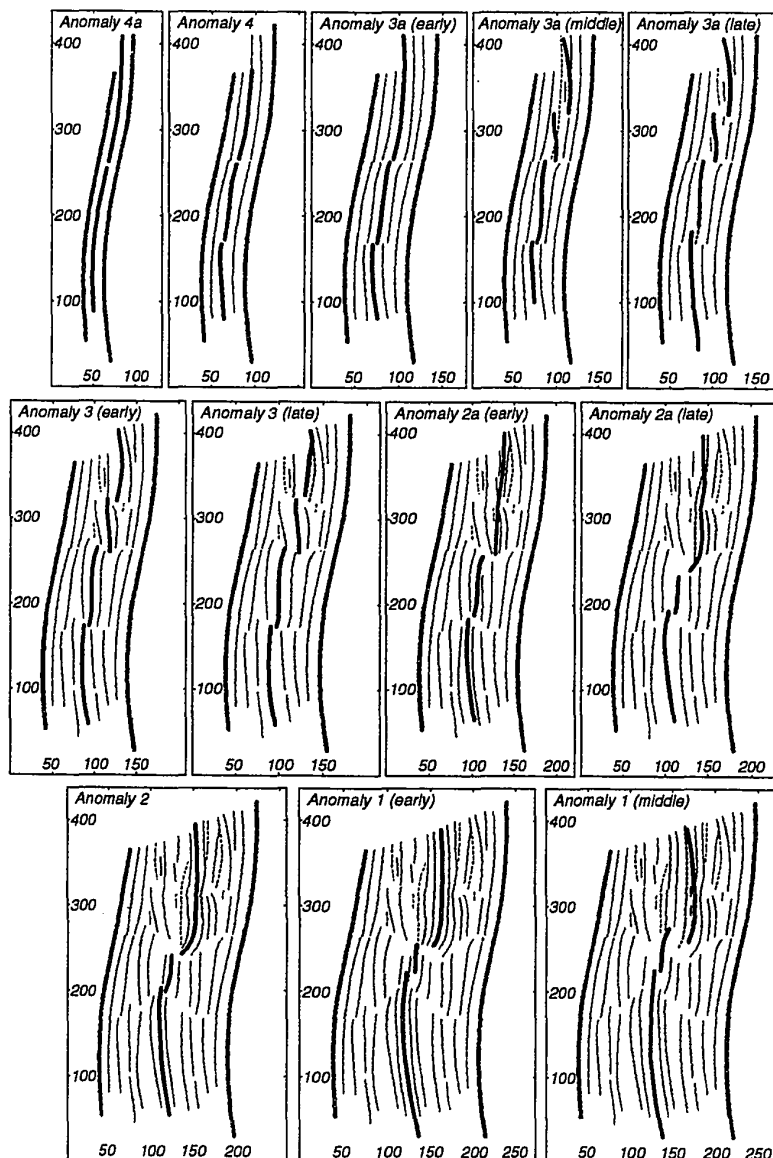


**Figure 2.4.** Tectonic reconstruction of KR. Detailed explanation of structures and events are discussed in text and summarized in Tables 2.1 and 2.2. In the reconstruction panels, the active spreading axis is a bold black line, positive magnetic anomalies are gray, and abandoned spreading axes are dashed. The lower left corner of each panel is centered on a reference point on the present North American plate at  $67^{\circ}\text{N}/22.2^{\circ}\text{W}$ . Basemap annotations show distances in kilometers from this point.

Table 2.1. Chronology of events on KolbeinseyRidge based on reconstruction shown in Figure 2.4.

Anomaly	Event
5	Continuous, sinuous ridge axis.
4a	Initiation of right-stepping offset A (proto-Spar).
4	Initiation of right-stepping offset B.
3a	Counterclockwise reorientation of ridge segments. New segment 4 is established ~12 km east of the prior axis by either ridge jump or ultrafast propagation. Initiation of right-stepping offset C. Duelling ridge tips at offsets A and B.
3	Growth of segment 3 by northward propagation at offset C and southward propagation at offset A. Eastward migration of segment 3 by asymmetric spreading. Continued duelling at offset B.
2a	Segments 3 and 4 merge, eliminating offset C. Segment 3' propagates to its southernmost limit. Segment 1 propagates north.
2	No net migration of nontransform offset A. Segment 1 propagates north.
1	Faster northward propagation of segment 1. Segment 2 propagates north. Segment 3' migrates east by either a ridge jump or ultrafast propagation.

lived dueling propagation. Alternatively, the segments could have experienced symmetric spreading that decreased towards their tips.

By A3 time the amount of overlap at each discontinuity had diminished. Offset B occurs at K-172, north of its A4 position, which constitutes the beginning of the steady northward propagation of segment 1. By the end of A3 segment 3 was located east of the axis of symmetry defined by the A3A anomalies, indicative of a period of asymmetric spreading that added crust more quickly to the North American plate. Segment 4 experienced the opposite sense of asymmetric spreading, moving the axis towards the west. Segment 3 propagated south over this period, resulting in the migration of offset A to K-260. Offset C remained stable at K-325.

Another period of rapid ridge reorganization occurred between A3 and A2A. By the end of A2A segment 1 propagated northward to K-185, and segment 3 propagated south to K-238. Over this period segments 3 and 4 merged into a continuous segment (segment 3'), thus eliminating offset C. The merger was accommodated by the continued eastward migration of segment 3 and westward migration of segment 4. Migration continued throughout A2A time following closure of offset C, resulting in the bifurcation of A2A-E and A2A-W at K-350. The eastward migration of segment 3 has the added effect of widening offset A. This, in concert with the southward propagation of segment 3, resulted in the transferal of a wide swath of lithosphere from the Eurasian plate to the North American plate. The swath of transferred lithosphere is expressed in the observed magnetic field as the corridor of disrupted magnetic fabric that extends northwest from the northwest part of modern segment 2 (Figure 2.2).

By the end of A2 segment 3' was oriented orthogonally to the spreading direction. We infer that the A2 axis extended as far south as the A2A axis (K-238) based on the anomaly pattern south of the Spar Offset, and speculate that the strike of the A2 axis was parallel to A2A-E. Although offset A did not migrate along strike between A2A and A2, acoustic imagery of Spar Offset reveals no evidence for a fossil transform fault here. Segment 1 continued its northward propagation between A2A and A2, resulting in the northward migration of offset B and progressive decrease in length of segment 2.

Between anomaly 2 and the present, segment 1 has continued propagating northward, and the propagator tip is currently located at K-238 (68°43'N). The northern tip of the present segment 1 spreading axis is located asymmetrically between the A2A anomalies, and that A2 is absent west of segment 2. These observations can be accounted for by the northward propagation of segment 1 into crust older than A2-W, resulting in this crust being transferred to the Eurasian plate.

Following its brief period of stability, the Spar Offset reversed its migration direction in response to the northward propagation of segment 2 that began after A2. In its present configuration, the northern tip of segment 2 abuts A2W. The outer pseudofault of segment 2 intersects A2A-W, indicating that the southern tips of A2A-W and A2-W have been incorporated into the offset zone between segments 2 and 3'. A short positive anomaly located east of the segment 2 tip is interpreted to be part of the southern tip of A2-W thus translated to the east. The

northward propagation of segment 2 has left a wake of disrupted magnetic fabric that trends southeast from the north tip of segment 2 through the interior of Spar Offset, and extends to the southern tip of A2A-E.

North of Spar Offset, the spreading axis underwent a  $\sim 7^\circ$  counterclockwise reorientation following anomaly 2. A series of discontinuous, low-amplitude positive anomalies occur between the modern axis and A2-W, which are coincident with the predicted position of the spreading axis at 500 ka assuming symmetric spreading. We interpret these low-amplitude anomalies to mark the site of the abandoned early-Bruhnes spreading center, indicating that the reorientation of the axis began later than 730 ka. Anomaly 1 crosscuts A2-E at K-330, indicating the ridge reorientation occurred either by a lateral jump or a fast southward propagation event rather than by asymmetric spreading. An oblique, negative anomaly that converges on the south tip of segment 3' may mark the inner pseudofault of a southward propagator; however, anomalies between the modern axis and A2-W are not well organized, and the modern axis may be superimposed on A2-W crust.

#### INITIAL SEGMENTATION AND SUBSEQUENT MIGRATION OF DISCONTINUITIES ON KR

Although segmentation of KR first occurred with the birth of offsets A and B at A4A and A4 time, the most significant segmentation event was the clockwise reorientation at A3A time. In addition to increasing the offset across existing discontinuities, this event spawned a new offset and marked the beginning of a phase of ridge propagation and offset migration that has continued to the present. Why did the KR, which had been devoid of discontinuities since its inception, suddenly exhibit segmentation?

One explanation is that the segmentation and  $5^\circ$  reorientation occurred in response to a change in relative motion between the North American and Eurasian plates. On other slow, intermediate and fast spreading ridges, changes in opening direction as small as  $2^\circ$  have triggered ridge reorientation, small-scale segmentation and subsequent offset migration [Hey and Wilson, 1982; Wilson et al., 1984; Carbotte et al., 1991; Sloan and Patriat, 1992; Cormier and Macdonald, 1994; ; Lonsdale, 1994]. The obliquity of the new segments did not persist, and by A2A the segment axes all exhibited strikes oriented either orthogonal or slightly clockwise to the present NAM-EUR pole of rotation. This indicates that a change in spreading direction was a transient event. An alternative is that increased magmatic vigor, perhaps due to the arrival of a pulse of upwelling mantle at the head of a Raleigh-Taylor instability, resulted in the realignment and growth of a segment. However, the synchronous initiation of several small segments and reorientation of the axial strike is difficult to reconcile with this model.

Following the segmentation event, the KR abandoned the broad, S-shaped regional morphology of the pre-A4A axis and assumed a geometry characterized by spreading-orthogonal segments separated by axial discontinuities. We speculate that the segmentation event provided a means for replacing the unstable, oblique section of the ridge axis with an orthogonal, minimum-energy configuration [Lachenbruch and Thompson, 1972; Oldenburg and Brune, 1975]. In

support I note that the present position of Spar Offset coincides with the point of maximum obliquity of the pre-A4A axis, and that the proto-Spar offset did not migrate far to the north or south. However, it is not clear why the axis would spontaneously break into so many small segments over such a short period of time. Therefore I prefer a scenario involving a brief local perturbation, probably related to an ephemeral, 5° clockwise change in the spreading direction, to initiate the realignment of the spreading axis; once segmented the ridge was physically disinclined to reassume its original sinuous geometry.

Several observations bear on the causes of along-strike migration of axial discontinuities that followed the segmentation event. Average migration rates of KR discontinuities range from 1.0 cm/yr to 2.3 cm/yr (Table 2.2), and the closely-spaced discontinuities have periodically migrated in opposite directions. We therefore consider unlikely a systematic regional driving mechanism, such as the absolute motion of the plate boundary relative to an asthenospheric reference frame inferred for the MAR at 24°-30°N and 47°-51°N [Schouten *et al.*, 1987], where nontransform offsets consistently exhibit similar migration directions over periods ~ 5 m.y. at rates ranging from 0.27 to 0.35 cm/yr. Given the location of the KR between the Iceland and Jan Mayen hotspots, a reasonable alternate driving mechanism is sub-axial asthenospheric flow away from mantle plumes. South of Iceland, asthenospheric flow is thought to control the morphology of Reykjanes Ridge [Vogt, 1971; Schilling, 1973; Vogt and Johnson, 1973; Searle and Laughton, 1981], The structural dissimilarity between KR and Reykjanes Ridge, however, suggest different relationships between the spreading ridges to the hotspots. In a regional sense Reykjanes Ridge is linear, continuous, oriented 30° oblique to the extension direction, and merges along strike with the South Iceland Volcanic Zone. In contrast, KR is oriented orthogonally to the extension direction, the southern KR is separated from the northern Iceland volcanic axis by the ~100 km-wide Tjörnes Fracture Zone [Sæmundsson, 1974], and the middle KR (segment 3') is offset from the plume-dominated northern KR by the 36 km wide Eggvin Offset. Geochemical evidence is also inconsistent with lateral asthenospheric flow under KR. On the southern KR, Pb isotope values indicate there is no Iceland plume component in KR magmatism, implying the absence of northward-directed plume flow beneath KR [Mertz *et al.*, 1991; Schilling, 1986]. North of Spar Offset, Schilling [1973] used La/Sm ratios to divide KR basalts into "normal" and "plume" groups across a boundary that coincides with the Eggvin offset, suggesting that Jan Mayen plume material is not flowing southward toward segment 3'.

The northward propagation of segment 1 may be driven by gravitational spreading forces associated with the positive relief of the southern KR. Spreading forces are proportional to the across-axis slope of the seafloor, and therefore the net force acting on a plate is proportional to the difference between axial and off-axis depths [Phipps Morgan and Parmentier, 1985]. On the southern KR the spreading axis occupies a 30-40 km wide ridge that exhibits ~ 500 m vertical relief (Figure 2.1) and average across-axis bathymetric slopes of 20-30 m/km. This range in slope is similar to those of the 95.5°W and Easter propagators, which exhibit across-axis slopes of

Table 2.2. Propagation rates of segments 1, 2 and 3. Reversal boundaries younger than 5.23 Ma are astronomically-calibrated values from Hilgen (1991); older boundaries are from Berggren et al. (1985).

Segment	Propagation	Time Interval	Rate (km Ma <sup>-1</sup> )
	Direction	Distance	
Segment 1: (North)		End A4 † Present	10.3
		K -169 † K - 238	
		End A4 † End A3	02.8
		K -169 † K -176	
		End A3 † End A2	12.1
Segment 1: (North)		K -176 † K -205	
		End A2 † Present	18.5
		K -205 † K - 238	
Segment 2 (South)		End A3A † End A2A	10.6
		K -267 † K - 238	
Segment 3 (North)		End A2 † Present	21.4
		K -238 † K - 276	

< 28 m/km and < 16 m/km, respectively [Hey *et al.*, 1989; Phipps Morgan and Parmentier, 1985]. Interestingly, segment 1 exhibits a maximum slope of ~35 m/km at 68°30'N, near the propagator tip. Other propagating rifts exhibit decreasing depth gradients with proximity to the propagator tip, and the increase observed near the 68°43'N propagator may be related to the rapid post-A2 northward advance of this ridge inferred from the anomaly pattern.

In contrast, segment 3' exhibits a much flatter across-axis slope (Figure 2.1) characterized by gradients of < 10 m/km, and gravitational spreading stresses are less likely to have contributed to propagation events around Spar Offset. Despite the long and almost continuous history of propagation at Spar Offset, the discontinuity is today located at nearly the same spot as the original proto-Spar, which corresponds to the region of greatest obliquity of the A5 spreading axis. We suggest that post-A3A propagation at the Spar Offset occurred as a means for establishing an energetically favorable ridge geometry. Over shorter spatial and time scales, near-field stresses related to magmatic forcing associated with the variation in melt supply through time [Pockalny and Gente, 1992; Sloan and Patriat, 1992] may have contributed to the growth and retreat of the neighboring segments. Thus propagation around Spar Offset may have been modulated by waxing and waning melt supplies, perhaps associated with the arrival and dissipation of mantle upwelling events.

## CONCLUSIONS

A significant implication of the inferred structural evolution of the KR is the reorganization of the axis into orthogonal segments following the A3A reorientation. We suggest that an ephemeral, catalytic change in plate motion triggered the axial reorientation, which initiated the subsequent large-scale dueling at Spar Offset and persistent northward propagation of segment 1. Elongation of segment 1 away from Iceland may be driven by gravitational stresses rather than asthenospheric flow, whereas the propagators at Spar Offset were more likely controlled by the position and magmatic input of subjacent mantle upwelling zones. In addition to these inferences, our reconstruction supports the following conclusions:

1. The KR axis was a sinuous but essentially continuous feature for 15 Ma after spreading initiated, until the first axial discontinuity appeared at A4A time. The axial structure of the KR changed from being continuous to highly segmented following a counterclockwise reorientation of the spreading axis after A4, which resulted in the separation of the ridge axis into 4 segments. The post-A4 structural evolution of the KR was accommodated by the elongation and shortening of adjacent segments, and the corresponding along-strike migration of axial discontinuities.
2. Spar Offset (69°N) initiated at A4A and was the site of a southward-directed propagator until A2A. Following a brief period as a stationary nontransform offset, the migration direction of Spar Offset reversed, and from A2 to the present the offset has marked the site of a northward-directed propagator.

3. The  $68^{\circ}43'N$  discontinuity initiated after A4 and has migrated northward since A3 in response to the northward propagation of the southern segment of the KR. This propagator remains active.
4. The spreading center north of Spar Offset was displaced eastward during two periods of fast propagation and/or lateral ridge jumps that resulted in the counterclockwise reorientation of the axis. The first event occurred after A4, and the second began after A2.

## CHAPTER 3

AXIAL STRUCTURE AND RECENT TECTONICS OF THE KOLBEINSEY RIDGE SEAFLOOR  
SPREADING CENTER

## ABSTRACT

I document the axial structure of the slow-spreading Kolbeinsey Ridge (KR), which lies between Iceland and the Jan Mayen Transform (66.6°N-71.75°N) based on recently collected swath bathymetry, acoustic imagery and magnetics, and existing shiptrack data. Kolbeinsey Ridge exhibits structural segmentation manifested in plan view by nontransform discontinuities and in profile by corresponding depth maxima. The two largest discontinuities, the Spar offset (69.0°N) and Eggvin offset (70.4°N) define the boundaries between three structurally unique segments. The Spar offset has experienced southward and northward along-axis migration, and structural patterns indicate that southward propagation across the offset stalled after anomaly 2a, followed by northward propagation of the southern KR that was accommodated by three episodes of advance after anomaly 2. The Eggvin offset is inferred to have remained at the same location along strike since the inception of spreading on KR, and has been nontransform throughout the 6 m.y. period covered by our acoustic imagery. The southern KR includes 3 smaller-scale segments, one which lies entirely on the Iceland insular shelf, and in general is characterized by a narrow topographic ridge that contains a shallow summit graben that hosts the axial neovolcanic zone. In contrast, the middle KR is contained within a well-developed axial valley 2-14 km wide and 500-2000 m deep, superimposed on a much broader topographic swell. The middle KR is further divided into 3 smaller-scale segments separated by axial discontinuities < 5 km wide that disrupt axial boundary faults but are not associated with an off-axis trace. The northern KR shoals to less than 500 m depth, and the southern half of the segment is associated with broad, shallow rift flanks that appear to be rifting apart over a relatively wide zone. Near the segment's northern intersection with the Jan Mayen transform, the axis is characterized by a constructional volcanic ridge 18 km wide and more than 1000 m high, contained within a deep, broad axial valley that deepens towards the transform and exhibits a maximum depth of 3700 m at the inside corner. Shallow crust extends between the northern KR axis and Jan Mayen Island to the east, and based on morphological evidence I suggest that the Jan Mayen hotspot is more likely located beneath the northern KR than near Jan Mayen Island, which is consistent with available geochemical data.

## INTRODUCTION

The slow-spreading (full rate ~ 2 cm/yr) Kolbeinsey Ridge (KR) lies on the opposite side of the Iceland hotspot from the Reykjanes Ridge, yet exhibits significant first-order morphological differences from its southern counterpart (Figure 3.1). In contrast to the oblique orientation and narrow, linear geometry of the Reykjanes Ridge axis, KR lies asymmetrically on a broad

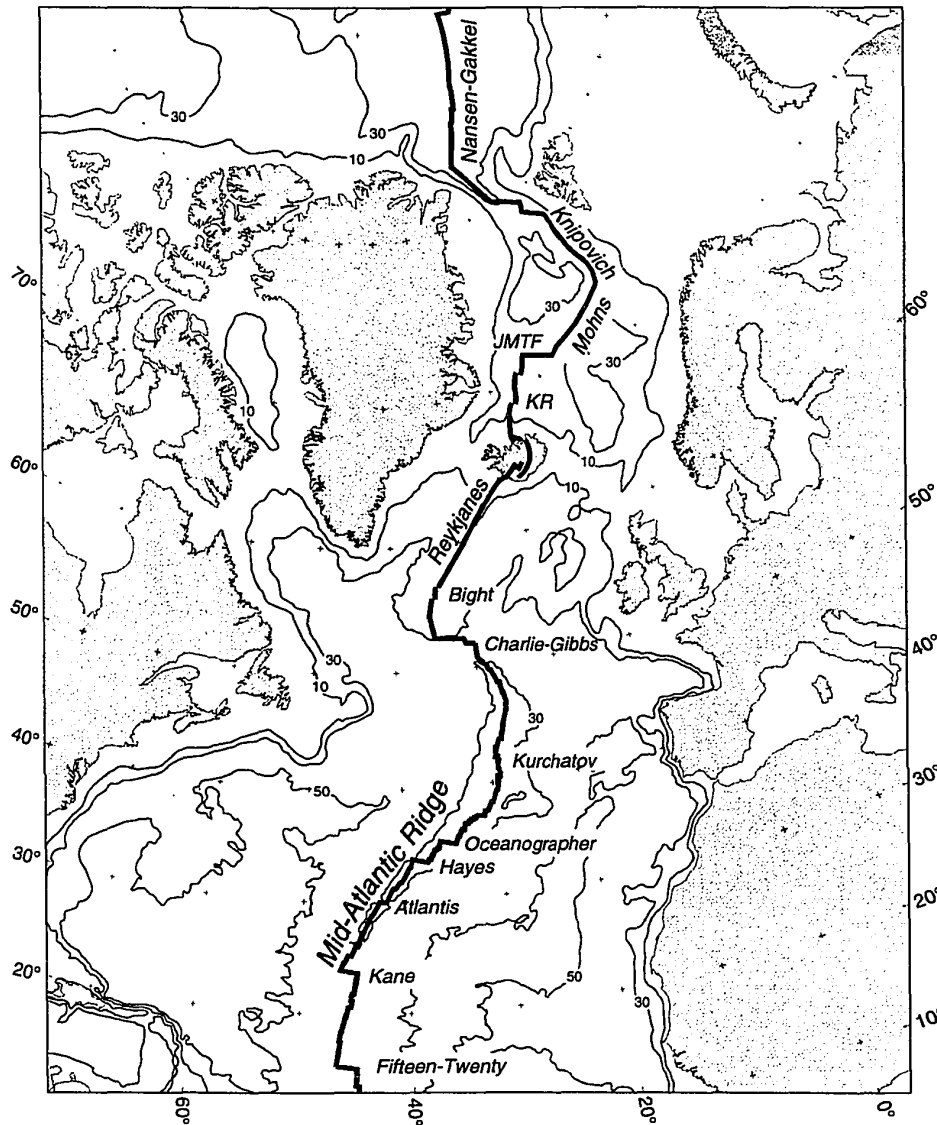


Figure 3.1. Location map showing Kolbeinsy Ridge with respect to the spreading centers and fracture zone of the Atlantic and Arctic Oceans. The plate boundary is bold, and depth contours are annotated in hundreds of meters. This is an oblique Mercator projection from the modern Euler pole for the North American and Eurasian plates [DeMets et. al., 1990]. Using this projection, fracture zones and transform faults that formed according to this pole of rotation trend horizontally across the page, and orthogonal spreading centers plot vertically.

topographic swell on the regionally shallow Iceland Plateau, and is oriented orthogonal to the spreading direction. Geochemical studies of basalts dredged from KR exhibit extremely low  $\text{Na}_2\text{O}$  contents and a wide range in incompatible-element ratios [Devey *et al.*, 1994; Klein and Langmuir, 1987; Mertz *et al.*, 1991; Schilling *et al.*, 1983], which suggests a dynamically melting, adiabatically ascending mantle source [Devey *et al.*, 1994]. Surprisingly, isotopic characteristics basalts from the southern and middle KR segments indicate that Iceland plume material is not involved in KR volcanism, in contrast with the gradient observed along Reykjanes Ridge. The northern KR contains enriched basalts that, based on the morphological evidence presented below, I suggest are related to the Jan Mayen hotspot.

Early geophysical surveys documented the regional setting and tectonic evolution of the Norwegian-Greenland Sea [Johnson *et al.*, 1972; Talwani and Eldholm, 1977; Vogt *et al.*, 1980; Vogt *et al.*, 1982], and as shown in Chapter 2 the KR between Iceland and 70°N has experienced a complex history of reorganization since anomaly 5 involving ridge propagation, asymmetric spreading, and rapid lateral migration of the ridge axis that were accommodated by either ultrafast propagation or synchronous ridge jumps. To date, however, most sampling and geophysical surveys of the Kolbeinsey Ridge have occurred south of 70°00'N, and as a result the northern KR and its intersection with the Jan Mayen Transform Fault (JMTF) have not been well constrained, and important first-order characteristics of the ridge crest have remained unknown, including details of the location and morphology of the spreading axis and the nature of the axial discontinuities (transform vs. nontransform).

This paper presents new results from recent swath bathymetry and side scan sonar surveys along the axis of Kolbeinsey Ridge. In conjunction with existing trackline data from previous cruises, these data reveal the detailed axial structure of the Kolbeinsey Ridge, and provide structural information that I use to characterize the nature, scale and recent behavior of large and small axial discontinuities along the segmented ridge crest. In addition to revealing aspects of the structure and evolution of the ridge, these new data provide an improved geophysical framework for understanding existing geochemical data, and provide a more accurate basis for future work. The following sections present the general tectonic setting and history of the ridge, describe the methods I used to collect and analyze our data, and discuss the ridge's axial structure and its recent tectonic evolution based on these observations.

## METHODS

We surveyed the KR between 68°20'N and the Jan Mayen Transform Fault (JMTF) at 71°45'N using Sea Beam swath bathymetry and the SEAMAP seafloor imaging systems (Figure 3.2). These data were collected during parts of two different cruises of the USNS Kane, and both systems operated concurrently using the technique of *de Moustier et al.* [1990]. Both cruises were navigated using the Global Positioning System. Sea Beam is a hull-mounted 12 kHz echo sounder that images swaths of seafloor equal to 75% of the water depth [Renard and Allenou, 1979; Farr,

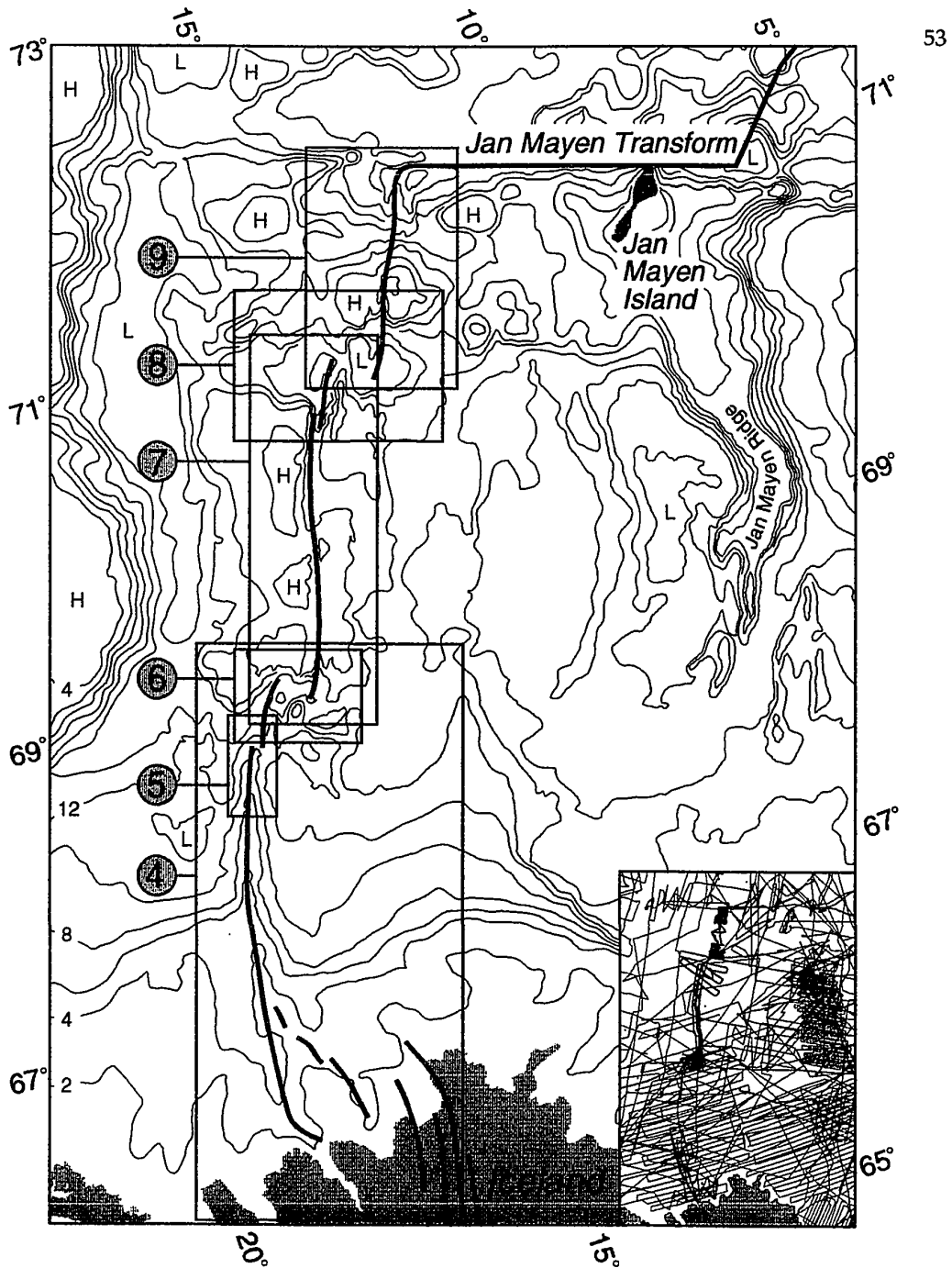


Figure 3.2. Regional bathymetry of the Greenland Sea around Kolbeinsey Ridge (oblique Mercator projection from NOAM/EUR pole). The KR spreading axis (bold line) is divided into three major segments oriented orthogonal to the extension direction, except where the axes bend toward major ridge offsets. Depth contour interval is 200 m, annotated in hundreds of meters. Closed contours around highs are marked H; lows are marked L. Numbered boxes indicate the locations of Figures 3.4-3.9. Inset shows trackline coverage used to generate the bathymetry.

1980]. SEAMAP is a shallow-towed, side-scanning swath imaging system that simultaneously acquires side scan and bathymetry data [Whittaker *et al.*, 1991]. SEAMAP was designed and built by the Hawaii Mapping Research Group at the University of Hawaii, and is operated by the U. S. Naval Oceanographic Office. The system is nearly identical to the HAWAII MR1 mapping system [Rognstad, 1992], and operates at 11 kHz (port) and 12 kHz (starboard) using transducers that are normally towed at a depth of 80 - 100 m. The SEAMAP side scan swath width varied from 10 to 18 km during our surveys, and bathymetry swaths extend to the first acoustic multiple (total swath ~340% of the water depth) and occasionally to the second multiple (~570% of depth). In one formal comparison of simultaneously-collected Sea Beam and SEAMAP bathymetry data, the RMS error between the data sets was found to be less than 30 m [Lingsch, 1994].

Side scan data were processed to remove speckle and stripe noise, then merged with ship navigation and gridded to produce digital mosaics of acoustic imagery using the methods described by Davis *et al.* [1992]. Side scan images presented herein are displayed such that high backscatter is black and acoustic shadow is white. SEAMAP uses interferometry to measure bathymetry, and the processing techniques involved in transforming raw acoustic data into bathymetry soundings are similar to those of the defunct SeaMARC II system described by Blackinton *et al.* [1983] Matsumoto [1990] and Shor [1990]. During parts of the survey the depth sensor in the towfish malfunctioned. In order to calculate total water depth (the sum of towfish depth and altitude) during these periods, I modeled towfish depth using the ship's speed and checked the resulting bathymetry where tracklines crossed. Navigated SEAMAP and Sea Beam bathymetry data were combined, filtered and plotted using the Generic Mapping Tools System [Wessel and Smith, 1991]. In areas covered by side scan but not bathymetry, isobaths were hand-contoured using the side scan as a guide, and then digitized and incorporated into the bathymetry data set.

We constructed bathymetry maps by digitally superimposing gridded SEAMAP and Sea Beam soundings over a regional bathymetry grid generated from trackline bathymetry archived at the U. S. National Geophysical Data Center. The bathymetry and structure maps presented herein are all oblique Mercator maps projected from the pole of rotation between the North American and Eurasian plates. As demonstrated by Joseph *et al.* [1992], this projection emphasizes the geometry of plate boundaries relative to the spreading direction: transform faults, fracture zones and other features that are oriented parallel to the spreading direction are oriented horizontally in this projection; structures that strike orthogonal to the spreading azimuth are oriented vertically. Figure 3.1 shows that the strike of the KR is regionally orthogonal to the spreading direction, in contrast to the oblique orientation exhibited by every other seafloor spreading center between 56°47'N and 82°30'N (the Reykjanes, Iceland, Mohns and Knipovich spreading centers).

## GEOLOGIC SETTING

The KR is ~600 km long, located between the subaerial Iceland spreading center and the Jan Mayen transform fault (Figure 3.2). Kolbeinsey Ridge forms a broad topographic high that is part of the Iceland Plateau in the Greenland Sea (Figure 3.2). The modern spreading axis lies east of the ridge's axis of topographic symmetry (Figure 3.2). The axis is offset by two right-stepping discontinuities, the Spar offset near 69°00'N, and an unnamed offset near 70°40'N [Johnson *et al.*, 1972; Vogt, 1986d]. We refer to the 70°40'N discontinuity as the Eggvin offset due to its proximity to Eggvin Bank.

The KR is a slow-spreading ridge, creating new seafloor at a full rate of < 2 cm/year since 12-14 Ma, prior to which it spread ~1.5 cm/year [Vogt *et al.*, 1980; 1981]. The pole of rotation between the North American and Eurasian plates is located at 62.4°N/135.8°E [DeMets *et al.*, 1990], and as a result the modern spreading velocity varies over the length of the ridge, from 1.85 cm/year (directed 105.2°) at 67°00'N to 1.70 cm/year (directed 110.7°) at 71°40'N. Spreading on the KR initiated at about Anomaly 20 time, when the Mid Atlantic Ridge (MAR) began propagating northward into the Greenland continental margin and progressively replaced the Aegir Ridge as the locus of spreading north of Iceland [Nunns, 1982]. Larsen [1988] inferred a propagation rate of 1-2 cm/year over this period. By anomaly 6 time the ridge had propagated north of the older, left-stepping East Jan Mayen Fracture Zone and established the modern right-stepping Jan Mayen transform [Talwani and Eldholm, 1977]. The northward propagation of the proto-KR cleaved off part of the Greenland margin, which was translated eastward and now constitutes the Jan Mayen Ridge [Talwani and Eldholm, 1977]. At Anomaly 5 time the Iceland spreading center was displaced to the east, establishing the Tjörnes fracture zone and isolating the KR from the spreading center to the south [Nunns, 1983; Sæmudsson, 1974].

## KOLBEINSEY RIDGE AXIAL PROFILE

We created an axial profile of the KR (Figure 3.3) by sampling our composite bathymetry grid along the inferred neovolcanic axis. The location of the neovolcanic axis was constrained by new magnetic and side scan data, and by aeromagnetic data [Vogt *et al.*, 1980]. KR is shallow relative to the mean zero-age depth of the Mid-Atlantic Ridge (MAR), which is ~2327 m [Malinverno, 1990]. Depth maxima occur at each of the major axial discontinuities (the Tjörnes, Spar and Eggvin offsets, and the Jan Mayen RTI), dividing the KR into three main segments: southern, middle and northern. The southern Kolbeinsey ridge (SKR) extends northward from the Iceland insular shelf, reaching its shallowest point near Kolbeins Ey (Kolbeins Island, ~67°09'N). Axial depth on the SKR increases monotonically north of Kolbeins Ey at a rate of 5 m/km, although a shorter wavelength variation of ~ 150 m is superimposed on the regional trend. A local depth maximum occurs at 68°43'N, and between this point and the Spar offset the axial depth increases at a rate of 8 m/km. This break in slope corresponds with the position of a right-stepping discontinuity discussed in more detail below. The middle Kolbeinsey ridge (MKR) spans 227 km

between the Spar and Eggvin offsets, and exhibits depth maxima at 70°00'N and 70°33'N that coincide with axial discontinuities. The northern Kolbeinsey ridge (NKR) is 125 km long and shoals within 400 m of the surface near 71.1°N, with rift flanks there as shallow as 25 m. The NKR does not exhibit significant local depth maxima, although sampling is sparse along the middle part of the segment.

#### TJÖRNES FRACTURE ZONE

The southern end of the KR is offset ~100 km west of the Iceland volcanic zone, across the Tjörnes fracture zone (Figure 3.4). The Tjörnes fracture zone is actually a structurally complex nontransform offset, characterized by three northwest-trending seismic zones. The southern part of the offset is defined by the Dalvik seismic zone, which strikes ~8° oblique to the NUVEL-1 plate motion azimuth. Most of the Dalvik seismicity has occurred on the western part of an inferred fault [Einarsson, 1991], including an offshore magnitude 7 right-lateral strike-slip event in 1963 [Sefánsson, 1966; Sykes, 1967] and an estimated magnitude 6.3 event near Dalvik in 1934 [Tryggvason, 1973]. The western end of the Dalvik system does not intersect the KR or any features associated with the KR, and an eastward continuation of the Dalvik system to the North Iceland Volcanic Zone (NIVZ) has not been demonstrated, although Einarsson [1991] suggested the fault zone may control the structure of the NW-SE Dalsmynni valley.

The central part of the Tjörnes offset is dominated by the seismic and structural expression of the Husavik fault, which is located ~30 km north of the Dalvik seismic zone and connects the Theistareykir fissure swarm in the NIVZ to Eyjafjardaráll Trough at the south end of the KR. Right-lateral strike-slip is expressed on the subaerial part of the fault system [Sæmundsson, 1974]. Offshore the fault zone is inferred to continue northwestward through a 296°-trending graben in Skjalfandi, along a negative gravity anomaly between the northern Flateyjarskagi peninsula and Flatey Island, and terminates at the southern tip of Eyjafjardaráll trough [Young *et al.*, 1985; Gudmundsson *et al.*, 1993]. The Husavik fault is seismically active, characterized by earthquake sequences onshore in 1755 and 1872 having magnitudes estimated up to 6-7 [Tryggvason, 1973], and offshore seismicity distributed along the western half of the fault [Einarsson, 1991].

The northern boundary of the TFZ is defined by the Grimsey seismic zone, a broad swath of seismicity that links the Krafla fissure swarm in the NIVZ to the KR near Kolbeins Ey. Fault plane solutions for two earthquakes indicate right-lateral strike-slip faulting oriented parallel to the trend of the seismic zone [Einarsson, 1991]. However, surface faulting is manifested as several (3-4) N-S trending fissure swarms arranged in a left-stepping, en echelon pattern. Most of the seismicity along the Grimsey seismic zone is concentrated along the fissure swarms [Einarsson, 1991]. At least three fissure swarms occur between the NIVZ and the axis of the KR, arranged in a left-stepping en echelon pattern. The ~350° strike of each fissure swarm is 25° oblique to the predicted spreading-normal direction, and the sense of obliquity is consistent with the rotated stress field expected between offset ridge tips [Macdonald *et al.*, 1984; Pollard and Aydin, 1984; Gudmundsson *et al.*, 1993]. Einarsson [1991] suggests that the fissure swarms result from shallow

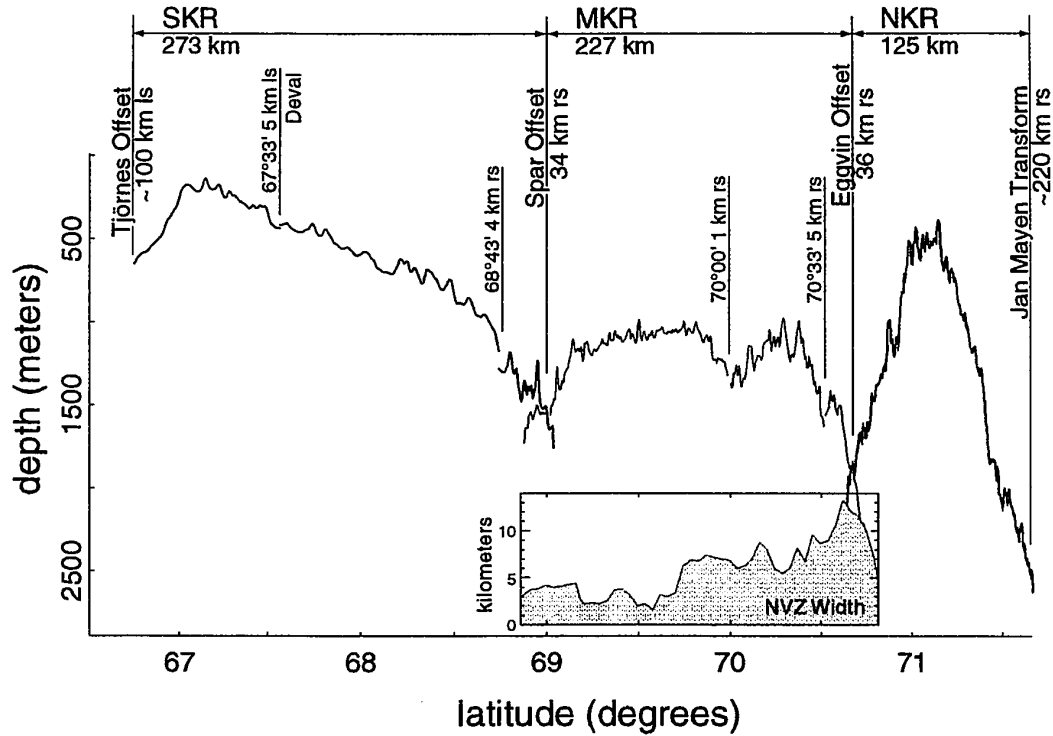


**Figure 3.3.** Kolbeinsey Ridge axial profile showing the partitioning of the KR into three major segments separated by depth maxima that correspond with axial discontinuities. The profile represents depths along the neovolcanic axis, which was identified from acoustic imagery and magnetic data. SKR = Southern Kolbeinsey Ridge segment; MKR = Middle; NKR = Northern. Resolution is lower on the SKR and NKR, where bathymetric coverage is less complete than the swath-mapped MKR. Inset shows axial neovolcanic zone (NVZ) width on the MKR. The sense of offset across axial discontinuities is indicated by ls (left-stepping) and rs (right-stepping).

crustal dilation, and that the larger earthquakes result from larger-scale shear related to transform motion. Several submarine eruptions have been documented within the offset zone, with most associated with fissure swarms in the northwest part of the offset. The fissure swarms of the Grimsey seismic zone are similar in geometry and scale to the fissure swarms on the Reykjanes Peninsula [Einarsson, 1991], and Taylor *et al.* [1994] propose that the TFZ may be a member of a new class of plate boundaries they term extensional transform zones.

#### SOUTHERN KOLBEINSEY RIDGE (SKR)

The southern KR (Figure 3.4) extends 273 km northward from the Tjörnes transform zone to the Spar offset, and contains three distinct segments separated by small nontransform offsets. In general the SKR axis is oriented orthogonal to the spreading direction and occupies a symmetric ridge, except near its southern and northern tips, where axial relief diminishes and the axis bends toward the Tjörnes and Spar offsets.

The SKR spreading axis is marked by a high-amplitude positive magnetic anomaly that follows the crest of the topographic ridge (Figure 3.4). As the southern end of the SKR is approached the axial anomaly bifurcates at 67.2°N, with one branch extending southeast over the volcanic centers of the Grimsey seismic zone, and the other continuing south along the KR axis. South of the bifurcation the axial anomaly becomes narrower and lower in amplitude, and can be traced past the end of the topographic ridge to ~66.7°N within Eyjafjardaráll Trough (ET). ET is an elongate sediment-filled graben that bends westward as it approaches its intersection at its southern tip with the Husavik fault system. Seismic sections reveal the trough contains sediments > 0.3 s thick [McMaster *et al.*, 1977], and the low-amplitude positive magnetic anomaly along ET may indicate the presence of dikes or sills intruded within the trough's sediments. The trough is seismically active [Einarsson, 1991], and seismic reflection profiles across the trough reveal growth faulting indicative of a history of subsidence and sedimentation [McMaster *et al.*, 1977]. I suggest ET is the tectonically active southern tip of the KR, without known recent extrusive volcanic activity but perhaps containing intrusive bodies. Seismic and volcanic activity elsewhere within the Tjörnes offset indicate that ET acts in concert with other features within the offset zone to accommodate the full extension across the plate boundary [Einarsson, 1991].

The SKR is divided into 3 subsidiary segments separated by small nontransform discontinuities. Between 66°48'N and 67°33'N the spreading axis lies entirely on the insular shelf, and occupies a ridge that displays up to 400 m of relief (Figure 3.4). The first clear bilateral symmetry of magnetic anomalies occurs at 67°10'N, where anomalies 2 and 2a are evident on either side of the ridge [Vogt *et al.*, 1980]. The central anomaly increases in width and amplitude here as well. The southern SKR segment contains the shallowest point on the SKR, near Kolbeins Ey, where boiling hydrothermal systems and recent eruptions have been documented [Olafsson *et al.*, 1990; Lackschewitz *et al.*, 1994].

The boundary between the south and middle SKR occurs where the spreading axis crosses the edge of the insular shelf, where the topographic ridges of the axis are offset in a left stepping

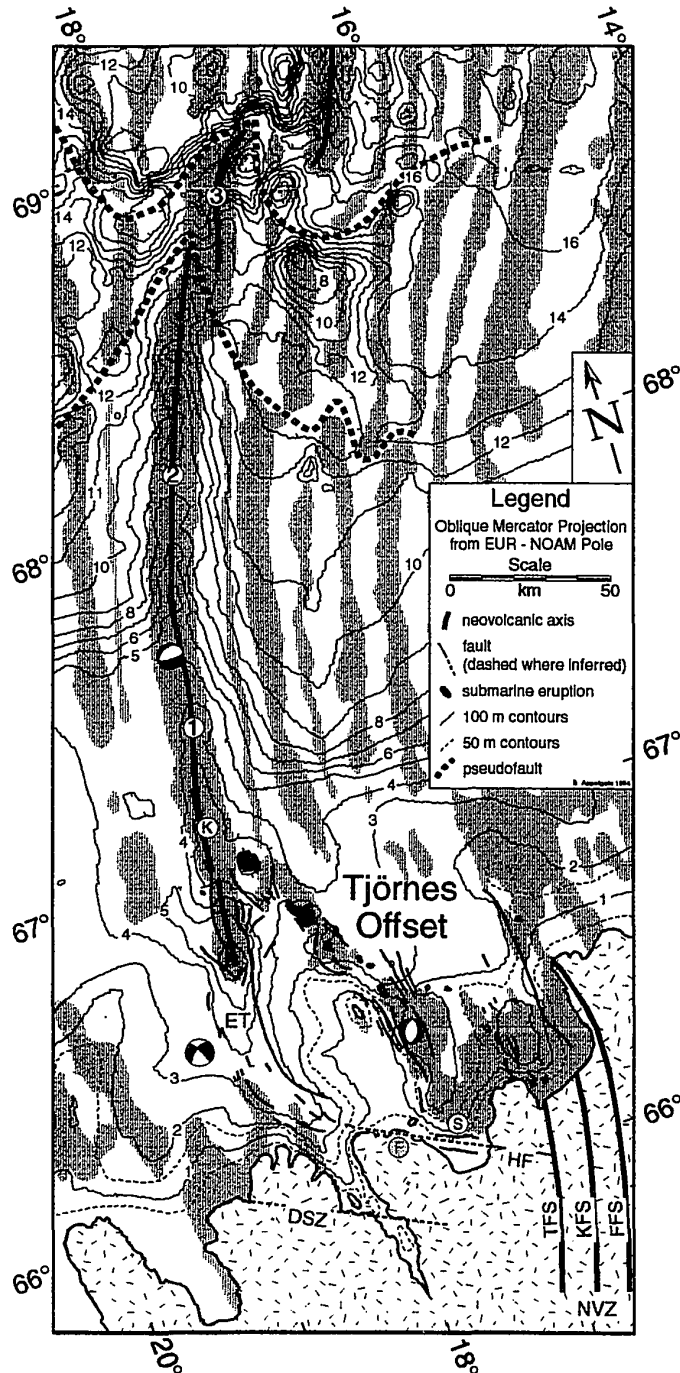


Figure 3.4. Bathymetry, magnetic anomaly pattern, and structure of the SKR and Tjörnes Offset. Magnetics are residual (total field - IGRF) aeromagnetic data from the U.S. Naval Oceanographic Office Project MAGNET [Vogt *et al.*, 1980]; shaded areas are positive. Structural data around Tjörnes Offset are from Sæmundsson [1974] and McMaster *et al.* [1977]. Segments 1, 2 and 3 of the SKR are numbered; ET is Eyjafjardaráll Trough; DSZ is Dalvík Seismic Zone; K is Kolbeins Ey; S is Skalfandi; F is Flateyjarskagi Peninsula.

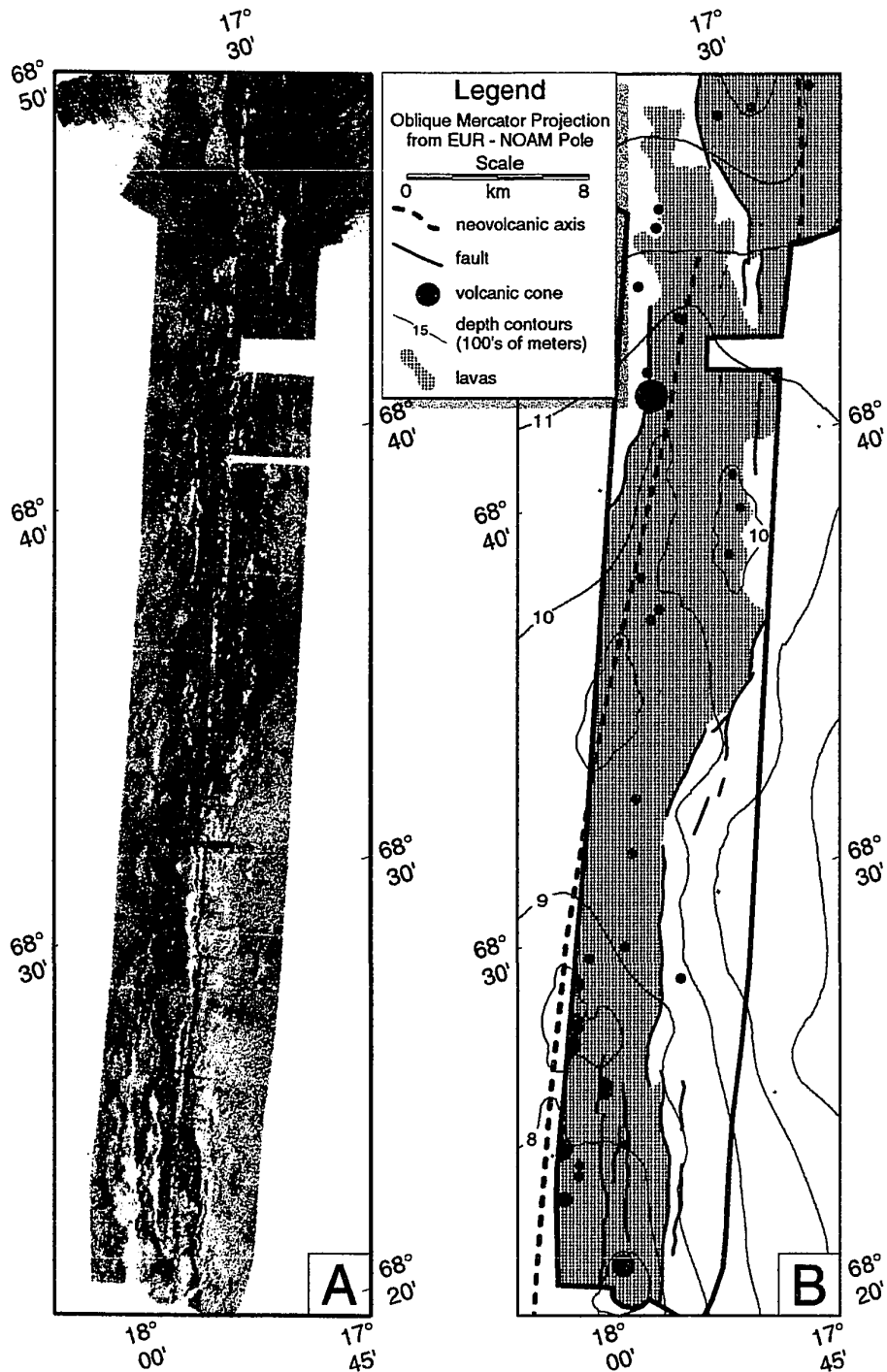
sense by ~ 10 km. The axial depth gradient does not appear to be disrupted at this offset, based on the synthesis of trackline bathymetry used to generate Figure 3.3. The central magnetic anomaly bends smoothly between the offset ridges, and north of this point the anomaly is wider and displays greater positive amplitude [Vogt *et al.*, 1980]. Anomaly 2 is not bent or offset on either side of the axis, indicating that this discontinuity developed later than ~1.8 Ma.

North of the 67°33'N offset the spreading axis occupies a narrow (~50 km wide) ~ 500 m high ridge that juts outward from the Iceland insular shelf. Axial depth increases northward at the rate of 5 m/km, although the overall relief of the ridge remains nearly constant. The ridge decreases in width to the north, and in these respects this segment of the SKR is a mirror-image of the Reykjanes Ridge south of Iceland. However, the middle SKR is the only part of the Kolbeinsey Ridge that bears a physical resemblance to the Reykjanes Ridge, and the scales of these two features are much different: measured from the shelf break to the Bight transform, the Reykjanes Ridge is 888 km long [Appelgate and Shor, 1994], compared to 130 km for the SKR between the shelf and the 68°43'N nontransform offset.

In contrast to the Reykjanes Ridge, the middle SKR is neither oblique nor does it exhibit the *echelon* volcanic ridges that dominate the volcanic morphology of Reykjanes Ridge. The crest of the middle SKR is partially imaged in Figure 3.5, which shows that the volcanic axis is composed of aligned, coalesced cones and ridges. The path of the inferred volcanic axis is constrained by the location of the central magnetic anomaly, and therefore the volcanic features imaged south of 68°40'N probably represent only the eastern flank of the volcanic axis. The network of ridges and cones can be traced to a northern terminus at ~68°43'N, although a field of flat-lying lavas (which fill low areas between older, higher relief cones) extends north to 68°48'N. Although the middle SKR regionally occupies a topographic ridge, Figure 3.5 indicates the volcanic axis occupies a shallow graben defined by small-throw, inward-facing faults.

The middle SKR terminates at 68°43'N, where the volcanic axis is offset at a right-stepping nontransform discontinuity. The eastern side of the discontinuity was not imaged, so the scale of overlap and offset cannot be measured, although the position of the volcanic axis north of the discontinuity suggests an offset of < 10 km. South of the discontinuity, axial boundary faults on the east side of the neovolcanic zone step eastward at 68°33'N. The 68°43'N discontinuity coincides with a change in gross spreading center morphology from axial high to axial valley. North of 68°43'N the northern SKR volcanic axis lies within a valley defined by inward-facing fault scarps, and the southern end of the valley's western boundary fault is evident as an east-facing fault between the offset volcanic axes.

The 68°43'N discontinuity marks the northern tip of a northward-directed propagating ridge. Disruptions in the magnetic anomaly patterns east and west of the ridge axis define a V-shaped wake that record the northward migration of this discontinuity (Figure 3.4). This discontinuity appears to have initiated after Anomaly 4a time and migrated northward at an average rate of about 10.3 km/my, although since Anomaly 2 the propagation rate has accelerated to



18.5 km/m.y. The middle SKR lies farther west than the northern SKR, so that the northward-propagating middle SKR has replaced the dying northern SKR with a spreading axis located west of its previous position. Another consequence of the passage of the propagator is the transfer of lithosphere from the North American plate, through the overlap zone, onto the Eurasian plate in a manner described generally by Hey et al. [1980; 1989]. We note that the propagating middle SKR occupies a topographic ridge, and this propagator may be driven by gravity-spreading stresses according to the model of Phipps Morgan and Parmentier [1985]. Although this ridge is adjacent to the Iceland hotspot, a plume geochemical signature is not observed north of the Tjörnes offset [Schilling et al., 1983; Schilling, 1986; Mertz et al., 1991; Devey et al., 1994], suggesting that a sub-asthenospheric flow mechanism [Hey and Vogt, 1977; Schilling et al., 1982; Vogt, 1971] does not apply here.

#### SPAR OFFSET

The Spar offset (Figure 3.6) is a right-stepping nontransform axial discontinuity that separates the SKR from the MKR. The volcanic axes of the ridges are offset by 34 km, measured parallel to the 107° local spreading azimuth and neglecting inward curvature of the axes near the ridge tips. We recognize volcanic and tectonic tips of each segment in the side scan imagery. Volcanic tips are defined as the end of axial constructional volcanic ridges, which here also coincide with the terminus of the central magnetic anomaly. Tectonic tips are defined as the farthest reach of axial boundary faults. At the Spar offset the opposing volcanic tips overlap by 15 km, measured perpendicular to the spreading direction, and the tectonic tips overlap by 27 km.

As the Spar offset is approached from the south, the northern SKR axis displays a sharp 30° clockwise bend at 68°55', and the volcanic axis and axial boundary faults generally strike ~045° over the northern 30 km of the axis. The northern SKR volcanic axis terminates at 69°02'N, evidenced by the disappearance of the axial volcanic ridge and the central magnetic anomaly. Axial lavas extend farther beyond this point, however, indicated by low-relief, high-backscatter surfaces evident several kilometers north and east of the end of the axial volcanic ridge.

Magnetic anomalies (Figure 3.4) indicate the SKR has recently propagated northward at the Spar offset, following an earlier period of southward propagation by the MKR. The structural relationship of several faults west of the axial valley reveals additional detail regarding the tectonic evolution of the northern tip of the SKR. South of 69°03'N, a fault system (Figure 3.6, fault set 2) located within low-backscatter seafloor several kilometers west of the neovolcanic zone strikes parallel to the volcanic axis, except near 69°03'N where it bends to the east. A different fault system (fault set 3) crosscuts set 2 at 69°03'N and extends northwest (parallel to the trend of the volcanic axis) to 69°08'N, where these faults bend to the east and crosscut N-S-trending scarps (fault set 0). We infer that the N-S scarps are older faults generated on the west side of the MKR, because they occur in low-backscatter seafloor and strike parallel to the MKR axis, and because magnetic anomalies indicate this crust was generated by the MKR. Although relative age assignments are difficult where sets of normal faults intersect, I suggest that fault set 3 (between

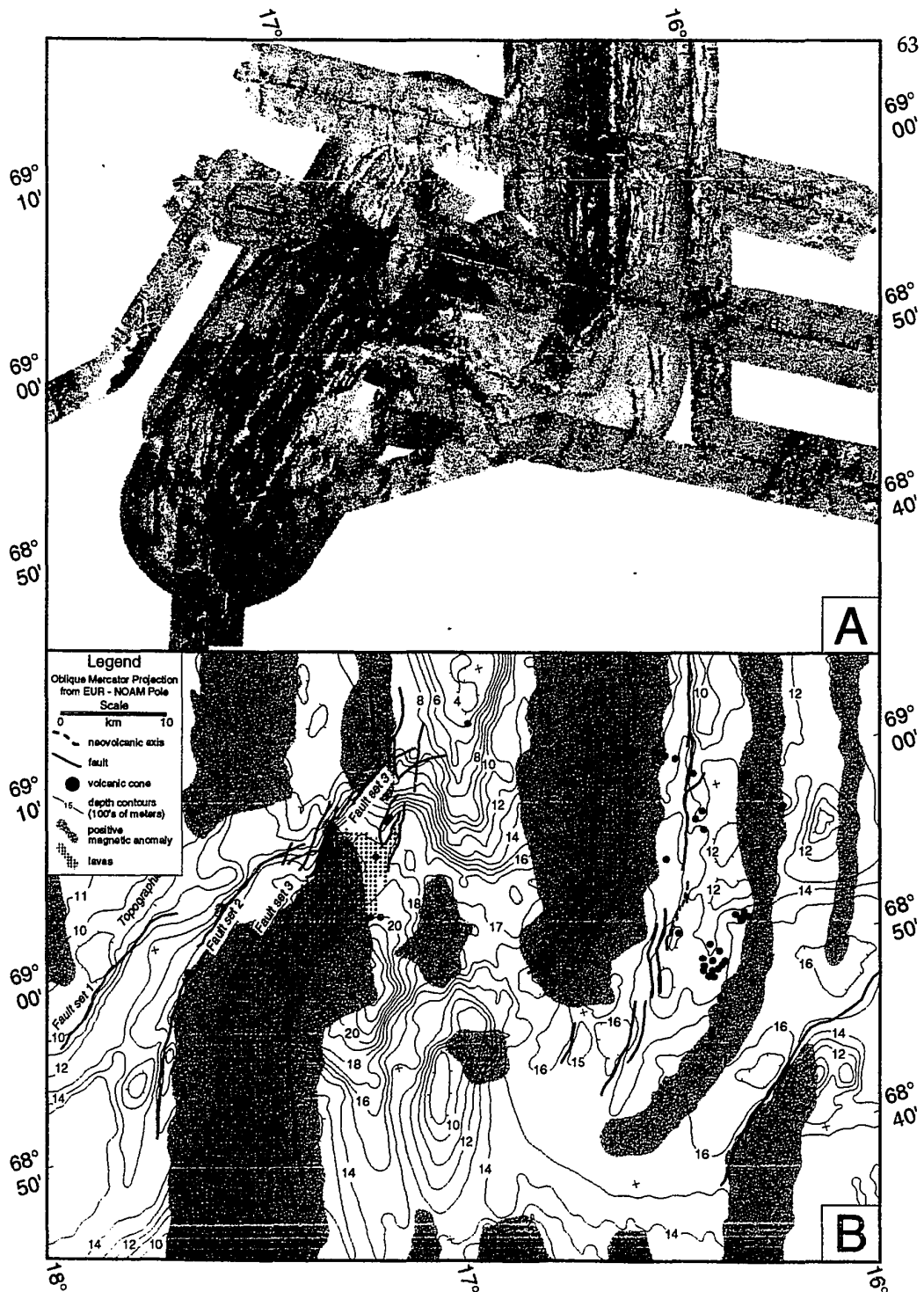


Figure 3.6. SEAMAP acoustic imagery (A) and structure map (B) of Spar Offset, a nontransform axial discontinuity. Shaded magnetic anomalies are positive residuals of total field magnetic measurements minus IGRF. In concert, the magnetic anomaly and fault patterns indicate a history of initial southward and subsequent northward propagation at the Spar Offset.

69°03'N - 69°08'N) postdates fault set 2 because it includes faults that define the present inner wall of the axial valley. Fault system 2 lies along the Brunhes/Matuyama boundary, and therefore these faults are inferred to be ~ 780 ka old. This age is consistent with the age predicted by assuming that the faults formed at the west edge of the inner valley and were rafted outward by seafloor spreading. Based on the observation that axial boundary faults curve inward towards axial discontinuities (for example, the southern tip of the MKR), I infer that the curvature of fault system 2 at 69°03'N records the location of the northern tectonic tip of the SKR at ~ 780 ka. The volcanic tip occurred farther south as indicated by the magnetic anomaly pattern, which is consistent with the general observation on modern ridges that the tectonic tip extends farther along strike than the neovolcanic zone [Hey *et al.*, 1986; Kleinrock and Hey, 1989]. More recently, SKR axial boundary faults (fault set 3) advanced northward through the older offset, establishing the crosscutting relationships evident at 69°03'N and 69°08'N.

Further evidence for the northward propagation of the northern SKR is provided by the geometry and structure of a topographic ridge located west of the SKR tip. The crest of the ridge shoals to ~ 1000 m and trends southwest from a shallow region north of the present SKR tip. The ridge displays low backscatter indicative of sedimented, relatively old seafloor. Faults that define the northern tectonic tip of the SKR, including those of fault set 3, extend up into the shallow region at 69°08'N. Fault set 2 defines the base of the topographic ridge between 69°03'N and 69°08'N. An additional fault system (fault set 1) occurs about 6 km west of fault set 2, and defines the base of the ridge from 69°01'N southwestward to at least 68°58'N. Although incompletely imaged, fault set 1 bends eastward at its tip, and is inferred to represent the northern tip of the SKR at ~1.2 Ma, based on its distance from the axial valley and the assumptions given above. The southeast flank of the topographic ridge marks the approximate position of the outer pseudofault of the SKR propagator, and the topographic ridge is inferred to consist of crust that originally formed on the west side of the MKR. The northward propagation of the SKR at the Spar offset thus occurred in a stepwise manner, characterized by the incremental northward advance of the SKR tip, which periodically stalled long enough for inward-curving tectonic fabric to be created and preserved.

The interior of the Spar offset contains several structural basins, including a 2400-m-deep basin located east of the SKR volcanic axis. Corridors of deep seafloor can be traced west and east of the offset, and correspond with pseudofaults revealed in the magnetic anomaly pattern (Figure 3.4). Thus the deep corridors record the approximate position of the offset through time, as has been demonstrated for other migrating offsets on the Mid-Atlantic Ridge [Kleinrock *et al.*, 1992; Pockalny and Gente, 1992; Sempéré *et al.*, 1993; Tucholke and Lin, 1994]. East of the offset, the corridor of deep bathymetry extends southeast from the modern overlap zone, and then follows a northeastward path across older seafloor. The deep bathymetry west of the offset mirrors this geometry (Figure 3.4), and indicates that the recent northward propagation of the northern SKR followed a period of southward propagation of the southern MKR.

Constraints on the extent of the southward MKR propagation are imposed by structures east of Spar offset. The southern tip of the MKR curves 35° in a clockwise sense as the Spar offset is approached. A system of fault scarps 8 km east of the MKR axis extends farther south than the present southern tip of the MKR, to the southern limit of our side scan imagery at 68°46'N. An additional west-facing fault scarp occurs in older crust to the east, and indicates that the MKR axis was once located at least as far south as 68°40'N. This fault defines the linear west flank of a shallow ridge near 68°43'N/16°00'W, and coincides with the outer pseudofault of the southward-propagating MKR.

#### MIDDLE KOLBEINSEY RIDGE (MKR)

The MKR spans 227 km between the Spar and Eggvin offsets, and is nearly orthogonal to the spreading direction over its entire length (Figure 3.7). In contrast to the positive relief exhibited by most of the SKR, the MKR contains an axial valley defined by long, straight boundary faults, except where the boundary faults curve toward the Spar and Eggvin offsets. Axial valley width varies along strike, from a minimum of <2 km on the southern part of the MKR to >13 km near the segment's northern terminus (Figure 3.3, inset). Axial valley relief is greatest near the segment tips (500 m south, 2000 m north), where most of the relief is accommodated by one or two major boundary faults rather than many small-offset faults.

The MKR is divided into three smaller segments by axial discontinuities at 70°00'N and 70°33'N that correspond with bathymetric maxima (Figure 3.3). The southern MKR segment is characterized by a 2-8 km wide axial valley that, in general, is narrowest along the central part of the segment and widens near the segment tips. The axial valley floor displays high backscatter indicative of relatively sediment-free lava flows. These high-backscatter lavas display a nearly uniform distribution throughout the axial valley, suggesting that relatively young lavas occur within the entire valley. Despite the widespread distribution of young lavas, the southern MKR contains few large constructional edifices. The ubiquitous presence of young lavas within the axial valley may be due to widely-distributed volcanic vents throughout the valley floor rather than specific volcanic centers. Alternatively, lavas on the southern MKR may be very fluid, allowing lavas that erupt at central vents to flow widely across the axial valley without building high-relief AVR.

The southern and middle MKR segments are separated by a 1450 m-deep saddle in the axial profile at 70°00'N (Figure 3.3). Despite the well-defined expression of this discontinuity in the axial profile, the structural expression of this offset in plan view is complex. In a regional sense the southern and middle MKR segments are offset by ~7 km in a left-stepping manner. Boundary faults on the west side of the axial valley are offset 7 km to the left at 69°45'N, although faults on the east side are not offset. As a result, the axial valley width increases north of 69°45'N (Figure 3.3, inset). Despite the structural discontinuity at 69°45'N, the volcanic axis of the southern MKR is continuous to 70°00'N. Lavas from the ridge overlie western boundary faults at 69°45'N, indicating that volcanism postdates movement along those faults. The ridge negotiates a gradual

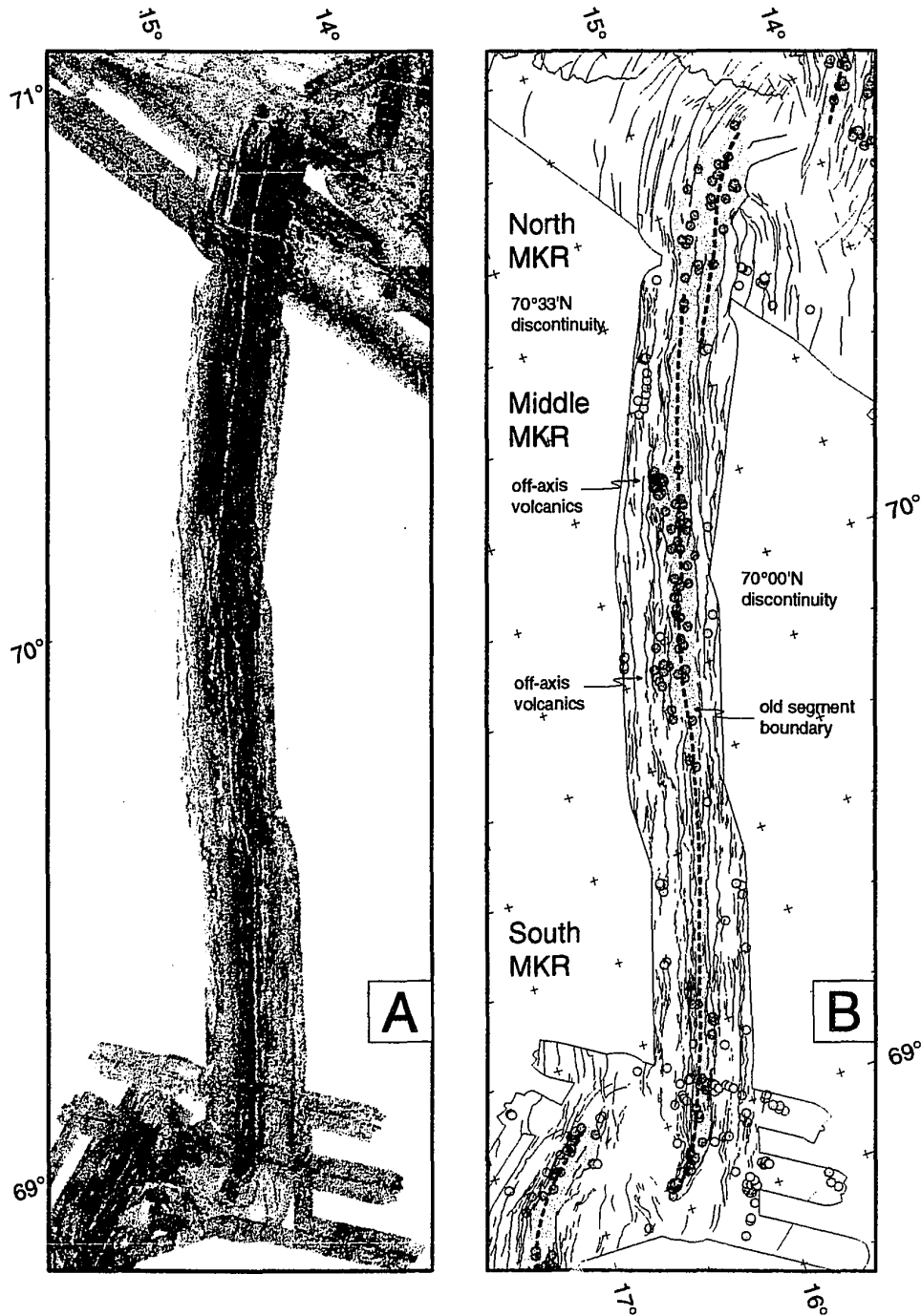


**Figure 3.7.** SEAMAP acoustic imagery (A) and structure map (B) of the middle segment of the Kolbeinsey Ridge. Faults are indicated by fine black lines, and the neovolcanic axis is marked by bold dashed lines. Axial lavas inferred from the backscatter distribution are shown by gray shading. Circular volcanoes are depicted by small circles (not to scale). Oblique Mercator projection from the NOAM/EUR pole.

westward bend between 69°40'N and 69°50'N, and at 70°00'N is offset from the volcanic axis of the middle MKR by a ~ 1 km right-stepping discontinuity. At 70°00'N the axial boundary faults display no evidence of disruption indicative of a long-lived discontinuity. We thus infer that the depth maximum at 70°00'N marks the present boundary between the magmatic systems of the southern and middle MKR, and that the position of this boundary was recently established by the propagation of the south MKR volcanic axis northward through a preexisting discontinuity at 69°45'N. The older offset was stable at 69°45'N long enough to establish a structural discontinuity marked by left-stepping boundary faults on the west side of the axial valley.

We observe no evidence of time-transgressive structures associated with the 70°00'N discontinuity, and therefore propose that the reorganization of the MKR volcanic axis occurred rapidly relative to the spreading rate. This sort of reorganization could have been as simple as the northward propagation of a dike beyond the previous position of the offset between these segments, as has been documented on the southern Juan de Fuca Ridge during a recent volcano-tectonic episode that involved fissuring and volcanic activity that extended 16 km through a preexisting nontransform offset [Chadwick *et al.*, 1991; Embley and Chadwick, 1994]. The northward growth of the southern MKR is also reminiscent of the rapid advance of spreading segments on the fast-spreading East Pacific Rise [Macdonald *et al.*, 1992; 1987], and may be indicative of locally high magma supply.

In contrast to the southern MKR, the middle MKR (70°00'N to 70°33'N) contains a robust axial volcanic ridge that dominates the physiography of the axial valley. The axial volcanic ridge can be subdivided into three smaller sections based on its morphology. Between 70°00'N and 70°10'N the ridge is comprised of a series of aligned, coalesced cones that individually vary in diameter from .5 to 2 km. At 70°10'N the character of the volcanic axis changes, and northward is constructed from a linear, high-relief ridge that does not contain discrete cones. Between 70°10'N and 70°27'N this AVR is 6 km wide and up to 500 m tall, rising to the same depth as the adjacent rift shoulders at 70°18'N (1000 m) and 70°22'N (900 m). The morphology of the volcanic axis changes once more at 70°27'N, where the AVR exhibits constituent volcanic cones and diminishes in relief. The ridge's northern terminus occurs at 70°33'N, where it merges along strike with an east-facing fault scarp that extends farther north.

The walls of the axial valley along the middle MKR are constructed from many subparallel, inward-facing faults. Although detailed bathymetry over the valley walls is sparse, no single fault appears to accommodate a majority of the valley's vertical relief. Changes in the structural architecture of the valley wall occur at roughly the same places where changes in AVR morphology are evident. At 70°10'N, boundary faults on the west side of the valley exhibit a 4 km left step. This site also contains a series of volcanic cones within a 28 km<sup>2</sup> field of low-relief, high-backscatter lavas that are inferred to have erupted off-axis relatively recently, based on their superposition over faulted, low-backscatter seafloor between the lava field and the primary AVR to the east. The structure of the axial valley changes again at 70°27'N, where relief on the axial

valley walls is consolidated along a single major boundary fault on either side of the valley. At this point the width and relief of the axial valley begin to increase toward the north (Figure 3.3).

The northern MKR is defined by an axial volcanic ridge that extends from 70°25'N to 70°47'N. The southern end of the ridge is offset 5 km to the east of the middle MKR, and the two ridges overlap by 12 km. Between the two ridges is a small-offset, east-facing fault scarp. This fault and the east wall of the axial valley define a shallow graben that contains the south tip of the northern MKR volcanic axis. The axial volcanic ridge displays up to 500 m vertical relief, and is 5 km wide at 70°35'N. The northern MKR axial valley increases in width and relief north of 70°30'N, reaching maximum values of > 14 km and > 2000 m, respectively. On the west side of the axis, the valley wall is constructed from three offset, overlapping fault systems, although at any given location a single fault system predominates and accommodates most of the valley's relief (Figure 3.8). The east axial valley wall is constructed from a major scarp that is cut by ravines on its upper slope and obscured by talus ramps on its lower slope. An embayment in the east wall at 70°40'N corresponds with an area where a network of NW-trending faults intersects the valley wall. The embayment may represent the net effect of slope destabilization and mass wasting at the intersection of the NW-trending faults with the east valley wall. The northern tip of the MKR abuts much shallower crust of the NKR, and here axial boundary faults bend northwest and penetrate several kilometers upslope into old, low-backscatter crust.

#### EGGVIN OFFSET

The right-stepping Eggvin nontransform offset (Figure 3.8) separates two structurally dissimilar spreading axes. In contrast to the well-defined axial valley and volcanic axis of the northernmost MKR, the NKR is characterized by a broad zone of faulting that defines a pair of valleys that each contain volcanic cones and high-backscatter lavas. The western valley contains the largest volcanoes and greatest areal coverage of lavas, but lacks a positive magnetic anomaly. The eastern valley contains a positive magnetic anomaly that extends southward to 70°34'N, overlying both volcanic cones and lower-backscatter seafloor. Using this anomaly to identify the location of the NKR volcanic axis, the NKR and MKR are offset across the Eggvin discontinuity by 36 km, and overlap by 11 km. Backscatter amplitudes of the lavas, however, suggest that recent volcanism has occurred in both valleys, indicating that extension and volcanism may occur over a wider area on the southern NKR than is typical elsewhere on the KR.

Side scan and bathymetry data on either side of Eggvin offset indicate no evidence for a transform fault within the modern discontinuity or preserved in crust as old as 6 Ma to the east and west, indicating that this has been a nontransform discontinuity for at least that long. The off-axis trace of the Eggvin offset is expressed in the regional bathymetry (Figure 3.2) by a >500 m bathymetric step that separates deeper crust that formed on the MKR from shallower NKR crust. The trace of the Eggvin offset extends eastward along a flowline to the Jan Mayen Ridge. These observations suggest that an axial discontinuity has existed between these segments since the

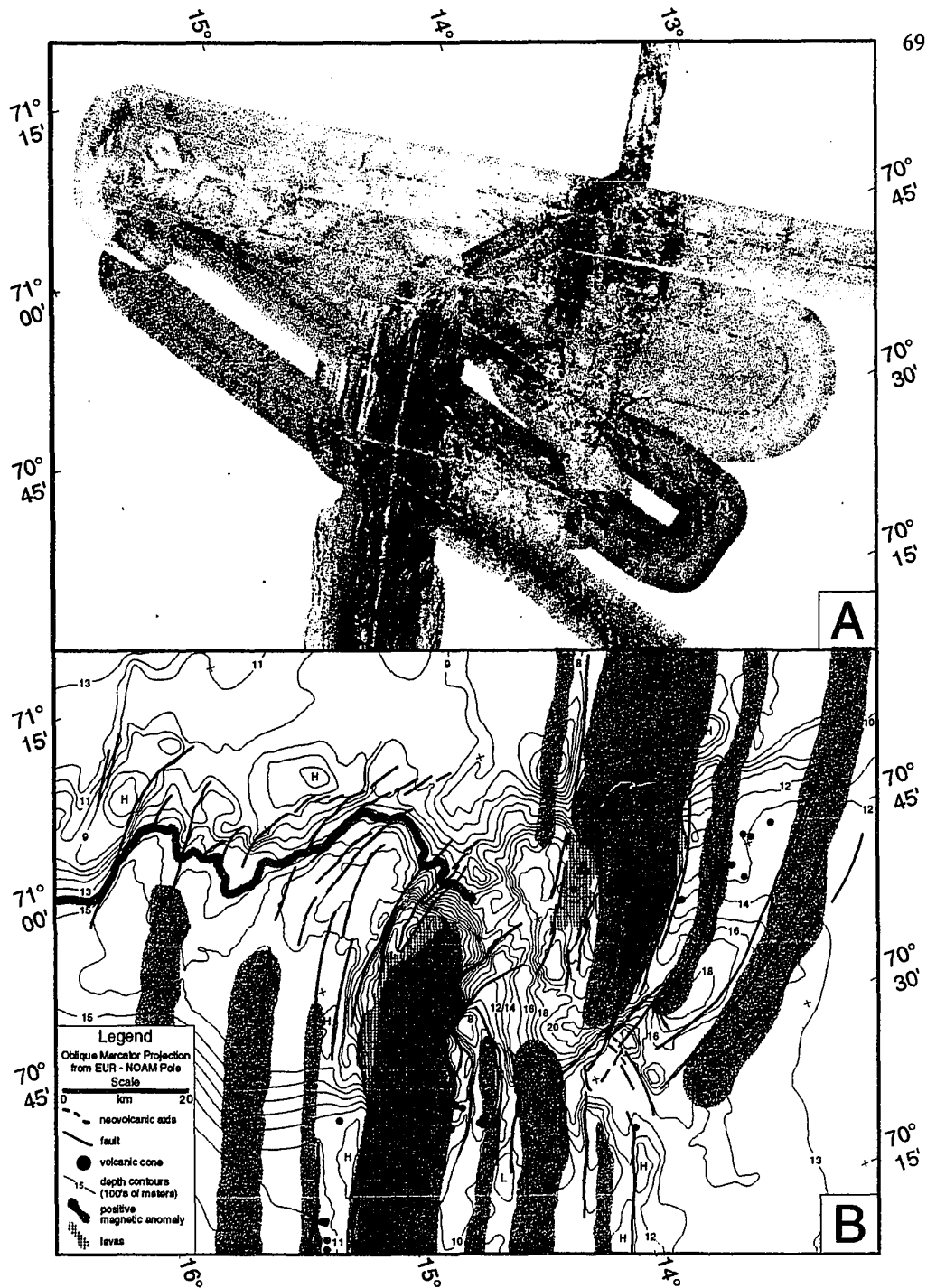


Figure 3.8. SEAMAP acoustic imagery (A) and bathymetry, magnetics, and structure map (B) of Eggvin Offset, a 36 km wide nontransform discontinuity. The absence of transform fault structures off-axis indicates this has been a nontransform discontinuity for at least 6 m.y. The 1400 m contour west of the offset (shaded) marks the approximate position of the discontinuity through time, characterized by two cycles of northward advance and retreat of the MKR.

inception of spreading on the Kolbeinsey Ridge, and that the discontinuity has not migrated significantly along axis over its history.

Despite the long-term stability of the Eggvin offset at this position, the structure of the discontinuity suggests that the opposing ridge tips periodically advance and retreat over a scale of ~10 km. This behavior is suggested by the presence of a pair of reentrants west of the offset that penetrate northward into the shallower NKR crust. Using the 1500 m isobath as an indicator for the northern tip of the MKR through time, two major cycles of advance and retreat of the MKR are evident, with the present ridge tip located ~10 km south of its position at 1 Ma. This behavior may be similar to “dueling” propagators described at the Cobb offset on the Juan de Fuca Ridge and elsewhere [Johnson *et al.*, 1983]. However, it is not clear from our data whether the advance/retreat cycles are driven by the along-strike propagation of one axial magmatic system at the expense of the other, or whether this is a tectonic phenomenon resulting from the shear stresses associated with a large nontransform offset juxtaposed against thick crust.

#### NORTHERN KOLBEINSEY RIDGE (NKR)

The NKR (Figure 3.9) is 125 km long, located between the Eggvin offset and the Jan Mayen transform fault (JMTF). The NKR displays more than 2000 m variation in axial depth, rising to ~500 m near its midpoint before plunging below 2500 m at its intersection with the JMTF (Figure 3.3). The structural complexity of the NKR evident around the Eggvin offset continues north to 71°25'N. Over this distance the available backscatter and magnetic data do not constrain a discrete volcanic axis. This part of the NKR exhibits a central valley 13 to 18 km wide, which contains a 300 m high, low-backscatter topographic ridge. The central valley is bounded laterally by steep inward-facing faults up to 500 m high, and flanking topography (Eggvin Bank) rises to within 25 m of the surface. Faults in the west side of the central valley are linear, and the basin on the west side of the valley is straight and continuous. The east side of the central valley is divided into two basins, separated by a ridge that extends obliquely into the valley from the east. A single swath of side scan imagery over the central valley and medial ridge reveals low backscatter seafloor, and the only evidence for recent volcanism is a cluster of small volcanic cones located in the valley east of the medial ridge between 71°00'N and 71°02'N.

Magnetic data do not indicate the presence of a continuous high-amplitude axial magnetic anomaly along this part of the ridge, although I present a tentative interpretation of the Brunhes anomaly based on limited magnetics coverage (Figure 3.9). The magnetic high that defines the southern axis of the NKR can be traced northward up the south flank of Eggvin Bank, along a path located east of the central valley. This trajectory crosses NE-trending faults and ridges that constitute the east side of the central valley. Positive magnetic values occur within the central valley's west basin, and over the northern parts of the medial ridge and eastern basin. These observations suggest that the Eggvin volcanic edifice is rifting apart in a complex manner, and that recent volcanic activity has not been concentrated along a specific axis.

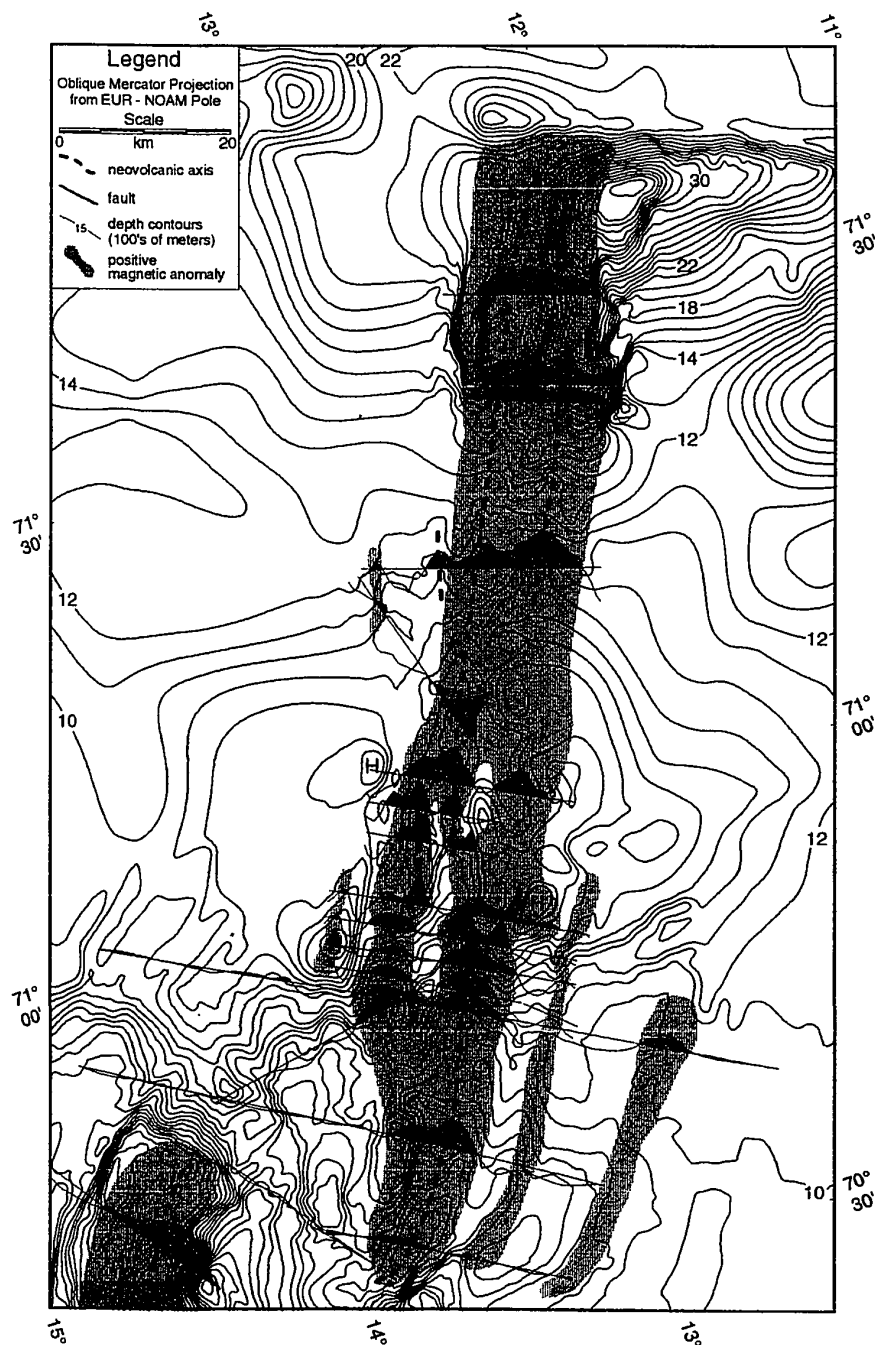


**Figure 3.9.** Bathymetry and magnetics of the northern Kolbeinsey Ridge segment. The shallow southern part of the segment is characterized by a much broader zone of faulting than typical of other KR segments, and the northern volcanic axis contains an exceptionally massive constructional volcanic system. Magnetic tracklines show total field minus IGRF, with inferred positive anomaly stripes shaded gray. Oblique Mercator projection from NOAM/EUR pole. Contour interval is 100 m, annotated in hundreds of meters.

North of 71°25'N the spreading axis is clearly expressed in both bathymetry and magnetic data, and occupies a robust volcanic ridge within an 18 km wide axial valley. The volcanic ridge appears to fill most of the axial valley, and is more than 1000 m high. The axial volcanic ridge bends eastward north of 71°37'N, and at its intersection with the JMTF (71°42'N, 12°00'W) the axial strike is nearly parallel with that of the transform. The east side of the axial valley is consistently deeper than the west, and reaches a maximum depth of 3900 m immediately southeast of the RTI.

## DISCUSSION

### *Structural and Geochemical Axial Segmentation*

All midocean ridges exhibit structural segmentation over a range of length scales, although the physical manifestation of segmentation differs between fast- and slow-spreading ridges. Detailed mapping on the slow-spreading Mid-Atlantic Ridge has revealed a hierarchy of spreading center segmentation based on the morphology of axial discontinuities [Sempéré *et al.*, 1990; Fox *et al.*, 1991; Grindlay *et al.*, 1991, Macdonald *et al.*, 1991]. The scale of a discontinuity has been related to its longevity and spatial stability. First-order discontinuities, which are the largest and most stable type within the hierarchy, are defined by transform faults [Macdonald *et al.*, 1991; Sempéré *et al.*, 1993]. Transform faults are typically greater than 20-30 km wide, exhibit age offsets greater than 2 Ma, and coincide with the deepest parts of axial depth profiles. Relative motion between the opposing lithospheric plates is accommodated across a relatively narrow (1-5 km wide) fault zone that follows a small circle about the NUVEL-1 relative pole of rotation [DeMets *et al.*, 1990], and within this zone transform motion is often concentrated along a single fault [Macdonald *et al.*, 1986; Tucholke and Schouten, 1988]. On the KR, the JMTF is a first-order discontinuity, and is the only transform fault observed between Iceland and the north end of the Kolbeinsey Ridge. South of Iceland, the closest transform fault is the Bight Transform at the southern end of the Reykjanes Ridge (56°47'N). Transform faulting is not observed subaerially on Iceland, making the total distance along the spreading axis without a transform fault roughly 2,200 km.

Second through fourth-order discontinuities occur at nontransform offsets, with higher order correlating to progressively smaller offset, decreasing disruption of axial valley boundary faults, smaller axial depth anomalies and shorter life spans. Second-order discontinuities disrupt axial boundary faulting, leave a wake of disrupted topography off axis, and often migrate along axis. The neovolcanic zone is typically offset 15 to 30 km across second-order offsets, and horizontal shear between offset ridge tips is distributed throughout the overlap zone rather than concentrated along a single transform. The Spar and Eggvin nontransform offsets are second-order discontinuities that exhibit different migration histories. The Spar offset has migrated along axis since anomaly 3A, first towards the south and more recently towards the north. The Eggvin offset is inferred to have remained near its present position throughout its history, although variations of ~ 10 km are inferred to have occurred over periods of < 1 m.y. On the SKR, I consider the 68°43'N offset to be a second-order discontinuity based on its inferred history

of propagation and the disruption evident in the axial boundary faults observed south of the offset. The degree of separation between the offset volcanic zones (4 km) is much less than typically observed at second-order discontinuities, however.

Third-order discontinuities are similar but smaller (< 10 km offset, < 200 m axial depth anomaly) than second order discontinuities, and do not disrupt axial boundary faults or leave off-axis trails of disrupted topography. These offsets may therefore be either shorter-lived features, or they may be incipient second-order offsets. The 70°00'N and 70°31'N discontinuities on the MKR are third-order offsets. Fourth-order discontinuities are small (< 4 km) offsets of the volcanic axis that probably represent ephemeral discontinuities between adjacent volcanic systems within the axial valley. On axial volcanic ridges, fourth-order discontinuities correspond to changes in orientation or gaps between ridges. The middle MKR segment exhibits morphological changes at 70°10'N and 70°27'N that correspond with slight changes in strike, and probably represent fourth-order segments.

Analyses of rocks dredged from the KR suggest that the observed structural segmentation of the KR may correspond with geochemical segmentation. Structural segmentation on fast spreading ridges usually corresponds with magmatic segmentation across first- through third-order discontinuities [Langmuir *et al.*, 1986; Sinton *et al.*, 1991], although on slow spreading centers the relationship between structural and magmatic segmentation is not as well known due to insufficient sampling density [Sempéré *et al.*, 1993]. On Kolbeinsey Ridge, Pb isotope values definitively indicate that no Icelandic plume component is involved in Kolbeinsey Ridge magmatism [Mertz *et al.*, 1991]. Rare-earth element (REE) patterns abruptly change at the Tjörnes offset from the enriched patterns typical of Iceland to light REE-depleted patterns more typical of normal MORB [Schilling, 1986]. Therefore the Tjörnes offset defines a geochemical boundary as well as a structural discontinuity. Based on La/Sm ratios, Schilling [1986] divides KR basalts into "normal" and "plume" groups separated by a boundary between 70°40'N and 71°04'N, which is the location of the Eggvin nontransform offset, suggesting that Eggvin offset may also define a geochemical segment boundary. These observations are consistent with a model of coincident magmatic and structural segmentation, although the geochemical inferences are based on a very small sample size north of 70°N and must be regarded as preliminary.

#### *Axial volcanism on the MKR*

Axial volcanism on the Kolbeinsey Ridge is manifested in three general forms, axial volcanic ridges, circular volcanoes, and high-backscatter pavements that probably represent low-relief lava flows. The most areally significant are the axial volcanic ridges of the middle and northern MKR and on the NKR north of 71°30'N, which I estimate to contain ~63, ~29 and 185 km<sup>2</sup> of material, respectively. Axial volcanic ridges are in some places composed of many small individual volcanic cones, such as on the northern NKR where the surface of the ridge is peppered with circular volcanoes 2 to 4 km in diameter. On the middle MKR segment, the southern axial ridge also appears to be mostly composed of a mosaic of volcanic cones.

Elsewhere, such as on the central part of the middle and northern MKR segments, the axial volcanic ridges appear more massive, containing smaller subsidiary ridges along their flanks and crest, although few circular cones. On the MKR, volcanic cones are observed individually and as parts of volcanic ridges, but in general are concentrated near the tips of each segment.

Small circular volcanoes are the dominant small scale volcanic morphotype within the axial valley elsewhere on the slow-spreading Mid-Atlantic Ridge [Smith and Cann, 1990; 1992; 1993]. The predominance of small volcanoes is thought to result from low magma flux in conjunction with rapid convective cooling, which limit the size of magma bodies, the proximity to the surface a magma batch can rise, and the rate at which it can be erupted [Nisbet and Fowler, 1978; Smith and Cann, 1993]. In contrast, fast spreading ridges are characterized by low-relief flows typical of low-viscosity magmas, fast eruption rates and/or large volumes of lava [Bonatte and Harrison, 1988]. The observed distribution of volcanic morphologies on the KR suggests significant along-strike variation in the processes controlling volcanism. The distribution of volcanic cones on the KR suggests that the tips of the segments are the only areas where the formation of individual volcanoes is favored, suggesting that these regions experience either lower magma flux, a greater degree of hydrothermal cooling, or both. The axial valley of the central part of the southern MKR is characterized by a high-backscatter floor (indicative of unsedimented lavas) but lacks discrete volcanic cones or even low-relief constructional volcanic topography. This region lies on the shallowest part of the southern MKR, where the thickest crust and highest magma supply is predicted [Lin *et al.*, 1990; Sempéré *et al.*, 1993]. By analogy with fast-spreading ridges, this region may be paved with low-viscosity lavas that issue from eruptive fissures too small to be resolved in our acoustic imagery. An alternate possibility is that this segment is experiencing a phase of amagmatic extension [e.g. Tucholke and Lin, 1994]. However, the high backscatter within the narrow axial valley and the gross morphology of this southern MKR are not characteristic of a magmatically-starved slow spreading ridge. The central part of the middle MKR also lacks volcanic cones, although a well-developed axial volcanic ridge is present, which probably results from focused volcanic activity along a fissure or fissure system.

*The NKR, and Eggvin Bank: Implications for the Jan Mayen hotspot*

The NKR bisects Eggvin bank, and shallow crust extends laterally on either side of the spreading axis. The regional bathymetry shows that a plateau lies between the NKR axis and Jan Mayen island. The plateau is bounded on the north by the JMTF, and exhibits a nearly consistent width of 125 km (measured north to south). The bathymetric step at the southern side of the plateau follows a small circle eastward from the Eggvin offset, which I use as evidence to suggest that the Eggvin offset has existed since the inception of spreading on the northern KR. A corollary to this interpretation is that the shallow crust south of JMTF was generated at the NKR spreading center, and the bathymetric expression of this crust implies that the NKR axis has been anomalously shallow over its entire history.

Present knowledge of the geochemistry of NKR is based on four samples dredged from two locations between the Eggvin offset and Jan Mayen transform fault (Figure 3.9). These rocks exhibit enriched light rare-earth element patterns, and are enriched in large-ion lithophile elements (La, P, and K) indicative of a mantle plume source, which *Schilling et al.* [1983] named the Jan Mayen hotspot. The morphology of the plateau leads us to propose that the source of the geochemical anomaly is located beneath the NKR, and the shallow bathymetry of the plateau represents the trace of the hotspot. The name of the hotspot is somewhat unfortunate, because it implies the plume source lies beneath Jan Mayen Island. If Jan Mayen Island is the focus of the plume source, and assuming the mantle plume is stationary and not a nascent feature, I would expect to see a hotspot trace extending in the direction of plate motion. This is not observed. The nature of Jan Mayen Island remains enigmatic, in that it contains active volcanoes [Imsland, 1986], and is located south of the JMTF on the north end of the Jan Mayen Ridge. The Jan Mayen Ridge is a crustal sliver that was rifted off the east coast of Greenland at the inception of spreading on the KR, and therefore Jan Mayen Island may overlie and have erupted through rocks of the Jan Mayen Ridge, which contains an upper continental rise sedimentary sequence several hundred meters thick [Talwani and Eldholm, 1977; Gairaud et al., 1978] that overlies crystalline rock that may be either continental [Johnson et al., 1972] or oceanic [Talwani and Eldholm, 1977] in provenance, and probably contains flood basalts associated with the opening of the KR [Nunns, 1982]. Volcanism on Jan Mayen has been attributed to a leaky transform [Imsland, 1986] and to the proximity of the Mohns/JMTF ridge-transform intersection [Sylvester, 1975].

## CONCLUSIONS

Our new maps of the axial structure of Kolbeinsey Ridge from the Spar offset to the Jan Mayen Transform, in conjunction with a synthesis of existing bathymetry and magnetic data, constrain the location and nature of the spreading axis. Our observations support the following conclusions:

1. The Kolbeinsey Ridge is divided into three major segments (southern, middle, and northern). Major segment boundaries are characterized by depth maxima in the axial profile, which correspond to large axial discontinuities at 69°00'N (the Spar offset) and 70°40'N (the Eggvin offset). The SKR and MKR are further subdivided by smaller offsets; on the NKR fine-scale segmentation cannot be resolved from the available data. The geochemistry of the small number of rock samples from KR is compatible with a model of coincident structural and geochemical segment boundaries.
2. The Spar offset is a 34 km wide nontransform discontinuity that has evolved via propagation events on the opposing ridge segments. The first event involved the southward propagation of the MKR, which stalled south of the present offset ~ 3 Ma. The second event involved the northward propagation of the SKR sometime after 2.8 Ma. Structural data from acoustic imagery indicate that northward propagation occurred incrementally, characterized by three discrete northward advancements of the SKR tectonic tip.

4. The Eggvin offset is a 36 km wide right-stepping nontransform offset. This discontinuity has existed as a nontransform offset for at least 6 my, and is inferred to have persisted at this location since the inception of spreading on the KR.
3. Small offsets are inferred to have migrated along axis. On the SKR, the 68°43'N discontinuity has moved northward at an average rate of 10 km/m.y. for ~ 8 my. On the MKR, the discontinuity at 70°00'N is inferred to have recently formed as the result of the rapid growth of a new volcanic ridge that extends northward from the southern MKR.
5. The NKR is shallow, volcanically robust, and contains rocks that exhibit plume-like geochemical characteristics. Shallow seafloor extends from NKR to Jan Mayen Island, east of which the depth increases. This morphology indicates that if a distinct Jan Mayen hotspot exists, it probably lies beneath the NKR rather than Jan Mayen Island. This inference is compatible with the available geochemical data for the NKR.
6. No transform faults exist between Iceland and the north end of the Kolbeinsey Ridge. South of Iceland, the closest transform fault is the Bight Transform at the southern end of the Reykjanes Ridge (56°47'N). Transform faulting is not observed subaerially on Iceland, making the total distance along the spreading axis without a transform fault roughly 2,200 km.

## REFERENCES

- Appelgate, B., and A.N. Shor, The northern Mid-Atlantic and Reykjanes Ridges: Spreading center morphology between 55°50'N and 63°00'N, *Journal of Geophysical Research*, 99, 17935-17956, 1994.
- Batiza, R., and D. Vanko, Volcanic development of small oceanic central volcanoes on the flanks of the East Pacific Rise inferred from narrow-beam echo-sounder surveys, *Marine Geology*, 54, 53-90, 1983.
- Bell, R.E., and W.R. Buck, Crustal control of ridge segmentation inferred from observations of the Reykjanes Ridge, *Nature*, 357, 583-586, 1992.
- Berggren, W.A., D.V. Kent, J.J. Flynn, and J.A. VanCouvering, Cenozoic geochronology, *Geological Society of America Bulletin*, 96, 1407-1418, 1985.
- Bergman, E.A., and S.C. Solomon, Earthquake swarms on the Mid-Atlantic Ridge: Products of magmatism or extensional tectonics?, *J. Geophys. Res.*, 95, 4943-4965, 1990.
- Blackinton, J.G., D.M. Hussong, and J. Kosalos, First results from a combination side-scan and seafloor mapping system (SeaMARC II), in *15th Annual Offshore Technology Conference*, pp. 307-314, Houston, Texas, 1983.
- Bogdanov, Y.A., A.M. Sagalevich, M.I. Kuz'min, and A.P. Kuznetsov, Geologic structure of the rift zone of the Reykjanes Ridge at 58°N, *Oceanology*, 1985.
- Bonatti, E., and C.G.A. Harrison, Eruption styles of basalt in oceanic spreading ridges and seamounts: Effect of magma temperature and viscosity, *Journal of Geophysical Research*, 93, 2967-2980, 1988.
- Carbotte, S., S.M. Welch, and K.C. Macdonald, Spreading rates, rift propagation, and fracture zone offset histories during the past 5 my on the Mid-Atlantic Ridge; 25°-27°30'S and 31°-34°30'S, *Marine Geophysical Researches*, 13, 51-80, 1991.
- Chadwick, W.W., R.W. Embley, and C.G. Fox, Evidence for volcanic eruption on the southern Juan de Fuca Ridge between 1981 and 1987, *Nature*, 350, 416-418, 1991.
- Cormier, M.H., and K.C. Macdonald, East Pacific Rise 18°-19°S: Asymmetric spreading and ridge reorientation by ultrafast migration of axial discontinuities, *Journal of Geophysical Research*, 99, 543-564, 1994.
- Crane, K., The spacing of rift axis highs: Dependence upon diapiric processes in the underlying asthenosphere?, *Earth and Planetary Science Letters*, 72, 405-414, 1985.
- Crane, K., L.E. Johnson, B. Appelgate, R. Buck, C. Jones, E.G. Gurvich, L. Moscalev, A.V. Gebruk, V.N. Lukashin, S.V. Luk'yanov, A.D. Scherbinin, V.V. Serova, and M.V. Rudenko, Investigating the Reykjanes Ridge near 59°50'N with the Russian Mir submersibles (abstract), *Eos Trans. AGU*, 73, Fall Meeting Suppl. (43), 530, 1992.
- Dauteuil, O., and J.-P. Brun, Oblique rifting in a slow-spreading ridge, , 361, 145-148, 1993.

- Davis, R., S. Zisk, M. Simpson, M. Edwards, A. Shor, and E. Halter, Hawaii Mapping Research Group bathymetric and sidescan data processing, *International Conference on Signal Processing and Technology*, 77, 777, 1992.
- de Moustier, C., P.F. Lonsdale, and A.N. Shor, Simultaneous operation of the Sea Beam multibeam echo-sounder and the SeaMARC II bathymetric sidescan sonar system, *IEEE Journal of Oceanic Engineering*, 15, 84-94, 1990.
- Delaney, J.R., H.P. Johnson, and J.L. Karsten, The Juan de Fuca - hot spot - propagating rift system: New tectonic, geochemical, and magnetic data, *Journal of Geophysical Research*, 86, 11747-11750, 1981.
- DeMets, C., R.G. Gordon, D.F. Argus, and S. Stein, Current plate motions, *Geophys. J. Int.*, 101, 425-478, 1990.
- Devey, C.W., C.-D. Garbe-Schönberg, P. Stoffers, C. Chauvel, and D.F. Mertz, Geochemical effects of dynamic melting beneath ridges: Reconciling major and trace element variations in Kolbeinsey ( and global) mid-ocean ridge basalt, *Journal of Geophysical Research*, 99, 9077-9095, 1994.
- Edwards, M.H., The morphotectonic fabric of the East Pacific Rise: Implications for fault generation and crustal accretion, Ph. D. dissertation thesis, Columbia University, 1991.
- Edwards, M.H., D.J. Fornari, A. Malinverno, W.B.F. Ryan, and J. Madsen, The regional tectonic fabric of the East Pacific Rise from 12°50'N to 15°10'N, *Journal of Geophysical Research*, 96, 7995-8017, 1991.
- Einarsson, P., Earthquakes and present-day tectonism in Iceland, *Tectonophysics*, 189, 261-279, 1991.
- Embley, R.W., and W.W. Chadwick, Volcanic and hydrothermal processes associated with a recent phase of seafloor spreading at the northern Cleft segment: Juan de Fuca Ridge, *Journal of Geophysical Research*, in press, 1994.
- Farr, H.K., Multibeam bathymetric sonar: Sea Beam and Hydrochart, *Marine Geodesy*, 4, 77-93, 1980.
- Fleischer, U., The Reykjanes Ridge: A summary of geophysical data, in *Geodynamics of Iceland and the North Atlantic Area*, edited by Kristjánsson, pp. 17-31, Reidel, Holland, 1974.
- Fox, P.J., N.R. Grindlay, and K.C. Macdonald, The Mid-Atlantic Ridge (31°S-34°30'S): Temporal and spatial variations of accretionary processes, *Marine Geophysical Researches*, 13, 1-20, 1991.
- Gairaud, H., G. Jacquart, F. Aubertin, and P. Beuzart, The Jan Mayen Ridge: Synthesis of geological knowledge and new data, *Oceanologica Acta*, 1, 334-358, 1978.
- Gardner, J.V., M.E. Field, H. Lee, B.E. Edwards, D.G. Masson, N. Kenyon, and R.B. Kidd, Ground-truthing 6.5kHz side scan sonographs: What are I really imaging?, *Journal of Geophysical Research*, 96, 5955-5974, 1991.
- Goslin, J., and D. Aslanian, Asymmetry of the mantle structure beneath the Mid-Atlantic Ridge, *Geophysical Research Letters*, 19, 1165-1168, 1992.

- Grant, J.A., and R. Schreiber, Modern swath sounding and sub-bottom profiling technology for research applications: The Atlas Hydrosweep and Parasound systems, *Marine Geophysical Researches*, 12, 9-20, 1990.
- Grindlay, N.R., P.J. Fox, and K.C. Macdonald, Second-order ridge axis discontinuities in the South Atlantic: Morphology, structure, and evolution, *Marine Geophysical Researches*, 13, 21-49, 1991.
- Gudmundsson, A., S. Brynjolfsson, and M.T. Jonsson, Structural analysis of a transform fault-rift zone junction in North Iceland, *Tectonophysics*, 220, 205-221, 1993.
- Hagen, R.A., N.A. Baker, D.F. Naar, and R.N. Hey, SeaMARC II survey of recent submarine volcanism near Easter Island, *Marine Geophysical Researches*, 12, 297-315, 1990.
- Hammond, S.R., and J.R. Delaney, Evolution of Axial Volcano, Juan de Fuca Ridge (abstract), *Eos Trans. AGU*, 66, 925, 1985.
- Hey, R., F.K. Duennebieer, and W.J. Morgan, Propagating rifts on midocean ridges, *Journal of Geophysical Research*, 85, 3647-3658, 1980.
- Hey, R.N., M.C. Kleinrock, S.P. Miller, T.M. Atwater, and R.C. Searle, Sea Beam/deep-tow investigation of an active oceanic propagating rift system, Galapagos 95.5°W, *Journal of Geophysical Research*, 91, 3369-3393, 1986.
- Hey, R.N., J.M. Sinton, and F.K. Duennebieer, Propagating rifts and spreading centers, in *The Eastern Pacific Ocean and Hawaii*, edited by E.L. Winterer, D.M. Hussong, and R.W. Decker, pp. 161-176, Geological Society of America, 1989.
- Hey, R.N., and P.R. Vogt, Spreading center jumps and sub-axial asthenosphere flow near the Galapagos hotspot, *Tectonophysics*, 37, 41-52, 1977.
- Hey, R.N., and D.S. Wilson, Propagating rift explanation for the tectonic evolution of the northeast Pacific-the pseudomovie, *Earth and Planetary Science Letters*, 58, 167-188, 1982.
- Imsland, P., The volcanic eruption on Jan Mayen, January 1985: Interaction between a volcanic island and a fracture zone, *Journal of Volcanology and Geothermal Research*, 28, 45-53, 1986.
- Jackson, D.R., D.P. Winebrenner, and A. Ishimaru, Application of the composite roughness model to high-frequency bottom backscattering, *Journal of the Acoustical Society of America*, 79, 1410-1422, 1986.
- Jacoby, W.R., Morphology of the Reykjanes Ridge crest near 62°N, *Journal of Geophysics*, 47, 81-85, 1980.
- Johnson, G.L., J.R. Southall, P.W. Young, and P.R. Vogt, Origin and structure of the Iceland Plateau and the Kolbeinsey Ridge, *Journal of Geophysical Research*, 77, 5688-5696, 1972.
- Johnson, G.L., P.R. Vogt, and E.D. Schneider, Morphology of the northeastern Atlantic and Labrador Sea, *German Hydrographic Journal*, 24, 49-73, 1971.
- Johnson, H.P., J.L. Karsten, J.R. Delaney, E.E. Davis, R.G. Currie, and R.L. Chase, A detailed study of the Cobb Offset of the Juan de Fuca Ridge: Evolution of a propagating rift, *Journal of Geophysical Research*, 88, 2297-2315, 1983.

- Johnson, L.E., Small scale geochemical variation on the Reykjanes Ridge between 59°43'N and 59°55'N (abstract), , 73, *Fall Meeting Suppl.*, 605, 1992.
- Joseph, D., B. Taylor, and A. N. Shor, New sidescan sonar and gravity evidence that the Nova-Canton Trough is a fracture zone, *Geology*, 20, 1992.
- Kappel, E., and W.B.F. Ryan, Volcanic episodicity and a non-steady state rift valley along the northeast Pacific spreading centers: Evidence from SeaMARC I, *Journal of Geophysical Research*, 91, 13925-13940, 1986.
- Karson, J.A., and P.A. Rona, Block-tilting, transfer faults, and structural control of magmatic and hydrothermal processes in the TAG area, Mid-Atlantic Ridge 26°N, *Geological Society of America Bulletin*, 102, 1635-1645, 1990.
- Klein, E.M., and C.H. Langmuir, Global correlations of ocean ridge basalt chemistry with axial depth and crustal thickness, *Journal of Geophysical Research*, 92, 8089-8115, 1987.
- Kleinrock, M.C., and R.N. Hey, Detailed tectonics near the tip of the Galapagos 95.5°W propagator: How the lithosphere tears and a spreading axis develops, *Journal of Geophysical Research*, 94, 13801-13838, 1989.
- Kleinrock, M.C., B.E. Tucholke, J. Lin, and M.A. Tivey, The trace of non-transform offsets and the evolution of Mid-Atlantic Ridge spreading segments between 25°25'N and 27°10'N over the past 30 m.y. (abstract), *Eos Trans. AGU*, 73, 538, 1992.
- Lachenbruch, A.H., and G.A. Thompson, Oceanic ridges and transform faults: Their intersection angles and resistance to plate motion, *Earth and Planetary Science Letters*, 15, 116-122, 1972.
- Lackschewitz, K.S., J. Dehn, and H.J. Wallrabe-Adams, Volcaniclastic sediments from mid-oceanic Kolbeinsey Ridge, north of Iceland: Evidence for submarine volcanic fragmentation processes, *Geology*, 22, 975-978, 1994.
- Langmuir, C.H., J.F. Bender, and R. Batiza, Petrological and tectonic segmentation of the East Pacific Rise, 5°30'-14°30'N, *Nature*, 322, 422-429, 1986.
- Larsen, H.C., A multiple and propagating rift model for the NE Atlantic, in *Early Tertiary Volcanism and the Opening of the NE Atlantic*, edited by A.C. Morton, and L.M. Parson, pp. 157-158, Geological Society of London, London, 1988.
- Laughton, A.S., R.C. Searle, and D.G. Roberts, The Reykjanes Ridge crest and the transition between its rifted and non-rifted regions, *Tectonophysics*, 55, 173-177, 1979.
- Lawson, K., R.C. Searle, J.A. Pearce, R.B. Owens, S. Allerton, P. Browning, P. Kempton, C. Mevel, B. Murton, and H. Schouten, High resolution imaging and sampling of the Mid-Atlantic Ridge north of Kane Transform [MARNOK] (abstract), *Eos Trans. AGU*, 72, *Fall Meeting Suppl.*, 476, 1991.
- Lewis, B.T.R., Periodicities in volcanism and longitudinal magma flow on the East Pacific Rise at 23°N, *Geophysical Research Letters*, 6, 753-756, 1979.
- Lin, J., G.M. Purdy, H. Schouten, J.-C. Sempéré, and C. Zervas, Evidence from gravity data for focused magmatic accretion along the Mid-Atlantic Ridge, *Nature*, 344, 627-632, 1990.

- Lin, J., B.E. Tucholke, M.C. Kleinrock, and J.A. Goff, Variations in crustal faulting and magmatic accretion along the Mid-Atlantic Ridge and off-axis: Results from the western flank of the MAR at 25-27 Deg N (abstract), *Eos Trans. AGU*, 73, 538, 1992.
- Lingsch, S., Quantitative comparison of two swath bathymetry systems: Sea Beam and SEAMAP, in *Oceans 94*, pp. 265-275, IEEE Oceanic Engineering Society, Washington DC, 1994.
- Lonsdale, P., Segmentation of the Pacific-Nazca spreading center, 1°N-20°S, *Journal of Geophysical Research*, 94, 12197-12225, 1989.
- Lonsdale, P., Geomorphology and structural segmentation of the crest of the southern (Pacific-Antarctic) East Pacific Rise, *Journal of Geophysical Research*, 99, 4683-4702, 1994.
- Macdonald, K., J.C. Sempere, and P.J. Fox, East Pacif Rise from Siqueiros to Orozco Fracture Zones: Along-strike continuity of axial neovolcanic zone and structure and evolution of overlapping spreading centers, *Journal of Geophysical Research*, 89, 6049-6069, 1984.
- Macdonald, K.C., D.A. Castillo, S.P. Miller, P.J. Fox, K.A. Kastens, and E. Bonatti, Deep-Tow studies of the Vema Fracture Zone; Tectonics of a major slow slipping transform fault and its intersection with the Mid-Atlantic Ridge, *Journal of Geophysical Research*, 91, 3334-3354, 1986.
- Macdonald, K.C., P.J. Fox, S. Miller, S. Carbotte, M.H. Edwards, M. Eisen, D.J. Fornari, L. Perram, R. Pockalny, D. Scheirer, S. Tighe, C. Weiland, and D. Wilson, The East Pacific Rise and its flanks 8°-18°N: History of segmentation, propagation, and spreading direction based on SeaMARC II and Sea Beam studies, *Marine Geophysical Researches*, 14, 299-344, 1992.
- Macdonald, K.C., D.S. Schierer, and S.M. Carbotte, Mid-ocean ridges: Discontinuities, segments, and giant cracks, *Science*, 253, 986-994, 1991.
- Macdonald, K.C., J.C. Sempere, P.J. Fox, and R. Tyce, Tectonic evolution of ridge-axis discontinuities by the meetin, linking, or self-decapitation of neighboring ridge segments, *Geology*, 15, 993-997, 1987.
- Malinverno, A., A quantitative study of the axial topography of the Mid-Atlantic Ridge, *Journal of Geophysical Research*, 95, 2645-2660, 1990.
- Matsumoto, H., Characteristics of SeaMARC II phase data, *IEEE Journal of Oceanic Engineering*, 15, 350-360, 1990.
- McMaster, R.L., J.G. Schilling, and P.R. Pinet, Plate boundary within Tjörnes Fracture Zone on northern Iceland's insular margin, *Nature*, 269, 663-668, 1977.
- Mertz, D.F., C.W. Devey, W. Todt, P. Stoffers, and A.W. Hofmann, Sr-Nd-Pb isotope evidence against plume-asthenosphere mixing north of Iceland, *Earth and Planetary Science Letters*, 107, 243-255, 1991.
- Minster, J.B., and T.H. Jordan, Present-day plate motions, *Journal of Geophysical Research*, 83, 5331-5354, 1978.
- Müller, R.D., and W.R. Roest, Fracture zones in the North Atlantic from combined Geosat and Seasat data, *Journal of Geophysical Research*, 97, 3337-3350, 1992.

- Murton, B.J., and L.M. Parson, Magmatic and tectonic relationships at oblique spreading centers: Evidence for mantle controls on axial valley morphology (abstract), *Eos Trans. AGU*, 72, Fall Meeting Suppl., 455, 1991.
- Murton, B.J., and L.M. Parson, Segmentation, volcanism and deformation of oblique spreading centres: A quantitative study of the Reykjanes Ridge, *Tectonophysics*, 222, 237-257, 1993.
- Nisbet, E.G., and C.M.R. Fowler, The Mid-Atlantic Ridge at 37° and 45°N: Some geophysical and petrological constraints, *Geophysical Journal of the Royal Astronomical Society*, 54, 631-660, 1978.
- Nishimura, C.E., P.R. Vogt, L. Smith, and J.D. Boyd, Investigation of a possible underwater volcanic eruption on the Reykjanes Ridge by airborne sonobuoys and AXBT's, *Eos Trans. AGU*, 70, 1301, 1989.
- Nunns, A., The structure and evolution of the Jan Mayen Ridge and surrounding regions, in *Studies in Continental Margin Geology, AAPG Memoir 34*, edited by J.S. Watkin, and C.L. Drake, American Association of Petroleum Geologists, 1982.
- Nunns, A.G., Plate tectonic evolution of the Greenland-Scotland Ridge and surrounding regions, in *Structure and Development of the Greenland-Scotland Ridge*, edited by M.H.P. Bott, S. Saxov, M. Talwani, and J. Thiede, pp. 11-30, Plenum, New York, 1983.
- Olafsson, J., K. Thors, U. Stefansson, S.P. Jakobsson, W.J. Jenkins, F.T. Manheim, R.F. Commeau, and R.R. Jones, Geochemical observations from a boiling hydrothermal site on the Kolbeinsey Ridge (abstract), *Eos Trans. AGU*, 71, 1650, 1990.
- Oldenburg, D.W., and J.N. Brune, An explanation for the orthogonality of ocean ridges and transform faults, *Journal of Geophysical Research*, 80 (17), 2575-2585, 1975.
- Owens, R.B., R.C. Searle, P. Field, L.M. Parson, and S. Spencer, The first non-transform offset on the Reykjanes Ridge (abstract), *Eos Trans. AGU*, 72, Fall Meeting Suppl., 467-468, 1991.
- Parmentier, E.M., and J. Phipps Morgan, Spreading rate dependence of three-dimensional structure in oceanic spreading centres, *Nature*, 348, 325-328, 1990.
- Parson, L.M., B.J. Murton, R.C. Searle, D. Booth, J. Evans, P. Field, J. Keeton, A. Laughton, E. McAllister, N. Millard, L. Redbourne, I. Rouse, A. Shor, D. Smith, S. Spencer, C. Summerhayes, and C. Walker, En echelon volcanic ridges at the Reykjanes Ridge: A life cycle of volcanism and tectonics, *Earth and Planetary Science Letters*, 117, 73-87, 1993.
- Phipps Morgan, J., and Y.J. Chen, Dependence of ridge-axis morphology on magma supply and spreading rate, *Nature*, 364, 706-708, 1993.
- Phipps Morgan, J., and E.M. Parmentier, Causes and rate-limiting mechanisms of ridge propagation: A fracture mechanics model, *Journal of Geophysical Research*, 90, 8603-8612, 1985.
- Pockalny, R.A., and P. Gente, A model for the segmentation characteristics of a slowly spreading mid-ocean ridge (abstract), *Eos*, 73, 569, 1992.
- Pollard, D.D., and A. Aydin, Propagation and linkage of oceanic ridge segments, *Journal of Geophysical Research*, 89, 10017-10028, 1984.

- Purdy, G.M., J.-C. Sempéré, H. Schouten, D.L. DuBois, and R. Goldsmith, Bathymetry of the Mid-Atlantic Ridge, 24°-31°N: A map series, *Marine Geophysical Researches*, 12, 247-252, 1990.
- Rabinowicz, M., S. Rouzo, J.-C. Sempéré, and C. Rosemberg, Three-dimensional mantle flow beneath mid-ocean ridges, , 98, 7851-7870, 1993.
- Renard, V., and J.-P. Allenou, Seabeam, multi-beam echo-sounding in *Jean Charcot*: Description, evaluation, and first results, *International Hydrographic Review of Monaco*, 56, 35-67, 1979.
- Rognstad, M., HAWAII MRI: A new underwater mapping tool, in *International Conference on Signal Processing and Technology*, pp. 900-905, 1992.
- RRISP Working Group, Reykjanes Ridge Iceland Seismic Experiment (RRISP 77), *Journal of Geophysics*, 47, 228-238, 1980.
- Rudenko, M.V., Geomorphology of the rift zone of the Reykjanes Ridge at 58°30'N, *Oceanology*, 26, 475-480, 1986.
- Sæmundsson, K., Evolution of the axial rifting zone in northern Iceland and the Tjörnes Fracture Zone, *Geological Society of America Bulletin*, 85, 495-504, 1974.
- Schilling, J.-G., Iceland mantle plume: Geochemical evidence along Reykjanes Ridge, *Nature*, 242, 565-571, 1973.
- Schilling, J.-G., Geochemical and isotopic variation along the Mid-Atlantic Ridge axis from 79°N to 0°N, in *The Western North Atlantic Region*, edited by P.R. Vogt, and B.E. Tucholke, pp. 137-156, Geological Society of America, 1986.
- Schilling, J.-G., M. Zajac, R. Evans, T. Johnston, W. White, J.D. Devine, and R. Kingsley, Petrologic and geochemical variations along the Mid-Atlantic Ridge from 29°N to 73°N, *American Journal of Science*, 283, 510-586, 1983.
- Schilling, J.G., R.H. Kingsley, and J.D. Devine, Galapagos hotspot-spreading center system; 1, Spatial, petrological and geochemical variations (83°W-101°W), *Journal of Geophysical Research*, 86, 5593-5610, 1982.
- Schouten, H., H.J.B. Dick, and K.D. Clitgord, Migration of mid-ocean-ridge volcanic segments, *Nature*, 326, 835-839, 1987.
- Schouten, H., K.D. Klitgord, and J.A. Whitehead, Segmentation of mid-ocean ridges, *Nature*, 317, 225-229, 1985.
- Searle, R.C., P.R. Field, and R.B. Owens, Segmentation and a non-transform ridge offset on the Reykjanes Ridge near 58°N, *Journal of Geophysical Research*, 98, 1123-1134, 1994.
- Searle, R.C., and A.S. Laughton, Fine-scale sonar study of tectonics and volcanism on the Reykjanes Ridge, *Oceanologica Acta*, 4 (supplement), 5-13, 1981.
- Sempéré, J.-C., J. Lin, H.S. Brown, H. Schouten, and G.M. Purdy, Segmentation and morphotectonic variations along a slow-spreading center: The Mid-Atlantic Ridge (24°00'N-30°40'N), *Marine Geophysical Researches*, 15, 153-200, 1993.
- Sempéré, J.-C., G.M. Purdy, and H. Schouten, Segmentation of the Mid-Atlantic Ridge between 24°N and 30°40'N, *Nature*, 344, 427-431, 1990.

- Sempéré, J.-C., M. Rabinowicz, S. Rouzo, and C. Rosenberg, Three-dimensional mantle flow beneath spreading centers: Implications of the models (abstract), *Eos Trans. AGU, 73 Fall Meeting Suppl.*, 494, 1992.
- Sender, K.L., A. Shor, and R. Hagen, SeaMARC II Side-scan processing techniques (abstract), *Eos Trans. AGU, 70*, 1304, 1989.
- Shih, J.S.F., T. Atwater, and M. McNutt, A near-bottom geophysical traverse of the Reykjanes Ridge, *Earth and Planetary Science Letters*, 39, 75-83, 1978.
- Shor, A.N., SeaMARC II seafloor mapping system: Seven years of Pacific research, in *Australian Institute of Mining and Metallurgy Pacific Rim '90 Conference*, pp. 49-59, 1990.
- Shor, A.N., C.E. Nishimura, M. Czarnecki, and P.R. Vogt, Lava extrusion from the 1989 Reykjanes Ridge seismic swarm? Probably yes, *Eos Trans. AGU, 71*, 1602, 1990.
- Sinton, J.M., S.M. Smaglik, and J. Mahoney, Magmatic processes at superfast spreading mid-ocean ridges: Glass compositional variations along the East Pacific Rise 13°-23°S, *Journal of Geophysical Research*, 96, 6133-6155, 1991.
- Sloan, H., and P. Patriat, Kinematics of the North American-African plate boundary between 28° and 29° N during the last 10 Ma: Evolution of the axial geometry and spreading rate and direction, *Earth and Planetary Science Letters*, 113, 323-341, 1992.
- Smith, D.K., and J.R. Cann, Hundreds of small volcanoes on the median valley floor of the Mid-Atlantic Ridge at 24°-30°N, *Nature*, 348, 152-155, 1990.
- Smith, D.K., and J.R. Cann, The role of seamount volcanism in crustal construction at the mid-Atlantic ridge (24°-30°N), *Journal of Geophysical Research*, 97, 1645-1658, 1992.
- Smith, D.K., and J.R. Cann, Building the crust at the Mid-Atlantic Ridge, *Nature*, 365, 707-715, 1993.
- Stefánsson, R., Method of focal mechanism with application to two Atlantic earthquakes, *Tectonophysics* (209-243), 1966.
- Sykes, R.L., Mechanism of earthquakes and nature of faulting on the mid-oceanic ridge, *Journal of Geophysical Research*, 72 (8), 2131-2153, 1967.
- Sylvester, A.G., History and surveillance of volcanic activity of Jan Mayen Island, *Bulletin Volcanologique*, 39, 313-335, 1975.
- Talwani, M., and O. Eldholm, Evolution of the Norwegian-Greenland Sea, *Geological Society of America Bulletin*, 88, 969-999, 1977.
- Talwani, M., C.C. Windisch, and M.G. Langseth, Reykjanes Ridge crest: A detailed geophysical study, *Journal of Geophysical Research*, 76, 473-517, 1971.
- Taylor, B., K. Crook, and J. Sinton, Extensional transform zones and oblique spreading centers, *Journal of Geophysical Research*, 99, 19707-19718, 1994.
- Tron, V., and J.-P. Brun, Experiments in oblique rifting in brittle-ductile systems, *Tectonophysics*, 188, 71-84, 1991.

- Tryggvason, E., Seismicity, earthquake swarms and plate boundaries in the Iceland region, *Bulletin of the Seismological Society of America*, 63, 1327-1348, 1973.
- Tucholke, B., and J. Lin, A geological model for the structure of ridge segments in slow spreading ocean crust, *Journal of Geophysical Research*, 99, 11937-11958, 1994.
- Tucholke, B.E., and H. Schouten, Kane Fracture Zone, *Mar. Geophys. Res.*, 10, 1-39, 1988.
- Vogt, P., C. Bernero, L. Kovacs, and P. Taylor, Structure and plate tectonic evolution of the marine Arctic as revealed by aeromagnetism, *Oceanologica Acta*, SP, 25-40, 1981.
- Vogt, P.R., Asthenospheric motion recorded by the ocean floor south of Iceland, *Earth and Planetary Science Letters*, 13, 153-160, 1971.
- Vogt, P.R., The Iceland phenomenon: Imprints of a hotspot on the ocean crust and implications for flow below the plates, in *Geodynamics of Iceland and the North Atlantic area*, edited by L. Kristjansson, pp. 49-62, Reidel, Dordrecht, 1974.
- Vogt, P.R., Plumes, sub-axial pipe flow, and topography along the mid-oceanic ridge, *Earth and Planetary Science Letters*, 29, 309-325, 1976.
- Vogt, P.R., Imaging the ocean floor: History and state of the art, in *The Western North Atlantic Region*, edited by P.R. Vogt, and B.E. Tucholke, pp. 19-44, Geological Society of America, 1986a.
- Vogt, P.R., Magnetic anomalies and crustal magnetization, in *The Western North Atlantic Region*, edited by P.R. Vogt, and B.E. Tucholke, pp. 229-256, Geological Society of America, 1986b.
- Vogt, P.R., The present plate boundary configuration, in *The Western North Atlantic Region*, edited by P.R. Vogt, and B.E. Tucholke, pp. 189-204, Geological Society of America, 1986c.
- Vogt, P.R., Seafloor topography, sediments, and paleoenvironments, in *The Nordic Seas*, edited by B.G. Hurdle, pp. 237-410, Springer-Verlag, New York, 1986d.
- Vogt, P.R., and O.E. Avery, Detailed magnetic surveys in the Northeast Atlantic and Labrador Sea, *Journal of Geophysical Research*, 79, 363-389, 1974.
- Vogt, P.R., and G.L. Johnson, Seismic reflection survey of an oblique aseismic basement trend on the Reykjanes Ridge, *Earth and Planetary Science Letters*, 15, 248-254, 1972.
- Vogt, P.R., and G.L. Johnson, A longitudinal seismic reflection profile of the Reykjanes Ridge: Part II - implications for the mantle hot spot hypothesis, *Earth and Planetary Science Letters*, 18, 49-58, 1973.
- Vogt, P.R., G.L. Johnson, and L. Kristjansson, Morphology and magnetic anomalies north of Iceland, *Journal of Geophysics*, 47, 67-80, 1980.
- Vogt, P.R., L.C. Kovacs, C. Bernero, and S.P. Srivastava, Asymmetric geophysical signatures in the Greenland-Norwegian and southern Labrador Seas and the Eurasia basin, *Tectonophysics*, 89, 95-160, 1982.
- Wessel, P., and W.H.F. Smith, Free software helps map and display data, *Eos Trans. AGU*, 72, 441-446, 1991.
- White, R.S., D. McKenzie, and K. O'Nions, Oceanic crustal thickness from seismic measurements and Rare-Earth element inversions, *Journal of Geophysical Research*, 97, 19683-19715, 1992.

- Whittaker, C.C., M. Rognstad, and A.N. Shor, NAVOCEANO's new swath bathymetric and imaging system, in *Proceedings of the Marine Technology Society*, Marine Technology Society, New Orleans, 1991.
- Wilson, D.S., R.N. Hey, and C. Nishimura, Propagation as a mechanism of reorientation of the Juan de Fuca Ridge, *Journal of Geophysical Research*, 89, 9215-9225, 1984.
- Withjack, M.O., and W.R. Jamison, Deformation produced by oblique rifting, *Tectonophysics*, 126, 99-124, 1986.
- Young, K.D., M. Jancin, B. Boight, and N.I. Orkan, Transform deformation of Tertiary rocks along the Tjörnes Fracture Zone, North Central Iceland, *Journal of Geophysical Research*, 90, 9986-10010, 1985.
- Zhang, Y.-S., and T. Tanimoto, Ridges, hotspots and their interaction as observed in seismic velocity maps, *Nature*, 355, 45-49, 1992.